REVISITING STABILITY CHARTS FOR HOMOGENEOUS UNDRAINED SLOPES BY FINITE ELEMENT METHODS

by

Emre Abdullah Gurluk

A thesis submitted to the Faculty and the Board of Trustees of the Colorado School of Mines in partial fulfillment of the requirements for the degree of Master of Science (Civil and Environmental Engineering).

Golden, Colorado

Date _____

Signed: _____

Emre Abdullah Gurluk

Signed: _____

Dr. D. V. Griffiths

Thesis Advisor

Golden, Colorado

Date _____

Signed: _____

Dr. Junko Munakata

Professor and Department Head

Civil and Environmental Engineering

ABSTRACT

Slope stability charts are essential engineering tools that enable rapid calculation of the factor of safety; hence, they are frequently used during the early design phase of a project to compare design options. This thesis revisits various chart solutions for undrained slope stability by numerical analyses using state-of-the-art programs based on (i) elastic-plastic finite element analysis (EPFE) and (ii) rigid-plastic finite element limit analysis (FELA). In this study, parametric studies were performed using a wide range of soil and geometrical parameters, and the results were compared with chart solutions based on thousands of different cases.

Finite element methods do not require prior assumptions about the shape or location of the critical failure mechanism which simply follows the path of least resistance through the slope. The charts considered in this thesis for comparison, however, use limit equilibrium methods based on circular and composite circular assumptions. The finite element results observed several points of disagreement with the charts because of the availability of more realistic failure surfaces. Based primarily on the FELA analyses, stability charts in terms of dimensionless stability numbers were proposed and thoroughly validated using EPFE analyses. Then, they were extensively compared to the charts in the literature. It was found that the proposed charts, derived from finite element methods, improved the estimations of: (i) the factor of safety particularly for slopes having a large foundation layer or relatively flat gradients; (ii) two previously accepted parameters, namely the minimum stability number that can be obtained through a deep mechanism and the slope angle where the slope stability becomes independent of the depth of the foundation layer; and (iii) the factor of safety for slopes having a small foundation layer in the presence of reservoir water.

TABLE OF CONTENTS

LIST OF FIGURES

LIST OF TABLES

LIST OF SYMBOLS

ϕ'	Effective Friction Angle
ϕ_u	Undrained Friction Angle
c'	Cohesion
γ	Unit Weight
γ_w	Unit Weight of Water
q	Surcharge
S_u	Undrained Shear Strength
σ	Total Stress
ε	Strain
E	Young's Modulus
ν	Poisson's Ratio
F_{mc}	Failure Function
ψ	Dilation Angle
D	Depth Factor
H	Slope Height
H_w	Height of Reservoir Level Above the Toe
β	Slope Angle
μ_q	Dimensionless Adjustment Factor for Surcharge
μ_w	Dimensionless Adjustment Factor for Submergence
μ_t	Dimensionless Adjustment Factor for Crack
N	Stability Number
N_{Ave}	Average of Distinct N Values (For Distinct Values of Soil's Unit Weight)

LIST OF ABBREVIATIONS

$EPFE$	Elastic-Perfectly Plastic Finite Element Analysis
$FELA$	Finite Element Limit Analysis
FEM	Finite Element Method
LEM	Limit Equilibrium Method
FE	Finite Element
$SOCP$	Second-Order Cone Programming
SRF	Strength Reduction Factor
LF	Load Factor
FS	Factor Of Safety
UB	Upper Bound
LB	Lower Bound
FL	Failure Load
FL_{TRUE}	"True" Failure Load
FL_{LB}	The Predicted Failure Load by LB
FL_{UB}	The Predicted Failure Load by UB

ACKNOWLEDGMENTS

First and foremost, I want to thank my dignified supervisor, Dr. D. V. Griffiths, without whom I would not have been able to complete my dissertation. His never-ending, unwavering support and advice have been an inspiration to me throughout this course of study. He provided unending aid, counsel, criticism, inspiration, and tolerance.

I would like to express my appreciation to the Republic of Turkey Ministry of National Education, which provided me with a tremendous opportunity to study abroad and countless possibilities to advance my professional objectives.

I owe Dr. D. V. Griffiths even more gratitude and Dr. Chris Martin for giving me permission to use their state-of-the-art programs to complete this thesis.

My heartfelt thanks go out to my loved family for their unending support. My beloved mother Dürdane Gürlük and my dear father Rifat Gürlük deserve a lot of credit for their constant support and efforts in helping me achieve my goals. I would like to thank my sisters Eda Gürlük and Esra Yurt, as well as her husband Tarık Yurt, for their important contributions. I would like to express my greatest thanks to my niece Ayşe Beren Yurt for inspiring me, and I look forward to meeting them again.

For their companionship, suggestions, and encouragement throughout my study and stay in the US, my friends Alaa Elsaid, Yucel Alp, Salam Al-Sammarraie, Celal Emre Uyeturk, Erick Christian Cruz have my warmest appreciation.

Last but not least, I would like to convey my appreciation to the committee members who attended my thesis defense, Dr. Andres Guerra and Dr. Shiling Pei, for supporting me.

CHAPTER 1

INTRODUCTION

1.1 Background

The stability of earth slopes has a long history in the discipline of geotechnical engineering. It has always attracted the attention of researchers because of its extensive use in practice (e.g., highways, railroads, canals, dams, and open-pit mining) and its catastrophic results in the case of a failure. Stability assessments are often conducted to determine the stability of a natural slope, stability of a man-made slope during or after construction, the reasons for a slope failure, or the elements that may affect the probability of a landslide.

Undrained slope stability is one of the considerations in some practical problems, particularly for saturated clays or clayey soils with low permeability. It is considered a short-term stability analysis, and it might become critical in the case of sudden stress changes in low permeability soils needing a longer time for consolidation, which can be exemplified as follows:

- A quick excavation of a slope
- The construction phase of an earth dam
- A rapid drawdown in a reservoir level

Undrained stability assessments are performed in terms of total stresses, utilizing undrained shear strength of soils (s_u) and setting internal friction angle to zero ($\phi_u = 0$).

Slope stability charts summarize the stability evaluations of slopes with a variety of soil and geometrical parameters and under a variety of boundary conditions. They provide a rapid assessment of the slope's factor of safety, as well as an understanding of the potential failure mechanisms. While they can assist to compare design alternatives during the early stages of a

project, they are also effective engineering tools for verifying comprehensive analyses. Even though the charts are mainly derived for uniform soils and geometrical configurations, they can accurately estimate the factor of safety for more complex problems by employing proper approximations and simplifications to the real problem.

1.2 Problem Statement

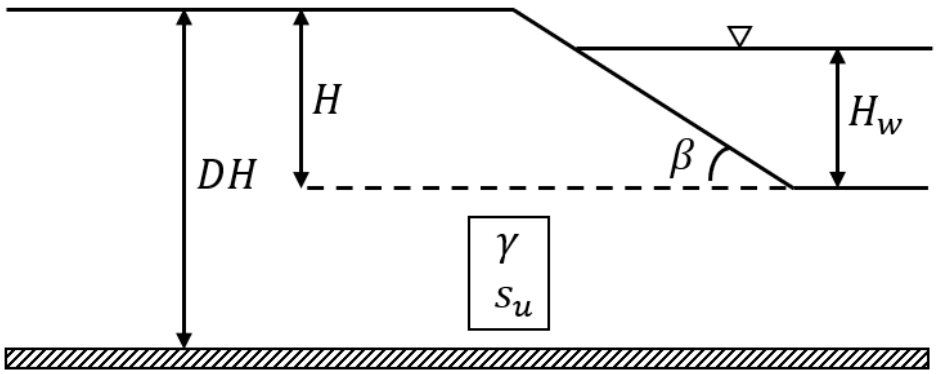

Figure 1.1 A general figure that states the problem with associated parameters discussed in the thesis

The main goal of this thesis is to develop stability charts for two-dimensional homogeneous undrained slopes with simple geometries by utilizing finite element methods. In order to accomplish this goal, comprehensive parametric studies involving a wide variety of geometrical and soil parameters are performed. These parameters are defined in Table 1.1 and illustrated in Figure 1.1.

Table 1.1 Definitions of the parameters used in the thesis

Parameter	***Definition***
H	slope height
H_w	height of the reservoir level above the toe
D	a dimensionless depth factor, where DH represents the depth to rigid base from the ground surface
β	slope angle
γ	saturated unit weight of soil
s_u	undrained shear strength of soil

All of these parameters are used throughout the thesis in the manner defined in this section. The soil is considered to be in a saturated undrained state with undrained shear strength s_u and $\phi_u = 0$, and it is homogeneous throughout.

1.3 Motivation of The Thesis

In practice, stability charts for homogeneous soil slopes are still commonly employed to calculate the factor of safety. However, despite the development of finite element methods for addressing slope stability problems in recent years, all the existing stability charts are based on limit equilibrium methods that enforce the failure mechanism to be in strict geometries such as circles or composite circles that consist of two arcs separated by a straight line. These limit equilibrium methods require prior assumptions regarding the form and position of failure surfaces and require a sufficient number of iterations to estimate the "true" factor of safety. Contrary to limit equilibrium methods, no prior assumption about the shape or location of the potential failure surface is needed for finite element-based solutions; the failure mechanism is developing naturally along the path of least resistance. Thus, the primary motivation of this study

is to revisit the existing stability charts using finite element methods, where the failure mechanisms are allowed to form "naturally" with no constraint imposed by the methodology.

Furthermore, the availability of two state-of-the-art finite element programs (Slope64 and OxLim) with distinct algorithms, namely Elastic-Plastic Finite Elements (EPFE) and Finite Element Limit Analysis (FELA) respectively, and their compatibility to perform such extensive parametric studies, serves as another motivation for this study to enable the validation of the proposed charts in this thesis.

1.4 Thesis Outline

This thesis consists of five chapters. Chapter 2 outlines the progressive evolution of slope stability methods and discusses three popular stability charts in the literature for undrained slopes. Following that, Chapter 3 explains the modeling techniques used in this thesis, describing two primary programs to perform the stability analyses in this study, Slope 64 and OxLim, with their corresponding algorithms, EPFE and FELA, respectively. Furthermore, this chapter presents the modeling and post-modeling processes of both programs for a representative slope problem whose variations will be studied by parametric analyses. Chapter 4 presents the results of the numerous parametric studies and discusses the findings. This chapter proposes stability charts for homogeneous undrained slopes both with and without external reservoir loading, and compares them to previously published charts. Finally, Chapter 5 summarizes the study and makes recommendations for further research.

CHAPTER 2

LITERATURE REVIEW

2.1 Overview

This chapter reviews previous research on the subject of slope stability. The gradual evolution of slope stability methods will be discussed, starting with the earliest studies in which all solutions were based on planar rupture surfaces, progressing to methods based on circular assumptions, and finally arriving at modern approaches such as finite element analyses.

Furthermore, the main charts in the literature used in the assessment of the stability of undrained clay slopes ($\phi_u = 0$) will be examined in detail. The similarities and differences between the charts will be highlighted, and the methods used in the derivation will be explained.

2.2 History of Slope Stability Methods

2.2.1 Early Approaches with Planar Failure Surface Assumption

Many of the fundamental principles and assumptions in slope stability calculations may be traced back to the work of Coulomb (1776), who developed a mathematical equation for shear strength in an earth pressure problem. He was able to estimate the location of the critical plane for which the active earth pressure reaches its maximum by employing a plane shear surface and taking into account overall equilibrium. By assuming a plane slip surface, he formulated the critical height of a vertical clay cut in terms of cohesion, internal friction angle, and the unit weight of soil. Rankine (1857) assumed and investigated planar rupture surfaces in his stress field solution for active and passive earth pressure predictions. A plane failure surface passing through the toe of the slope was also assumed by Francais (1820) and Culmann (1866) for stability analyzes.

2.2.2 Development of Limit Equilibrium Methods and Circular Failure Assumption

A memorandum published by Collin (1846) became one of the earliest pioneering works on the subject. Based on his field observations of several landslides in clays, he reveals that Coulomb's plane failure mechanism is not applicable, and the actual slide appears to be a curve. Kötter (1903) derived the differential equation of the distribution of the soil reaction on a curved failure surface for a cohesionless soil.

A geotechnical commission that worked between 1914 and 1922 was appointed by the Swedish State Railways to find out the cause of a series of recent landslides. In March 1916, a landslide occurred in the Stigberg Quay in the Göteborg port one year after being constructed. The commission was tasked with investigating the slide and making recommendations for the design of a replacement quay. The Stigberg slide was analyzed using the slip circle approach, devised by Hultin (1916) and Petterson (1916), assuming clay as a cohesionless material according to the concepts on that time. The circular slip assumption in the stability analysis of the construction of the quay was later depicted in Fellenius' seminal publication (1927) as seen in Figure 2.1. Fellenius (1927 and 1936), who had been the chairman of the commission, extended the scope of the circular slide method to include cohesive soils and soils having both friction and cohesion. Besides, he introduced a circular deep failure mechanism that passes below the toe and whose center is located above the mid-point of the slope. He revealed that this deep mechanism, later called a mid-point circle in the literature, was the most dangerous slip surface for homogenous purely cohesive slopes at slope angles less than 53°. Fellenius' solution for the stability of the $c' - \phi'$ soils had become a pioneering work for the development of the limit equilibrium methods. He divided the sliding mass into vertical slices and performed the stability analyses satisfying moment equilibrium. While this method was later called the

"Ordinary Method of Slices," the methods based on the circular stability analysis of slopes have also been called the "Swedish Circle Method."

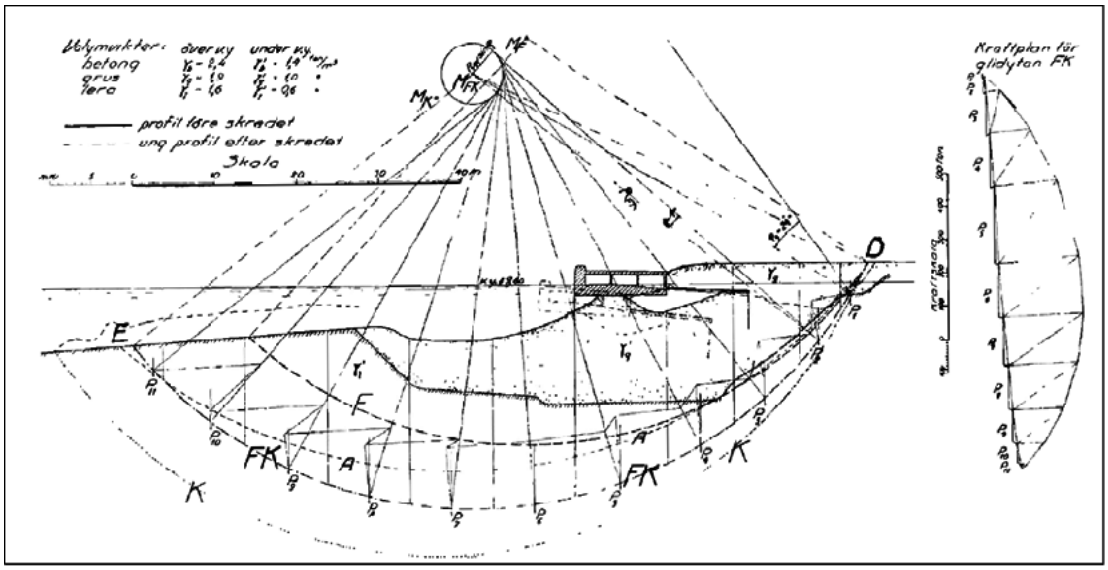

Figure 2.1 A circular slip surface assumption in the stability analysis of the construction of Stigberg Quay in Göteborg Harbor (Fellenius, 1927)

Prandtl (1921) introduced the concept of curved failures for strip footing bearing capacity problems, which is extended by Terzaghi (1943) taking into account the soil's cohesion, friction angle, and unit weight. Rendulic (1935) proposed that logarithmic spirals may be used as failure surfaces instead of circles for slope stability problems. Jaky (1936) presented a mathematical solution based on the equation of stress continuity along a toe circle making an angle of $45° - \phi'/2$ with the slope.

In 1937, Taylor published a seminal work on slope stability, in which he presented an overview of several methods developed by that time. He developed a mathematical approach to the friction circle method, which Glennon Gilboy and Arthur Casagrande developed as a graphical solution to the slope problems (Taylor, 1937). The outcome of the friction circle

method is a vector whose length equals the expression which in the notation of this paper is $\frac{2c'}{\gamma}$, where c' and γ represent the cohesion and unit weight, respectively. With the inspiration of this expression and dividing it by the slope height H, Taylor further modified it and introduced the new dimensionless expression, $\frac{c'}{FS\,\gamma H}$, called the "stability number," where FS is the factor of safety.

Using the stability number and a mathematical approach to the friction circle method, Taylor (1937) performed a trial-and-error procedure to determine the center of the most critical failure circle for each case of slope geometry and friction angle with the assistance of computing machines. Based on this study, he proposed a chart solution that delivers the stability number for homogenous slopes with a simple two-dimensional geometry. The chart solution is further discussed in Section 2.3.1. Moreover, Taylor performed a detailed comparison of the Culmann Method, the Jaky Method, the friction circle method with Jaky's slip circle assumption, and his friction circle method by searching for the most critical circular failure surface. Taylor also compared his stability results to the results obtained by the assumption of the logarithmic failure surface proposed by Rendulic. Although he found a close agreement in the results, he pointed out that the logarithmic spiral assumption requires the labor twice as that required by the friction circle method. Taylor compared the stability number results in his study to those obtained using Fellenius' slice method on the same slip surface, concluding that the ordinary method of slices is slightly more conservative.

After Fellenius (1927), many limit equilibrium methods built on the concept of the method of slices were developed in the following years. Table 2.1 summarizes several of these methods in terms of their applicable slip surface and equilibrium conditions.

Table 2.1 The summary of some remarkable limit equilibrium methods in the literature

Method	Applicability	Moment Equilibrium	Horizontal Force Equilibrium	Vertical Force Equilibrium	Comments
Ordinary Method of Slices (Fellenius 1927)	Circular Slip Surfaces	Yes	No	No	- Conservative - Unsuitable for high pore water pressure
Bishop Modified (Bishop 1955)	Circular Slip Surfaces	Yes	No	Yes	- Assumes horizontal side forces - Unsuitable for high pore water pressure
Janbu's Simplified (Janbu 1954)	Slip Surface of any Shape	No	Yes	Yes	- Assumes slide forces to be horizontal - Provides low factor of safety
Spencer's Method (Spencer 1967)	Slip Surface of any Shape	Yes	Yes	Yes	- Assumes slide forces to be Parallel to slope - Known to be the simplest method
Morgenstern and Price (1965)	Slip Surface of any Shape	Yes	Yes	Yes	- Assumes a varied side forces with pattern - Extremely time-consuming
Sarma's Method (Sarma 1973)	Slip Surface of any Shape	Yes	Yes	Yes	- Assumes predefined patterns for vertical forces - Calculates horizontal accelerationfor unstable equilibrium
General Limit Equilibrium - GLE (Fredlund and Krahn, 1977; Fredlund et al., 1981)	Slip Surface of any Shape	Yes	Yes	Yes	- Assumes a varied side forces with pattern - Extremely time-consuming

2.2.3 Development of Finite Element Methods for Addressing Slope Stability Problems

Using nonlinear stress-strain analyses in geotechnical engineering has revolutionized the way slope stability issues are addressed as it initiated the use of the finite element approach in the field. It can be said that this revolution was first accomplished by Clough and Woodward (1967). They were the first to introduce the finite-element method to the profession in a paper written for the first Berkeley conference on slope stability. Smith and Hobbs (1974) provided the results for $\phi_u = 0$ slopes and found that they agreed with Taylor's (1937) charts. Zienkiewicz et al. (1975) analyzed a $c' - \phi'$ slope and compared his results to the slip circle solutions in the literature. For a variety of slope geometries and soil properties, Griffiths (1980) demonstrated reasonable slope stability results by employing the finite element method with the assumption of elastic-perfectly plastic material. He then compared the results to the charts published by Bishop

and Morgenstern (1960). Kohgo and Yamashita (1988) compared the elastic-plastic finite element analyses to the limit equilibrium stability assessments and revealed good agreement between them. Griffiths (1989) analyzed an undrained clay slope in plane strain under gravity loading, using finite element methods with a strain-softening material. A finite element analysis case study performed on a progressive failure embankment using a nonlinear elastoplastic soil model was conducted by Potts et al. (1990). According to the findings, finite element analysis may produce predictions of the stability of strain-softening soils with sufficient precision for engineering purposes. Duncan (1996a) published an exhaustive summary of finite element analyses of slopes and embankments conducted by scholars over the past decades.

Griffiths and Lane (1999) published a seminal study using an elastic-plastic finite element analysis program, which is first introduced by Smith and Griffiths (1988), and employed the finite element method in conjunction with an elastic-perfectly plastic material model for assessing the factor of safety of slope stability problems using the strength reduction technique (Zienkiewicz et al., 1975). Griffiths and Lane (1999) presents the FE implementation to the five typical slope problems listed below, validating against the classical limit equilibrium problems:

- Homogenous slope with no foundation layer
- Homogenous slope with a foundation layer
- An undrained clay slope with a thin weak layer
- An undrained clay slope with a weak foundation layer
- Homogenous slope with horizontal free surface

The modeling techniques proposed by Griffiths and Lane (1999) and the accompanying software slope64 will be described in Chapter 3.

A study by Griffiths and Martin (2020) investigated undrained stability analysis of relatively flat slopes ($\beta < 10°$) and compared the stability number results and the associated failure mechanism obtained by using an elastic-plastic finite element (EPFE) analysis with strength reduction (performed by slope64 software), a finite element limit analysis (FELA) (performed OxLim software), and a MATLAB program that generates Taylor's solution with an assumed circular failure mechanism. The study concluded that although Taylor's slip circles are accurate for most slopes, they can differ from the FE results with up to %12 error on the unsafe side for flat slopes ($\beta < 10°$) with a small foundation layer. While Table 2.2 summarizes the results of the study, Figure 2.2 compares the failure mechanisms. The finite element limit analysis program OxLim and the theory behind it will be discussed in Chapter 3, and the program will be used as the primary instrument to perform the stability analyses throughout the thesis.

Table 2.2 Stability number results comparing to Taylor's for the relatively flat slopes (Griffiths and Martin, 2020)

	β = 5°				**β = 10°**			
	N_{FELA}	**N_{EPFE}**	**N_{Taylor}**	**ε_{Taylor} (%)**	**N_{FELA}**	**N_{EPFE}**	**N_{Taylor}**	**ε_{Taylor} (%)**
D = 1.0	22.5	23.1	25.1	12	14.2	14.4	15.0	6
D = 1.2	18.8	19.2	20.9	11	11.9	12.0	12.5	5
D = 1.5	15.1	15.3	16.8	11	9.7	9.7	10.0	3
D = 2.0	11.5	11.6	12.6	10	7.9	7.9	7.9	0
D = 3.0	8.7	8.7	8.8	1	6.5	6.5	6.5	0
D = 4.0	7.4	7.4	7.4	0	6.0	6.0	6.0	0

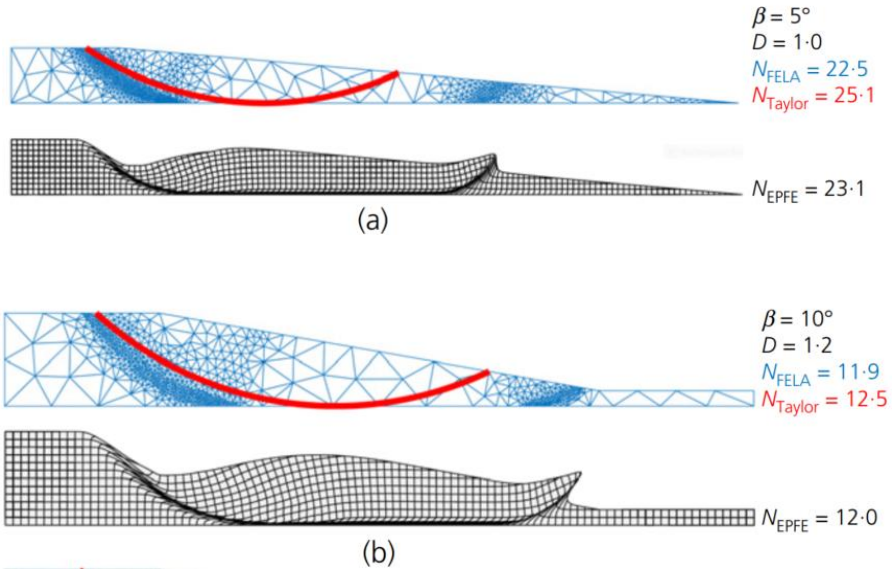

Figure 2.2 Stability results for (a) $\beta = 5°$ and $D = 1.0$; (b) $\beta = 10°$ and $D = 1.2$, where D is the depth factor illustrated in Figure 1.1 (Griffiths and Martin, 2020)

The stability of a vertical cut, in other words, a vertical slope where $\beta = 90°$ had been studied extensively. Early studies (Coulomb, 1776; Rankine, 1857; Culmann, 1866), assuming a planar rupture surface, leads to the equation below:

$$H_{cr} = \frac{4c}{\gamma} \tag{2.1}$$

where H_{cr} is the critical height for a stable vertical slope at $\beta = 90°$. After replacing the planar slips by circular slips in the analyses, Taylor (1937) and Janbu (1954) reduced this value to 3.83 from 4.0.

To date, this vertical cut problem has attracted the interest of researchers that study finite element limit analysis; Pastour et al. (2009), Kammoun et al. (2010), and Martin (2011) all agreed on the value of 3.78, rounded to the second decimal place, while the number is bracketed as follows:

$$3.7764904 < N < 3.7764911$$

Griffiths and Martin (2020) presented this vertical cut problem by using OxLim software and compared the failure mechanism to Taylor's solution, as illustrated in Figure 2.3.

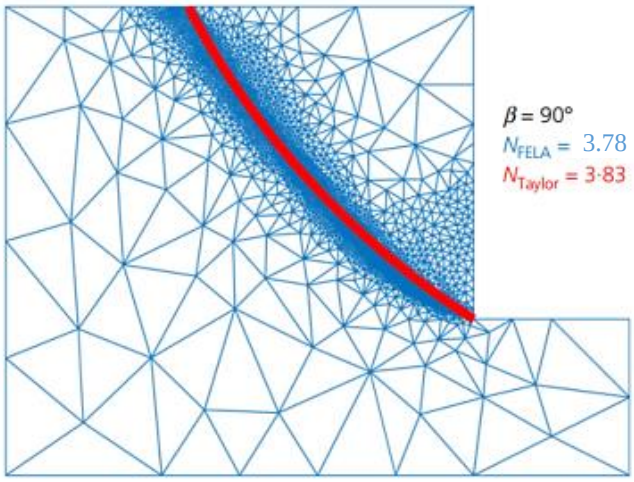

Figure 2.3 The stability analysis of a vertical cut by the finite element limit analysis (Griffiths and Martin, 2020)

2.3 Stability Charts for Homogeneous Undrained Slopes ($\phi_u = 0$)

Proposing chart solutions for slope stability analyses has always attracted the attention of researchers. Very early trials appeared in Fellenius (1927) study and had been considerably extended by Taylor (1937). In the later years, many important chart solutions have been proposed by researchers for different purposes, such as Janbu (1954), Spencer (1967), Hunter and Schuster (1968), Michalowski (2002), Baker (2003), Steward et al. (2011).

This section will discuss three main stability charts for the stability of undrained slopes with $\phi_u = 0$.

2.3.1 Taylor's Chart (1937)

Taylor (1937) developed a chart solution for the stability of homogeneous slopes having simple two-dimensional geometry by his mathematical approach to the friction circle method. He built the charts on the concept of the stability number which is a dimensionless expression showed below:

$$N_{Taylor} = \frac{c'}{FS\,\gamma\,H} \tag{2.2}$$

emphasizing Taylor's stability number N_{Taylor} is inversely proportional to factor of safety.

After searching for the most critical failure mechanism for different geometries by trial-and-error, Taylor presents the results in two stability charts (Figure 2.4 and Figure 2.5).

Figure 2.4 delivers the stability number for the slopes under both drained and undrained conditions depending on the internal friction angle and the slope gradient. However, this extensive chart does not comprise the solution for the $\phi_u = 0$ soil slopes flatter than 53°.

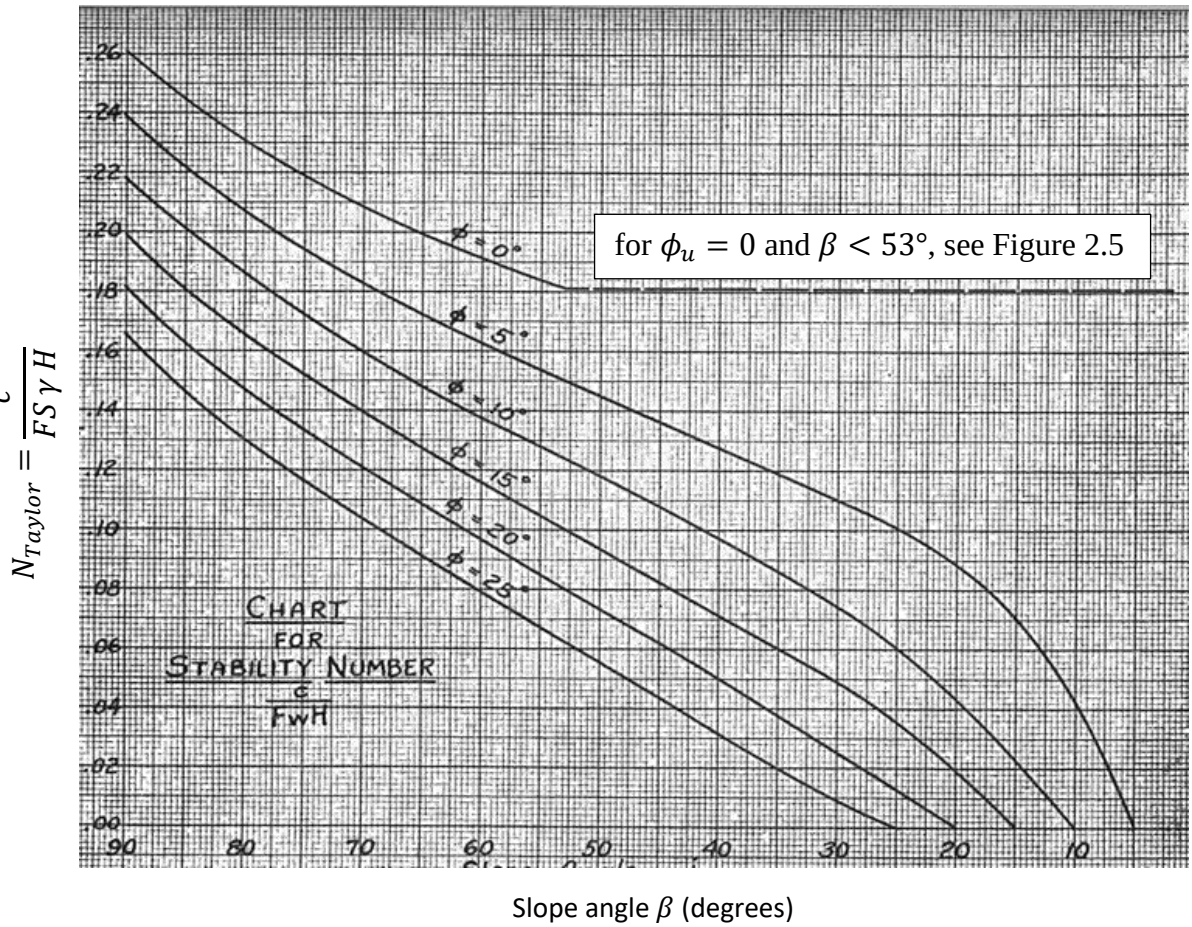

Figure 2.4 Stability chart for homogeneous slopes in simple geometries (Taylor, 1937)

Taylor proposed Figure 2.5 for this special case. According to Taylor (1937), for the flatter slopes with homogeneous soil having $\phi_u = 0$, the critical failure circle passes below the toe and has its center above the mid-point of the slope. As seen in Figure 2.5, the depth factor *D* becomes an additional consideration in the assesment of the stability number.

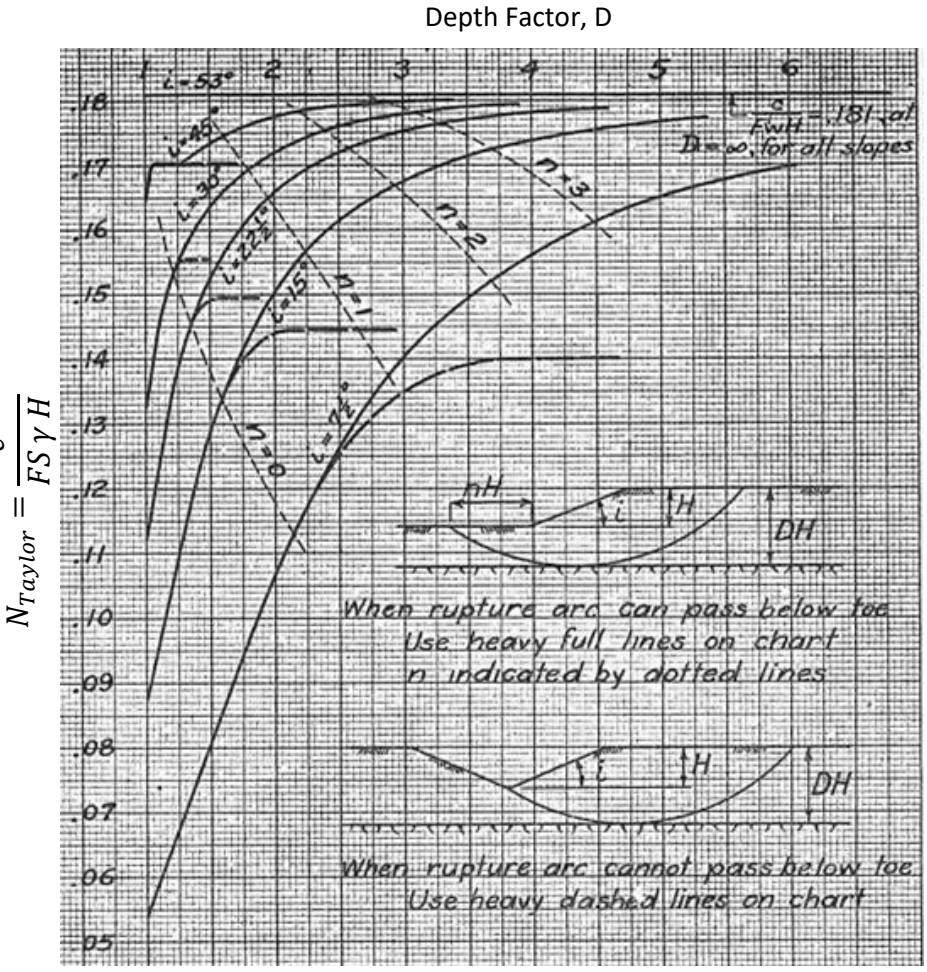

Figure 2.5 Taylor's stability chart for the slopes with $\phi_u = 0$ when $\beta < 53°$, showing the effect of the depth factor D on the stability number, where $i = \beta$ (Taylor, 1937)

It is worth to mention that Taylor presented all results of the stability analysis of soils with $\phi' > 0$ in Figure 2.4 because he indicated that the depth factor D does not have a significant effect on the stability number especially for the soils with $\phi' > 10°$ (Taylor, 1937).

Terzaghi (1943) combined Figure 2.4 and Figure 2.5 and presented the data published by Taylor (1937) on a single chart as shown Figure 2.6. This chart additionally delivers the type of failure mechanism corresponding to the stability number. Terzaghi re-defined Taylor's definition

of the stability number in a way that the stability number became directly proportional to the factor of safety and expressed like:

$$N = \frac{\gamma H_{cr}}{c'} \tag{2.3}$$

where H_{cr} is the maximum height of the stable slope. The factor of safety can be calculated by dividing the critical height (H_{cr}) obtained from the chart by the designed height of the slope (H).

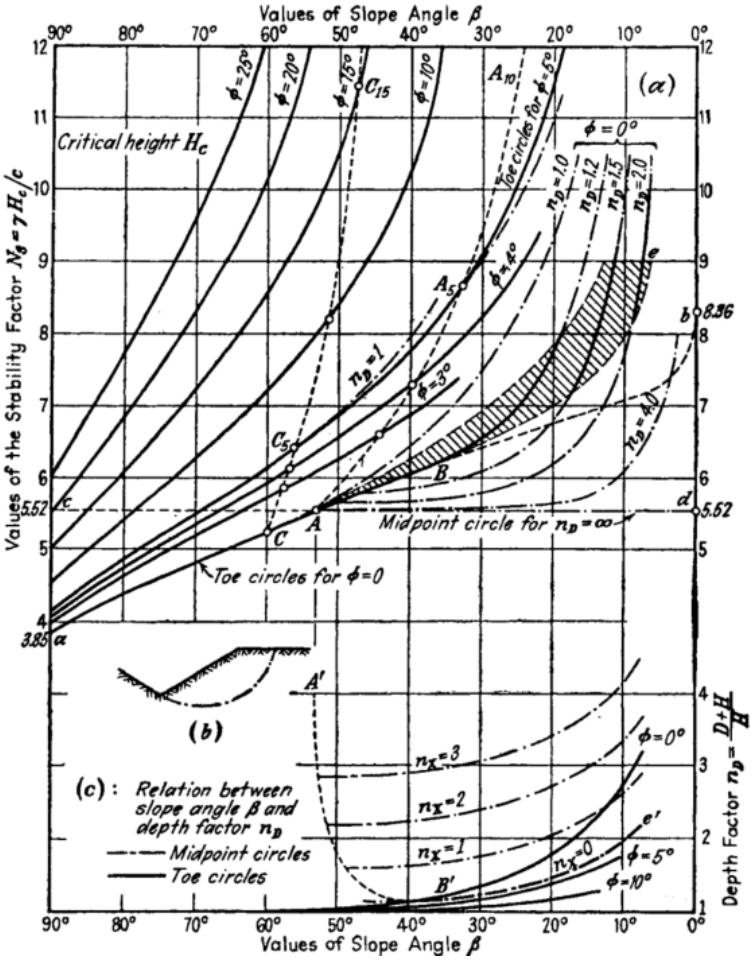

Figure 2.6 Taylor's stability chart after Terzaghi (1943)

Taylor's chart was later modified once again by Terzaghi and Peck (1948), and it reached its current popular version. Terzaghi and Peck presented the stability chart as two separate charts for undrained clays with $\phi_u = 0$ and $c' - \phi'$ soils. While the former for $\phi_u = 0$ is shown in Figure 2.7, the latter is not included since it is out of the scope of this thesis.

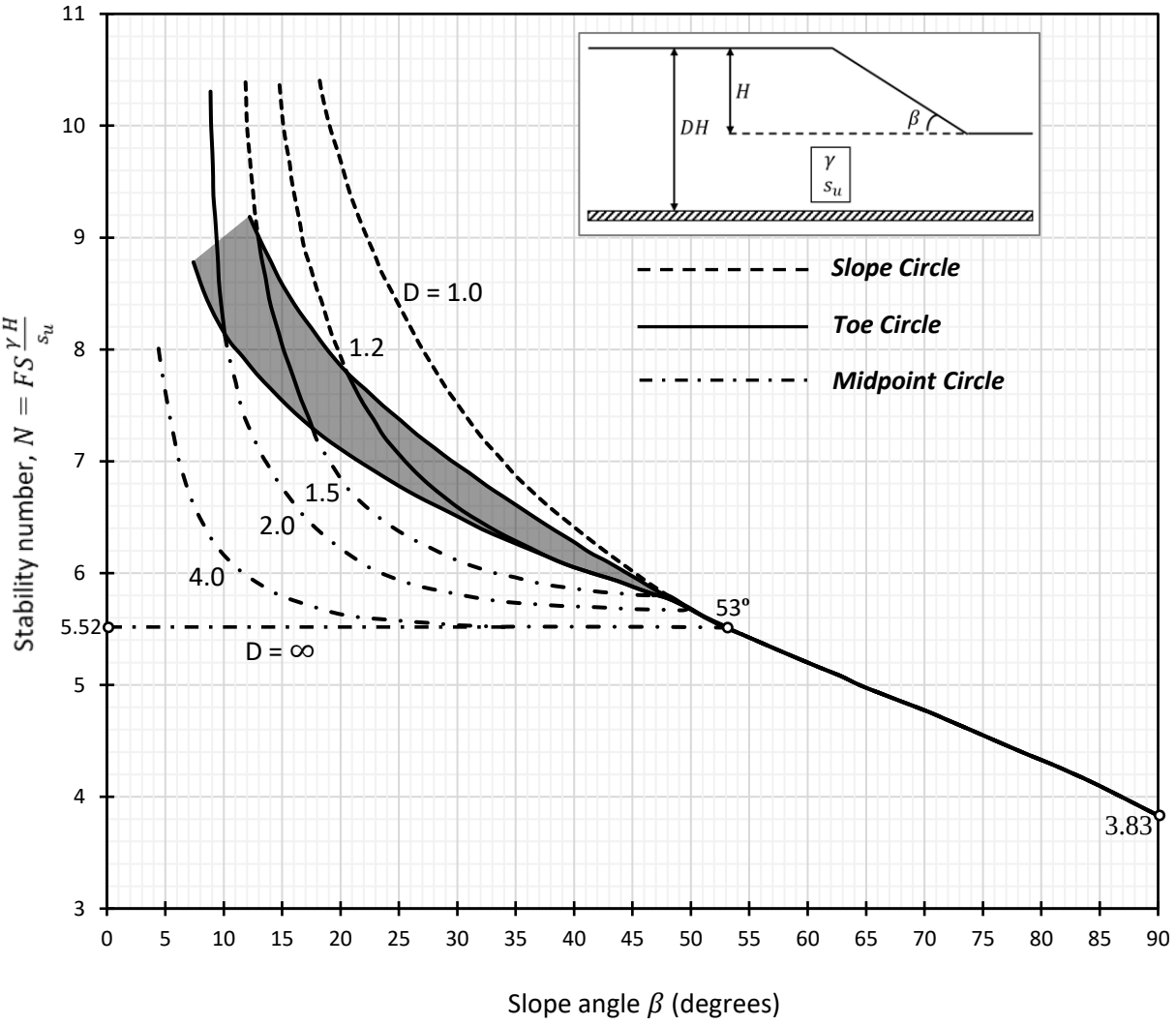

Figure 2.7 Taylor's stability chart for homogeneous undrained slopes with $\phi_u = 0$ in simple geometries (after Terzaghi and Peck, 1948)

After the modifications by Terzaghi and Peck, the current version of Taylor's chart for undrained clays with $\phi_u = 0$ brings a new type of failure mechanism called a "slope circle." Within the aspects of Figure 2.7, a slope circle means a circular slip that intersects with the face of the slope as illustrated in Figure 2.8(a). According to Terzaghi and Peck, slopes with flat geometry and shallow foundations, based on Taylor's data, are likely to develop a slope circle failure mechanism. While the dashed lines on Figure 2.7 represents the stability number obtained by a slope circle failure mechanism, the dash-dotted lines correspond to a mid-point circle failure mechanism. All types of slip surfaces are illustrated in Figure 2.8.

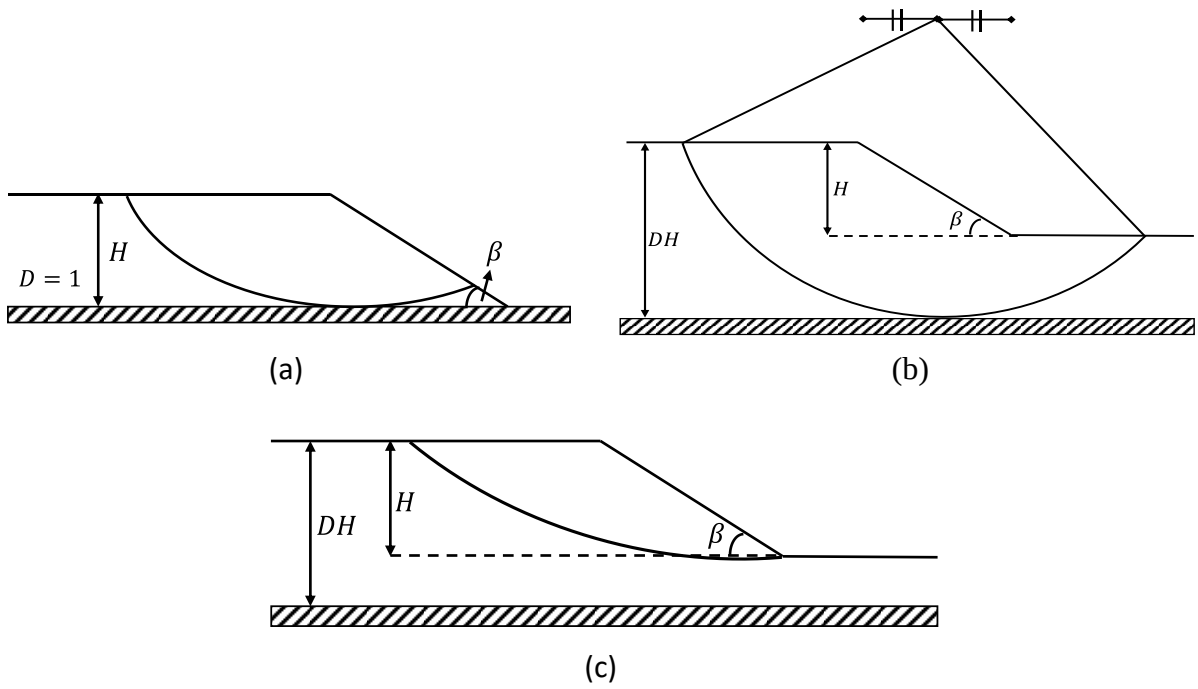

Figure 2.8 Slip circles: (a) slope circle; (b) mid-point circle; (c) toe circle

To maintain consistency throughout the thesis, the stability number N for the undrained clays with $\phi_u = 0$ will be described as follows:

$$N = FS\ \frac{\gamma H}{s_u} \tag{2.4}$$

where s_u is the undrained shear strength of the soil.

Fellenius (1927) revealed that the most critical sliding surface for slopes flatter than $53°$ is the one having infinitive depth in a homogenous pure cohesion soil ($\phi_u = 0$), and, accordingly, the maximum stable height of this type of slope is:

$$H_{cr} = \frac{c'}{0.181\gamma} \tag{2.5}$$

Taylor, in agreement with Fellenius, reported the value of 0.181 (in terms of N_{Taylor} given by Equation 2.2) as the maximum stability number that can be theoretically obtained by assuming a mid-point failure mechanism. However, larger N_{Taylor} values can be obtained by assuming a slip circle through the toe where $\beta \geq 53°$. Therefore, according to Taylor, all slopes steeper than $53°$ fail as a toe circle. This number can be interpreted as 5.52 in accordance with the definition of the stability number N given by Equation 2.4. It is indicated in Figure 2.7 as the stability number of slopes with $D = \infty$ where $\beta < 53°$, and all the steeper slopes fail in the form of a toe circle giving smaller N values. In other words, $N = 5.52$ in terms of Equation 2.4 represents the minimum stability number that can be obtained by a deep mechanism; however, according to Fellenius (1927) and Taylor (1937), it is only possible with an infinitely deep mid-point circle.

2.3.2 Janbu's Chart (1954)

Janbu (1954) made significant contributions to slope stability analysis in his PhD thesis. He investigated the stability of slopes in purely cohesive soil ($\phi_u = 0$) and slopes with $\phi' > 0$ under a variety of boundary conditions and created several stability charts. He also discussed the different definitions of factor of safety in the literature and suggested a rational selection of the definitions to the relevant circumstances. In addition, he introduced his own reasonable approach to the method of slices proposed by Fellenius (1927), which has become known as "Janbu's simplified method" (as mentioned in Table 2.1).

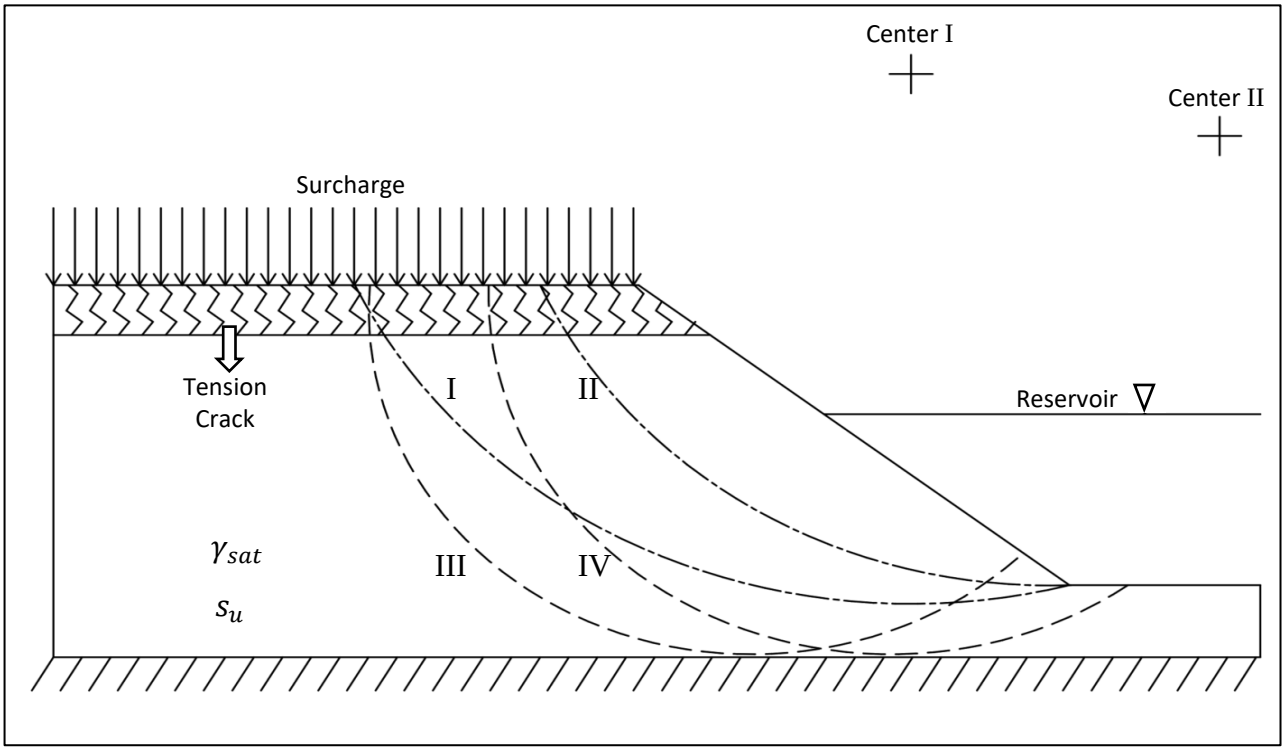

Figure 2.9 A homogeneous simple geometry slope under different boundary conditions and Janbu's assumed slip circles: I) a toe circle (the center lies above the slope); II) a toe circle (the center lies off the slope); III) a slope circle; and IV) a base circle

This section will only focus on Janbu's stability charts for soil slopes with $\phi_u = 0$. The rest of the charts can be found in Janbu's Ph.D. thesis (1954), in Janbu's technical report about slope stability computations (1968), and in Duncan (1996b).

Janbu (1954) derived a comprehensive mathematical solution to estimate the stability number for undrained slopes with $\phi_u = 0$ having simple geometry under different scenarios such as partial or complete submergence, tension cracks, and an external surcharge load on the slope crest.

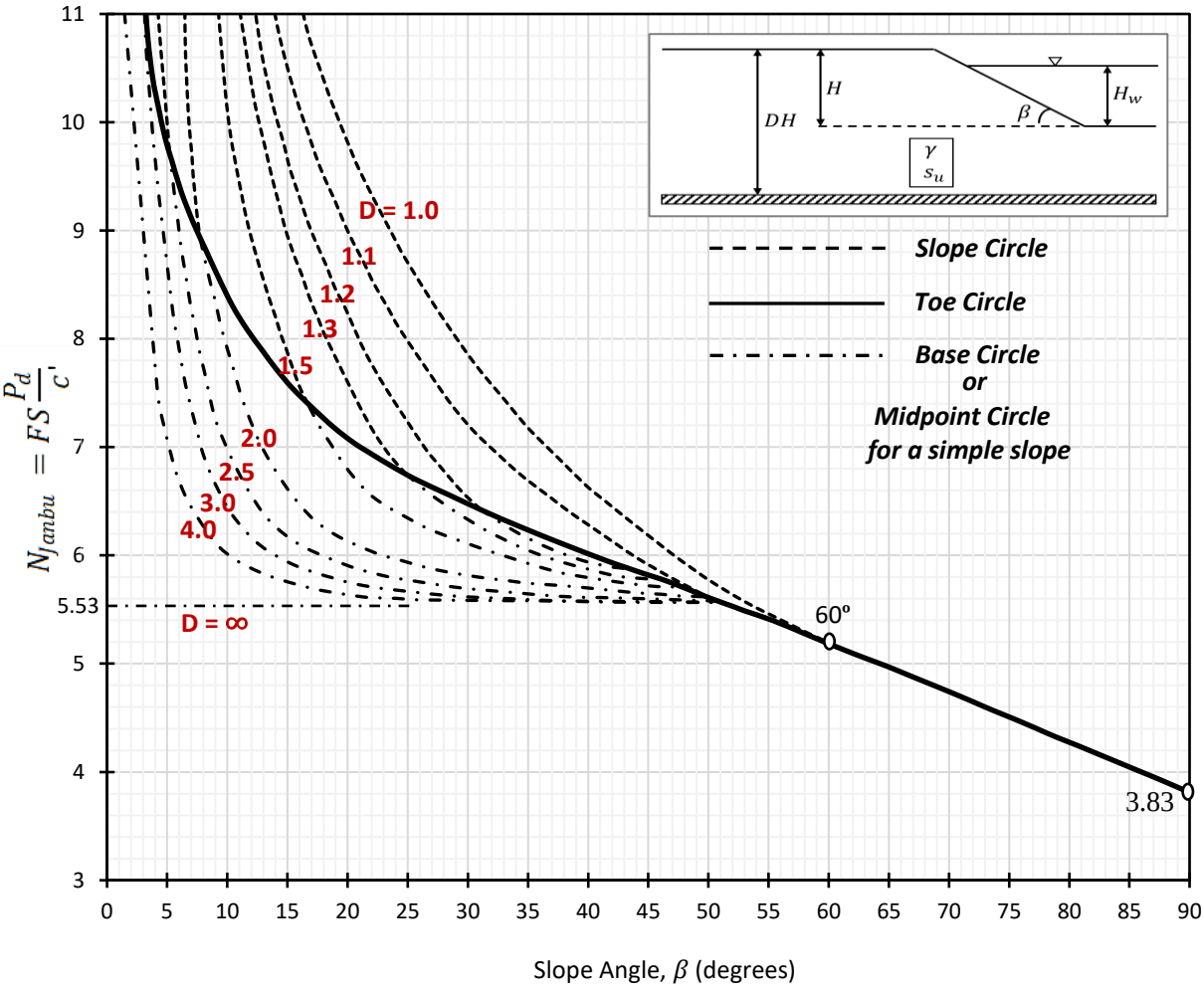

Figure 2.10 Stability number for simple slopes when $\phi_u = 0$ (after Janbu, 1954)

He based the method on the circular assumptions of the slip surface depicted in Figure 2.9, and he created charts to deliver the stability number after searching for the most critical slip circle for each case. The charts developed by Janbu are not only used for a single scenario but are also used for the combination of the scenarios in the assessment of the stability number.

Figure 2.10 is the centerpiece of Janbu's $\phi_u = 0$ solution which consists of a set of charts. This chart is the first step of the solution, and it delivers a stability number expressed below with a type of failure associated with it:

$$N_{Janbu} = FS\frac{P_d}{c'} \tag{2.6}$$

where

$$P_d = \frac{\gamma H + q - \gamma_w H_w}{\mu_q\, \mu_w\, \mu_t} \tag{2.7}$$

where

γ = average unit weight of soil
H = height of the slope above the toe
q = surcharge
γ_w = unit weight of water
H_w = height of reservoir level above the toe
μ_q = a dimensionless adjustment factor for surcharge ($\mu_q = 1.0$ when no surcharge)
μ_w = a dimensionless adjustment factor for submergence ($\mu_w = 1.0$ when empty reservoir)
μ_t = a dimensionless adjustment factor for tension crack ($\mu_t = 1.0$ when no tension crack)

It can be noticed that for a homogenous undrained slope without any additional condition (no surcharge, empty reservoir, and no tension crack) Equation 2.6 becomes equivalent to and Equation 2.7 to:

$$N = FS\ \frac{\gamma\ H}{s_u} \tag{2.8}$$

which means that a stability number obtained by Figure 2.10 can directly be used in the calculation of factor of safety for the simple slopes as used in Taylor's chart.

Janbu's stability chart differs from Taylor's in some respects. First of all, Janbu included more values of the depth factor D into the solution, which inherently minimizes the error if interpolation is needed. Secondly, Taylor's angle of $53°$ is updated, and the angle is proposed to be replaced by 60° instead. Despite the trend that the angle is still around $53°$ for large D values, Janbu pushed the largest angle where a slope or base circle can be the most critical to $60°$ due to the geometrical constraints for the slopes with either very shallow or no foundation ($D = 1.0$). Moreover, according to Janbu, a toe circle is presented by a solid line in Figure 2.10, whereas a shaded area is used in Taylor's chart (Figure 2.7) to illustrate slope geometries for which the most critical circle passes through the toe in the case of $\beta < 53°$.

For the stability of a vertical slope (cut), Janbu agrees with Taylor's estimate of 3.83. Additionally, the minimum theoretical stability number obtained from an infinitely large mid-point circle is proposed as 5.53, which is almost identical to Taylor's value (5.52).

Along with the value of the stability number and the failure type, Janbu also presented the position of the center of the critical slip circle. Figure 2.11 and Figure 2.12 give the dimensionless coordinates x_0 and y_0 of the center, respectively, where the origin is placed to the

toe of the slope. The real coordinates X_0 and Y_0 can be calculated by multiplying the dimensionless coordinates by the slope height H. It should be noted that these charts only deliver the coordinates of the slip circle for the analysis of a simple slope. In the case of additional boundary conditions such as a surcharge, the corresponding charts can be found in the original study.

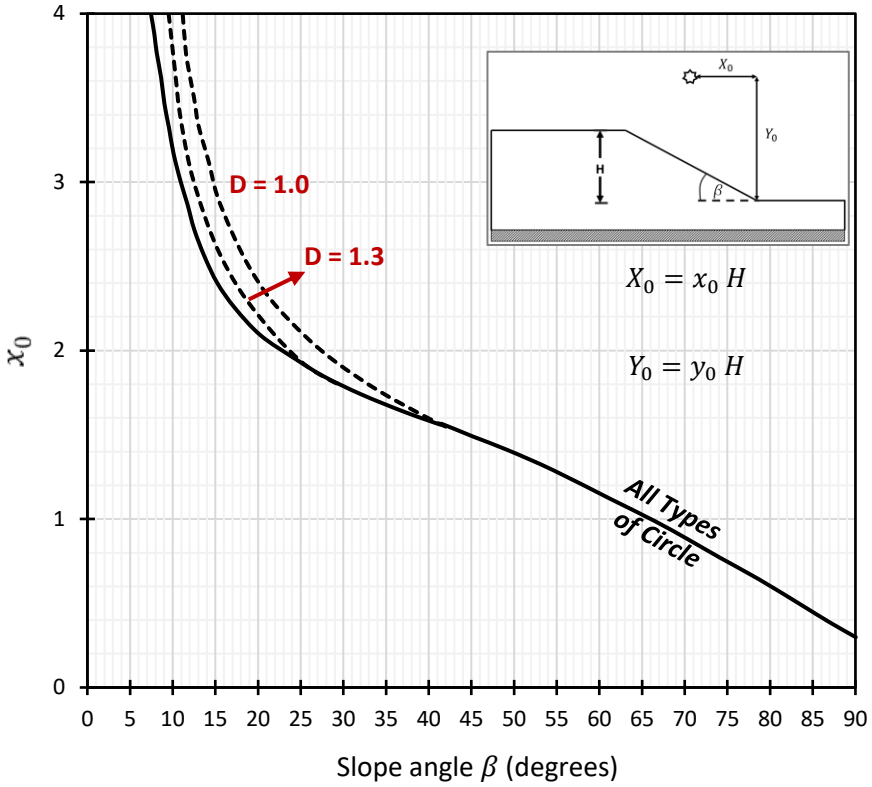

Figure 2.11 X coordinates of the center of the critical slip circle for simple slopes (after Janbu, 1954)

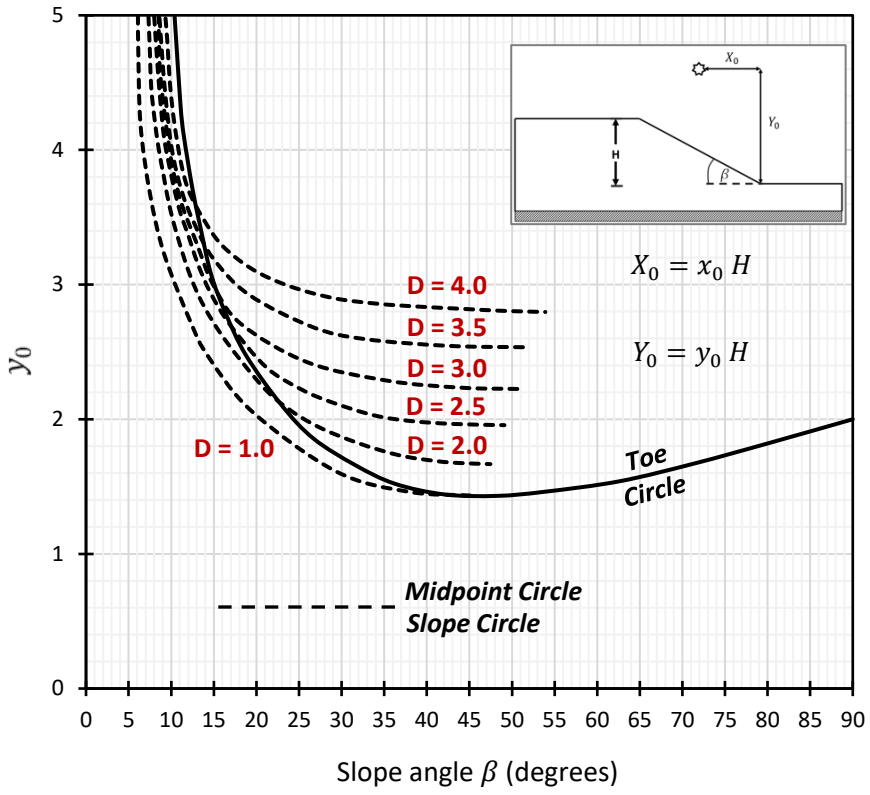

Figure 2.12 Y coordinates of the center of the critical slip circle for simple slopes (after Janbu, 1954)

On the other hand, when the reservoir is not empty, and the slope is partially or completely submerged, Equation 2.6 and Equation 2.7 yield

$$FS = N \frac{\mu_w s_u}{\gamma H - \gamma_w H_w} \tag{2.9}$$

Under such conditions, the adjustment factor of submergence μ_w can be obtained with the aid of Figure 2.13 for a toe circle and Figure 2.14 for a base or slope circle. However, since the reservoir water might change the governing type of failure mechanism suggested by Figure 2.10, it is sensible to use the smaller μ_w from both charts in the calculation of factor of safety.

For the reservoir problems, it is important to emphasize that Janbu (1954) did not consider the effect of the depth factor D on a toe circle mechanism.

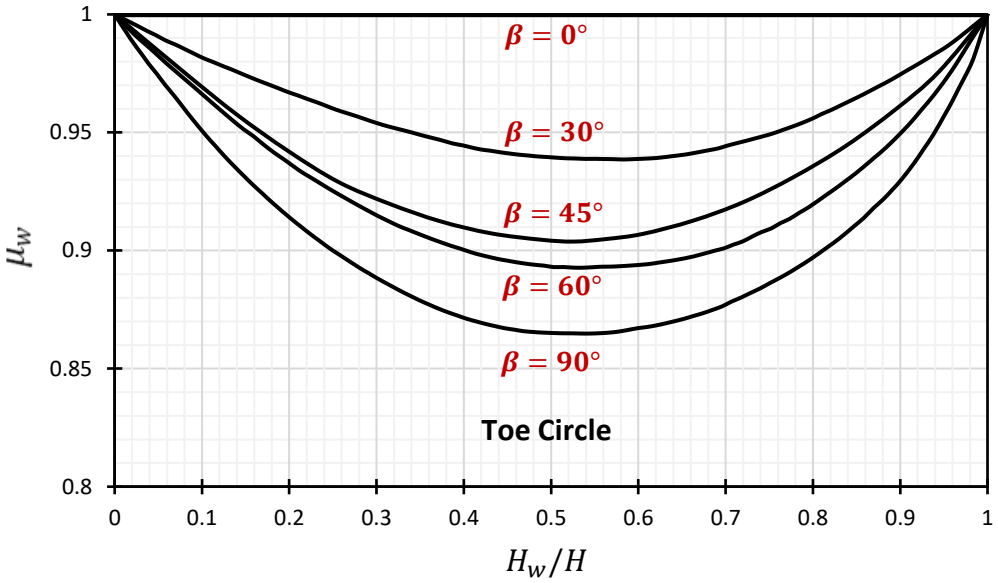

Figure 2.13 An adjustment factor μ_w of submergence for a toe circle

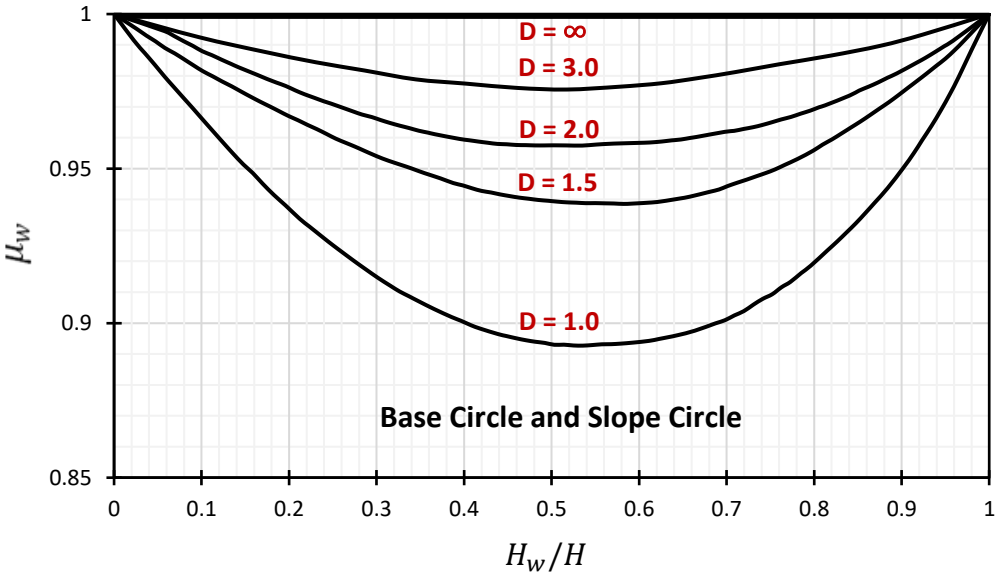

Figure 2.14 An adjustment factor μ_w of submergence for a base or slope circle

2.3.3 Steward, Sivakugan, Shukla, and Das's Chart (2011)

Steward et al. (2011) revisited Taylor's two design charts and performed a parametric study by hundreds of runs for the stability of several homogeneous slopes with varying geometries and soil conditions using SLOPE/W software with the Morgenstern and Price method.

The Morgenstern and Price method is one of the most common and developed limit equilibrium methods in the literature with some of the advantages listed below:

- applicable to complex geometric slopes
- applicable to both circular and non-circular geometries of the assumed slip surface
- satisfies both force and moment equilibrium, so calculates FS for both
- considers both shear and normal interslice forces
- allows user-specified interslice force function, which may increase the accuracy of the analysis

Steward et al. (2011) did not mention the interslice force function used in the derivation of the proposed charts even though SLOPE/W offers many options for the selection of the interslice force function as following:

- constant
- half-sine
- clipped sine
- trapezoidal
- data-point specified

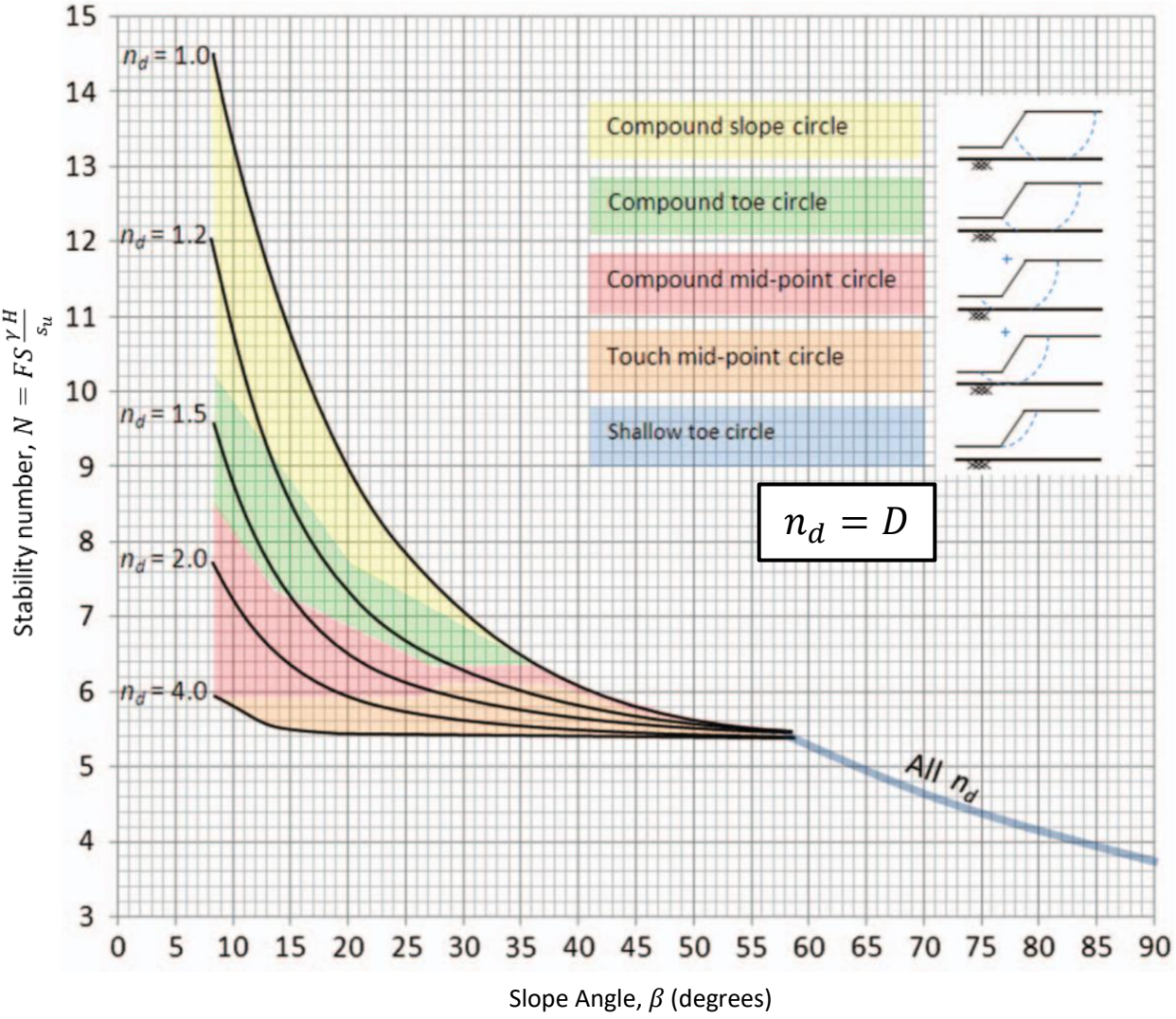

Figure 2.15 Stability chart for $\phi_u = 0$ proposed by Steward et al. (2011)

According to the SLOPE/W results obtained using the Morgenstern and Price method, the stability chart proposed by Steward (2011) for the stability of an undrained ($\phi_u = 0$) soil slope is shown in Figure 2.15. Although the chart has a similar trend with Taylor and Janbu's stability charts, it introduces a new type of failure mechanism for the analysis of homogenous slopes. Steward et al. (2011) concluded that the most critical slip, which delivers the lowest

factor of safety, might be a compound failure surface having two circular arcs connected by a straight line at the face of the rigid base.

Each failure mechanism is coded with a different color and is also illustrated in Figure 2.15. Accordingly, there are five failure types in total, which are:

- a compound slope circle
- a compound toe circle
- a compound mid-point circle
- a touch mid-point circle (tangent to the rigid base)
- a shallow toe circle

It is worth pointing out that a slope circle tangent to the rigid base is not a type of output failure mechanism in Figure 2.15, whereas Taylor and Janbu's charts proposed that a slope circle is the most dangerous slip for slopes flatter than a certain degree with a shallow foundation.

Another difference highlighted in this chart is that the failure is a shallow toe circle for the slopes when $\beta > 58°$, which is slightly different than the angles of $53°$ and $60°$ suggested by Taylor (1937) and Janbu (1954), respectively.

Steward et al. (2011) did not specify the values for the minimum stability number that can be obtained by a tangent deep mechanism and the stability number for a vertical cut; however, in Figure 2.5, these values appear to be around 5.40 and slightly less than 3.80, respectively.

2.4 Summary

This chapter mentioned the progressive development of slope stability methods with some remarkable studies; as a starting point, the initial research used planar rupture surfaces,

progressed to circular failure assumptions, and finally arrived at modern techniques like finite element methods that do not require a prior assumption about the form or position of the failure slip.

Three popular stability charts suggested in the literature, namely Taylor (1937), Janbu (1954), and Steward et al. (2011), for estimating the factor of safety of undrained slopes were examined in detail, and the followings could be concluded:

- While Taylor and Janbu's charts are based on the strict assumptions of circular failure surfaces, Steward et al.'s chart is derived by using the Morgenstern and Price Method (1965) and involves composite circular failure mechanisms composed of two arcs separated by a straight line on the rigid stratum
- Janbu's chart solutions are the most comprehensive ones available for estimating the factor of safety for additional boundary conditions such as a surcharge, reservoir loading, and tension cracks.
- Taylor, Janbu, and Steward et al. specify the slope angle at which the factor of safety becomes independent of the depth factor D as $53°$, $60°$ and $58°$, respectively. In spite of the proposed angle of $60°$ by Janbu (1954), the stability curves for a variety of D values meet around $53°$, consistent with Taylor's chart; however, the special geometrical case of $D = 1$ is stated to fail as a slope circle for slopes flatter than $60°$
- Fellenius (1927) mention that there is a minimum stability number that can be obtained by a mid-point circle which has infinite radius and proposes this value as 5.52. Taylor (1937) and Janbu (1954) closely agreed on the proposed value. Despite that this stability number is not specified by Steward et al. (2011), the number appears to be approximately 5.40 in their stability chart.

CHAPTER 3

MODELING TECHNIQUE

3.1 Overview

This chapter discusses the numerical methods utilized in this thesis's parametric research. Thousands of simulations were conducted to meet the aim of this thesis employing two primary approaches, namely an elastic-plastic finite element with strength reduction technique (EPFE) and the finite element limit analysis (FELA). slope64 software was used for the EPFE analyses in the study, whereas OxLim software performed the FELA analyses.

Both methods rely on the finite element technique. The following are the key benefits of finite element methods for slope stability analysis over conventional limit equilibrium methods that use the method of slices:

- It is not necessary to make any prediction about the shape or position of the failure mechanism prior to any analysis. "Failure mechanism" naturally takes place through the path of least resistance.
- Assumptions regarding side forces are not necessary. Global equilibrium is maintained until "failure" is observed.

The following subsections describe the overarching principles of slope64 and OxLim programs, briefly explaining their approach and assumptions, which are mostly centered on simulating a homogeneous undrained slope in this thesis.

This chapter demonstrates the implementation of slope64 and OxLim programs on a representative slope stability problem relevant to the parametric studies addressed in Chapter 4.

For this reason, the factor of safety of the homogeneous clay slope shown in Figure 3.1 will be sought out by using both programs. The slope has the following soil parameters:

$$s_u = 40 \text{ kPa}; \quad \gamma_{sat} = 20 \text{ kN/m}^3$$

and the following geometrical parameters:

$$H = 10 \text{ m}; \quad D = 2.0; \quad \beta = 20°; \quad H_w = 4 \text{ m}$$

where D is the depth factor illustrated in Figure 1.1.

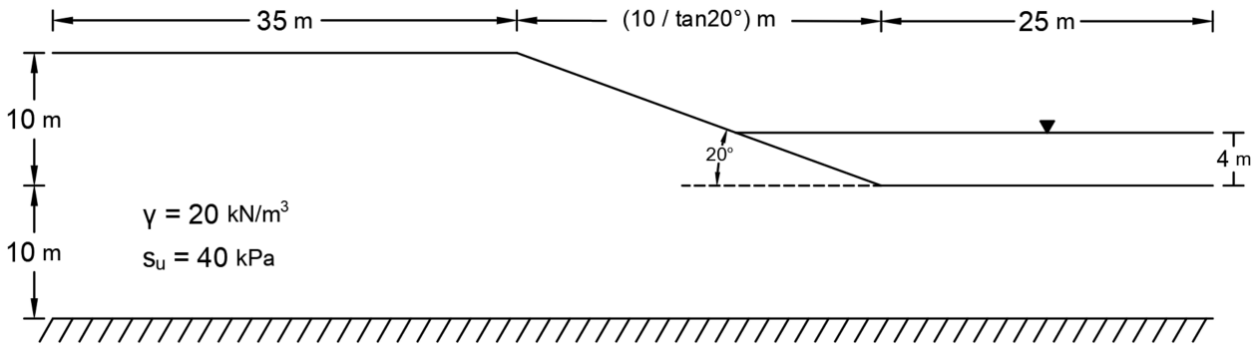

Figure 3.1 A representative slope stability problem discussed throughout Chapter 3

3.2 slope64

slope64 is a finite element slope stability program for 2D plane strain analyses of elastic-perfectly plastic soils with a Mohr-Coulomb criterion utilizing the strength reduction method. The program discretizes the soil into 8-noded quadrilateral elements with reduced integration, each comprising four Gauss points.

slope64 is based on Program 6.4 in the textbook, "Programming the Finite Element Method" by I.M. Smith, D.V. Griffiths and L. Margetts, 5th ed., 2014. The primary distinction of

slope64 is the ability of automated search of the strength reduction factor and the inclusion of water pressures.

3.2.1 General Philosophy of slope64

3.2.1.1 Soil Model and Fixed Parameters in the Analysis

The soil model the program uses is an elastic-perfectly plastic model (Figure 3.2) that comprises six soil parameters: friction angle ϕ', cohesion c', dilation angle ψ, Young's modulus E, Poisson's ratio v, and total unit weight γ.

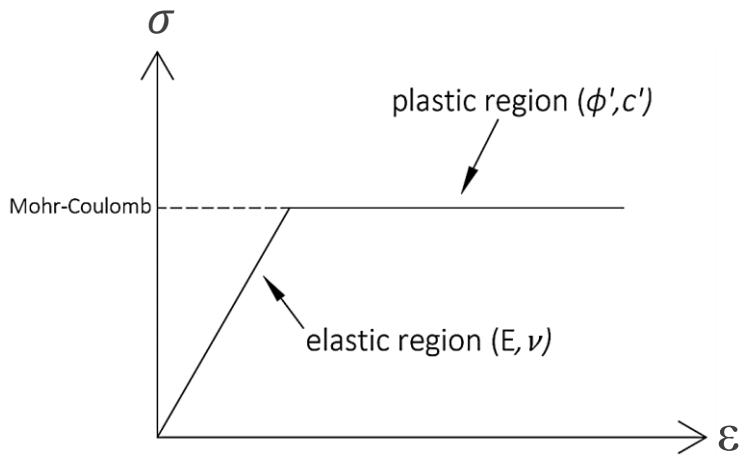

Figure 3.2 Elastic-perfectly plastic soil model where σ and ε are stress and strains, respectively

During plastic yielding, the dilation angle regulates the rate of plastic volumetric strains; nevertheless, taking into consideration that slope stability problems are relatively unconfined, Griffiths and Lane (1999) suggest setting the value of dilation to zero for any soil type even if the soil in the model is a frictional soil formation.

Elastic soil parameters, Young's modulus (E) and Poisson's ratio (v), have a significant impact on the displacements of the nodes; however, their effect on the computed value of the

factor of safety is negligibly small. Therefore, nominal values of $E = 1$ x 10^5 kN/m^2 and $\nu = 0.3$ are chosen for the analysis in accordance with Smith and Griffiths's recommendation (2014).

In summary, the main significant soil parameters in a slope stability problem based on finite element method are the same as in a traditional approach: total unit weight γ, shear strength parameters c' and ϕ', the slope's geometry and groundwater conditions.

3.2.1.2 Mohr-Coulomb and Tresca Failure Criteria

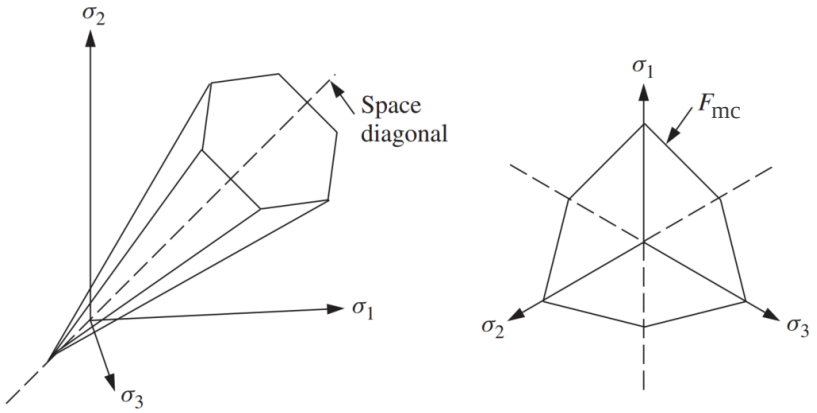

Figure 3.3 Mohr-Coulomb failure criterion in principal stress space (Smith and Griffiths, 2014)

Figure 3.3 depicts the Mohr-Coulomb criterion as an irregular hexagonal cone in principal stress space. The irregularity is caused by the omission of σ_2. Noting that assuming compression negative, the invariant form of this criterion derived from the geometry of Mohr's circle (Figure 3.4) can be stated in terms of principal stresses as follows:

$$F_{mc} = \frac{\sigma_1 + \sigma_3}{2}\sin\phi' - \frac{\sigma_1 - \sigma_3}{2} - c'\cos\phi' \tag{3.1}$$

This failure function F_{mc} can be interpreted as represented in Table 3.1.

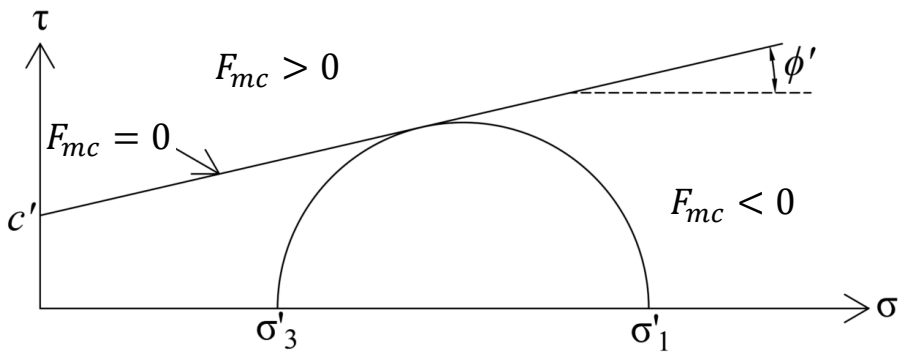

Figure 3.4 Shear stress vs. principal stress diagram for Mohr-Coulomb failure criterion

Table 3.1 Interpretation of the failure function, F_{mc}

Expression	***Meaning***
$F_{mc} < 0$	Below Mohr-Coulomb Failure Envelope (elastic)
$F_{mc} = 0$	On Mohr-Coulomb Failure Envelope (yielding)
$F_{mc} > 0$	Above Mohr-Coulomb Failure Envelope (yielding and must be redistributed)

To determine the undrained shear strength of clay samples, unconsolidated undrained (UU) triaxial tests are performed. During the test process, a confining pressure σ_3 is applied to a cylindrical soil sample with a cross-sectional area of A. Then, the sample is subjected to axial loading P until failure occurs where the maximum principal stress σ_1 can be calculated as $\sigma_1 = \sigma_3 + P/A$.

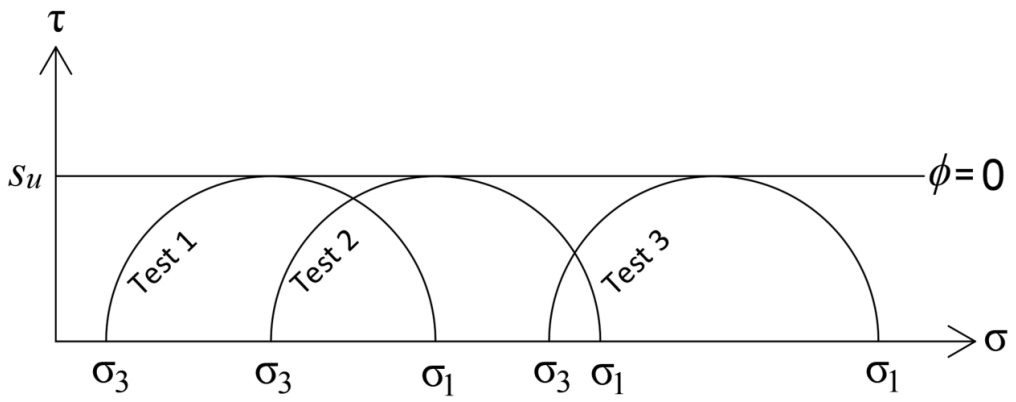

Figure 3.5 UU triaxial test results by Mohr's circles

When an unconsolidated undrained (UU) triaxial test is conducted, the soil does not gain strength during this phase because no consolidation occurred, and the void ratio stays constant. Thus, the undrained shear strength is not dependent on the confining pressure. After a series of tests at a variety of confining pressure, Mohr's circles of the results can be drawn as shown in Figure 3.5, and the undrained shear strength of the soil can be calculated by the following equation:

$$s_u = \frac{\sigma_1 - \sigma_3}{2} \tag{3.2}$$

As seen in both Equation 3.2 and Figure 3.5, the Mohr's circle expressions of UU triaxial test results match the maximum shear stress theory (Tresca yield criterion). Tresca criterion is a particular case of Mohr-Coulomb failure theory when $\phi_u = 0$, where the maximum shear stress is the difference between the maximum and minimum principal stresses divided by two, and yielding (failure) occurs when the maximum shear stress equals the yielding shear strength. Tresca yield criterion can be utilized for the saturated soils under undrained loading since the shear strength is independent of confining pressure.

When a model is first created, the soil is considered elastic, resulting in normal and shear stresses to be generated at all the Gauss points in the mesh. Once these stresses have been developed, they are then compared to the Mohr-Coulomb failure criterion. The location stays elastic as long as the stresses at any Gauss point are below the Mohr-Coulomb failure envelope ($F_{mc} < 0$). Yet, if they are on or above the failure envelope ($F_{mc} \geq 0$), the region is deemed to be yielding. Through the visco-plastic algorithm, yielding stresses are redistributed throughout the finite element mesh (Perzyna, 1966; Zienkiewicz and Cormeau, 1974).

3.2.1.3 Modeling Reservoir Loading on Slope

To simulate the external loading caused by the reservoir, normal stress is applied directly to the face of the slope at a rate equivalent to the water pressure at a certain depth (Griffiths and Lane, 1999). Naturally, the generated stress rises linearly with the water depth and stays constant throughout the horizontal foundation level. Then, the equivalent nodal loads due to the applied stress are calculated at each corresponding node and added to the gravity loads.

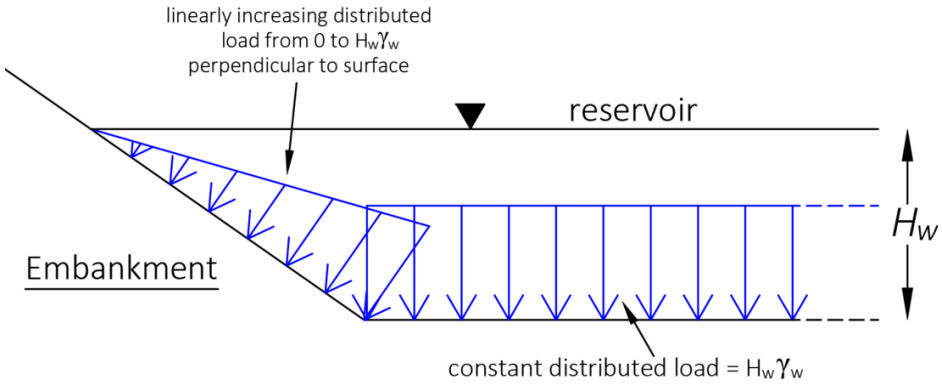

Figure 3.6 Detail of the stresses induced on the mesh surface due to free-standing reservoir loading

3.2.1.4 Initial Stress State and the Iterative Algorithm

Gravity loads calculated by Equation 3.3 are placed on each node of the FE mesh. Integrating the equation over each mesh element returns the gravity load, where [N] corresponds to the shape function and subscript "*e*" refers to the element number.

$$p^{(e)} = \gamma \int_{V^e} [\mathrm{N}]^T d(vol) \tag{3.3}$$

The volume of each element is determined by the integral which is then multiplied by the total unit weight of the soil to yield the net vertical gravity force of that mesh element. The calculated gravity force is utilized to produce the initial stress state of the problem by distributing it to every node, building a global gravity load vector once, and then assigning it to each node.

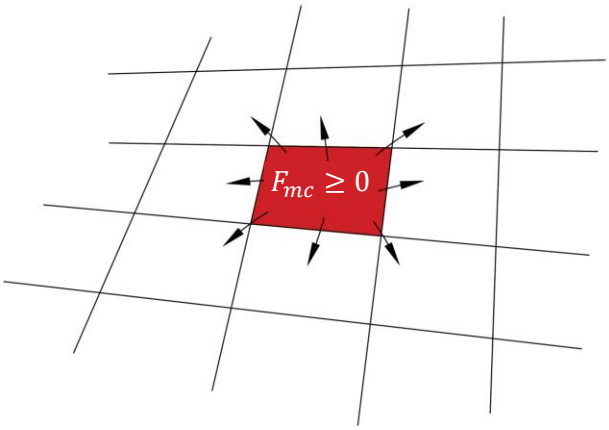

Figure 3.7 Stress redistribution to the neighbor elements

Calculations of shear and normal stresses are performed at all the Gauss points. Following that, the stresses are compared to the failure criterion (Table 3.1). The visco-plastic algorithm (Perzyna, 1966; Zienkiewicz & Cormeau, 1974) redistributes yielding stresses throughout the mesh (Figure 3.7), and convergence occurs when all stresses within the mesh

fulfill both the failure criterion and global equilibrium within a user-defined iteration ceiling and convergence tolerance.

3.2.1.5 Definition of Failure

Should the method run out of iterations within the user-defined ceiling value before converging, it means that the failure criterion and global equilibrium cannot be satisfied by a stress redistribution. If the algorithm cannot satisfy these criteria, "failure" is said to have occurred. In this case, both slope failure and numerical non-convergence take place at the same time, and this is accompanied by a steep rise in the nodal displacements within the FE mesh.

In other words, "failure" is defined for slope64 analyses in this study as the algorithm's inability to reach convergence within 1000 iterations combined with a steep increase in nodal displacements.

3.2.1.6 Strength Reduction Factor and Determination of Factor of Safety

While the gravity loads at each node are kept constant, a strength reduction factor (Zienkiewicz et al., 1975; Griffiths, 1980; Smith and Griffiths, 1988; Matsui and San, 1992; Griffiths and Lane, 1999) gradually weakens the shear strength parameters employed in the finite element mesh model of the soil, following equations below:

$$c'_{factored} = \frac{c'}{SRF} \tag{3.4}$$

$$\phi'_{factored} = \tan^{-1}\left(\frac{\tan\phi'}{SRF}\right) \tag{3.5}$$

An increasing trial value of the SRF is attempted until the algorithm fails to converge within the user-specified maximum number of iterations. The program begins by assigning the trial SRF value to 0.5 as a starting guess; then it chooses the next guess by increasing the previously converged guess by 0.5 until the non-convergence happens. When the non-convergence exists, a new trial value is computed by the Bisection Method taking into account the highest convergent and lowest non-convergent solutions. The program stops once the difference between these two boundary values is less than the user-specified FS tolerance value.

After multiple trials of increasing SRF values, the minimum value of SRF that leads to a non-convergence and therefore triggers the failure is referred to as the factor of safety of the soil slope.

$$FS \approx SRF_{failure}$$

Griffiths and Lane provide a more extensive description of the methodology (1999).

3.2.2 Modeling of the Example Problem by slope64

The example problem presented in Section 3.1 is modeled using by slope64 and a brief description of the modeling process is provided below.

slope64 program is provided for users with an executable file for Microsoft Windows operating system (slope64.exe). The program runs on the Command Prompt and requires a properly laid out data file (e.g., representative.dat). The summary of each iteration is displayed on the screen if the program is running well. If everything goes well, the following result files (presented in Table 3.2) will be created in the current working directory.

Table 3.2 Explanation of the output files generated by slope64

Output File	*Description*
representative.res	output file presenting the analysis results
representative.msh	PostScript file displaying the analyzed finite element mesh
representative.vec	PostScript file displaying nodal displacement vectors, which are magnified by a user-selected factor, corresponding to slope failure
representative..dis	PostScript file displaying the deformed mesh corresponding to slope failure (magnifying the nodal displacements by a user-selected factor)

3.2.2.1 Modeling Process in slope64

Figure 3.8 depicts the coordinate system and geometrical parameters of the FE mesh that will be generated by slope64. Parameters nx1, ny1, nx2, and ny2 indicate the number of mesh elements in the embankment and foundation in x and y directions.

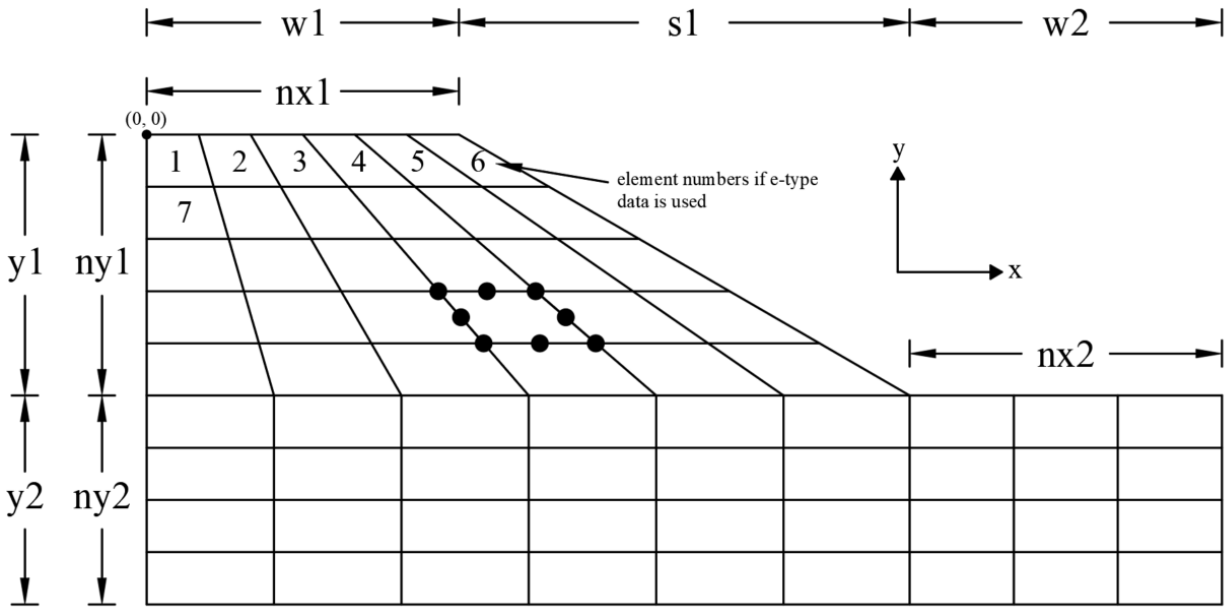

Figure 3.8 Dimensions of the slope model and finite element mesh layout

The data file of the representative problem for slope64 is demonstrated in Figure 3.9. A standard data file consists of the geometrical parameters, material properties, free surface coordinates (for a free surface and/or reservoir level if there exist), iteration ceiling, factor of safety tolerance value, and a magnification factor for the PostScript *.dis and *.vec files. The definition of each parameter is contained within the data file for the benefit of the user.

The representative slope stability problem (Figure 3.1) with a homogenous soil formation requires no e-type data since each mesh element has the same material properties. However, in the situation of requesting that different material properties be assigned to the mesh (e.g., a multi-layered soil), the element numbering process is carried out row by row, beginning at the mesh's upper left corner as shown in Figure 3.8.

A dense mesh can be created by setting the number of elements in both the x and y directions to high values; furthermore, by running the program with a low FS tolerance value (e.g., 0.01) and a high iteration ceiling (e.g., 1000), a rigorous estimation of the factor of Safety can be obtained by Slope64.

```
'-------slope64---------'
'Width of top of embankment (w1)'
35.0
'Width of sloping portion of embankment (s1)'
27.475
'Distance foundation extends to right of embankment toe (w2)'
25.0
'Height of embankment (h1)'
10.0
```

Figure 3.9 Data file for the analysis of the representative problem by slope64

'Thickness of foundation layer (h2)'

10.0

'Number of x-elements in embankment (nx1)'

70

'Number of x-elements to right of embankment toe (nx2)'

28

'Number of y-elements in embankment (ny1)'

20

'Number of y-elements in foundation (ny2)'

20

'Number of different property groups (np_types)'

1

'Material properties (phi,c,psi,gamma,e,v) for each group'

0.0 40.0 0.0 20.0 1.e5 0.3

'Property group assigned to each element (etype, data not needed if np_types=1)'

'Pseudo-static analysis: Horizontal acceleration factor (k_h)'

0.0

'Number of free surface points and their coordinates (nosurf, surf(2,nosurf))'

2

51.4849 -6.0000

87.4750 -6.0000

'Unit weight of water (gam_w)'

9.81

'Iteration ceiling (limit)'

1000

'Factor of Safety accuracy tolerance (fos_tol)'

0.01

'Magnification factor (ratmax) see p.625 of 5th ed for definition'

0.1

Figure 3.9 Continued

3.2.2.2 slope64 Post Processing

As previously stated, once slope64 has executed, it outputs four result files into the current working directory, which are listed in Table 3.2.

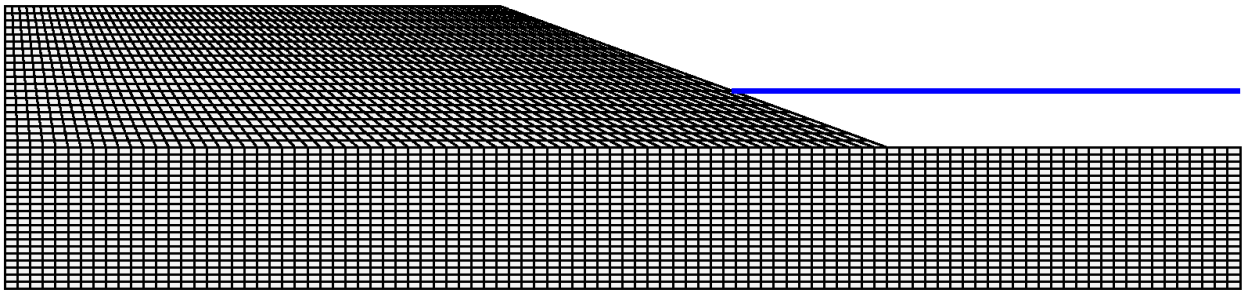

Figure 3.10 Undeformed mesh of the example problem, a homogeneous slope with a foundation layer and reservoir loading

The PostScript *.msh file in Figure 3.10 depicts the undeformed FE mesh generated by the corresponding data file. The blue line in the figure represents the reservoir water level ($H_w = 4\ m$) in the problem.

Figure 3.11 displays the generated *.dis file representing the deformed mesh at failure. This deformed mesh aids in the visualization of the failure mechanism. The failure mechanism in this case appears as essentially circular and tangent to the rigid base stratum.

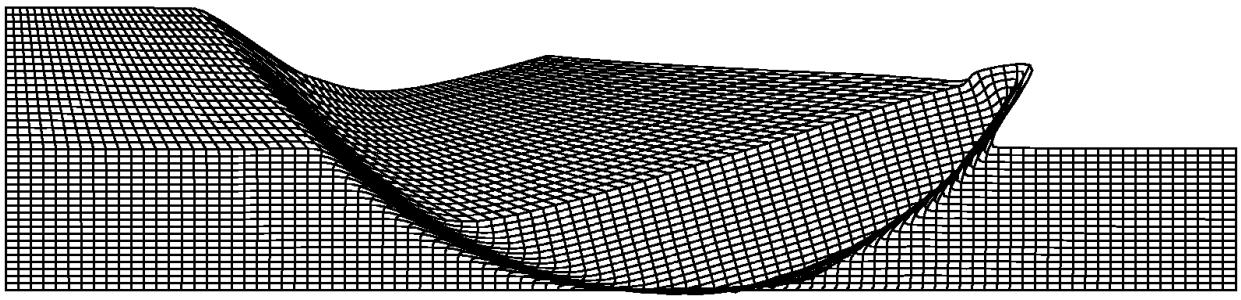

Figure 3.11 Deformed mesh of the example problem at failure

Another PostScript file with *.vec extension, which outputs the nodal displacement vectors at failure for each mesh element, is omitted from the thesis due to the lack of clarity in the visualization of a very dense mesh.

trial factor	max displ	iterations
0.5000	0.3241E-01	5
1.0000	0.4562E-01	52
1.2500	0.5414E-01	113
1.3750	0.5947E-01	162
1.4375	0.6284E-01	209
1.4453	0.6364E-01	254
1.4531	0.6920E-01	1000

Estimated Factor of Safety = 1.4531

Figure 3.12 The generated *.res file showing the results with the SRF trials and the FS estimation for the representative problem discussed in Chapter 3

The last output file is the *.res file, a result file, that presents the SRF trials with corresponding maximum nodal displacement and the number of iterations to converge, as illustrated in Figure 3.12. This file also gives the estimated factor of safety, which is the SRF value regarding the last non-converged SRF trial.

According to the *.res output file (Figure 3.12) of the representative problem (Figure 3.1), the user-specified iteration ceiling of 1000 was reached at $\mathrm{SRF} = 1.4531$. At this point, the Bisection Method stops since the convergence tolerance between successive SRF-values (0.01) has been met, and the lowest non-converged SRF value is assigned to FS.

A plot of each SRF trial with its corresponding maximum nodal displacement in Figure 3.13 demonstrates the jump in the maximum displacement when SRF ≈ FS, indicating that failure has taken place.

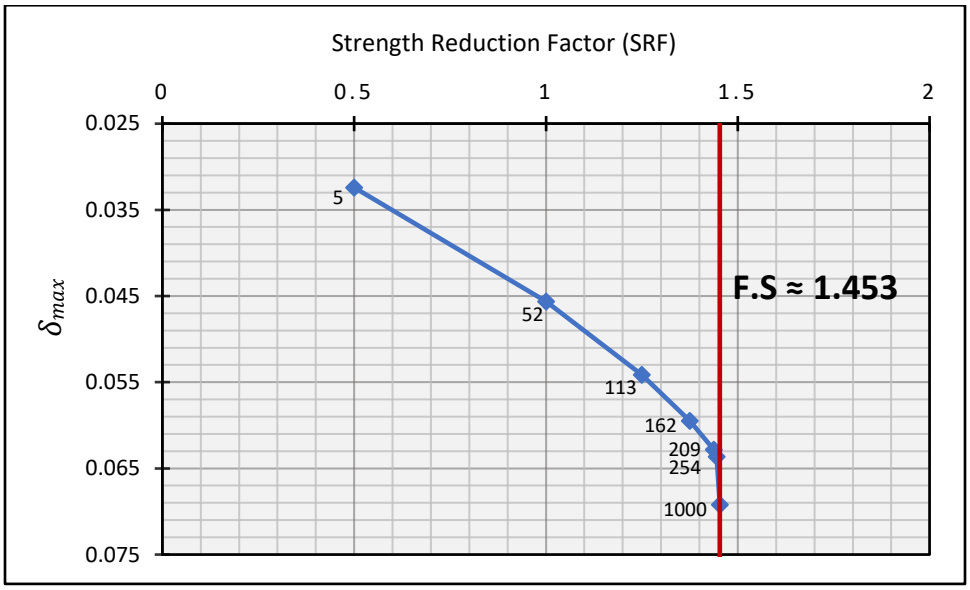

Figure 3.13 Maximum nodal displacement vs. SRF trials with number of iterations needed to converge for the problem addressed

Nodal displacements are beyond the scope of this thesis which is focused on failure and estimation of the factor of safety. However, the displacement values obtained by the analysis prior to failure are mainly dependent on the selected elastic parameters. If realistic deformations prior to failure are required, then suitable elastic parameters obtained from lab or field data would need to be input.

3.2.3 Python Scripts for Batch Run

Conducting a parametric study with thousands of simulations utilizing slope64 is undoubtedly a challenging task that demands data management and the automation of the modeling process. Therefore, the required slope64 analyses for the parametric studies discussed

in Chapter 4 were carried out by employing two Python scripts; one is required for the modeling process, the other is needed to manage the post-processing. The first Python script's algorithm is primarily composed of the following tasks:

- prompt user to enter the soil and geometrical parameters
- prompt user to determine the finite mesh density and FS tolerance value
- create subfolders in the program's running path for each H and H_w/H
- create a data file for each slope stability problem in the parametric study
- write parameters to a spreadsheet
- write a summary file
- write a Windows Batch File to run all cases in sequence
- split the batch file by the desired number of sub-batch files to conduct a simultaneous run

whereas the other Python script for the post-processing is based on the procedures as follows:

- read the summary file
- read FS estimates from each *.res file
- write FS estimates to the spreadsheet
- delete *.vec files to free up disk space

3.3 OxLim

OxLim, developed by Chris M. Martin at the University of Oxford since 2009, is a finite element limit analysis program combining Makrodimopoulos & Martin's (2006, 2007, 2008) lower-bound and upper-bound approaches together with an adaptive mesh refinement technique.

It has already been actively utilized to analyze plane strain problems (Martin, 2011; Martin and White, 2012; Mana et al., 2013; Dunne et al., 2015) as well as 3D problems (e.g., Martin et al., 2015; Dunne and Martin, 2017; Dunne et al., 2017).

While slope64 weakens the strength parameters until failure, OxLim multiplies the loads in the system by a load factor (LF) to set up the lower and upper bound solutions. The program identifies two constrained optimization problems that, when combined, allow for precise bracketing of the exact collapse load factor.

3.3.1 General Philosophy of OxLim

3.3.1.1 Limit Analysis

Limit analysis theory is derived by the upper and lower bound theorems of plasticity, developed by Drucker et al. (1951, 1952), and assumes a rigid-perfectly plastic material with an associated flow rule.

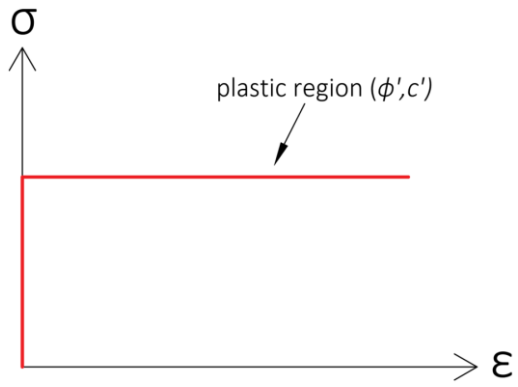

Figure 3.14 A rigid-perfectly plastic material model

The true solution lies in a range identified and bracketed by using these two independent bounding theorems. It should be noted that an iterative approach can minimize this interval, selecting possible lower and upper bound solutions that are closer to each other.

3.3.1.1.1 Lower Bound Theorem

The lower bound theorem refers to a statically admissible stress field that satisfies the equilibrium and balances the applied load without violating the failure criteria anywhere in the soil mass. This stress field always gives a lower bound solution in the prediction of failure load. Hence, the lower bound theorem leads to:

$$FL_{LB} \leq FL_{True}$$

where FL_{LB} is the predicted failure load obtained from a lower bound solution, and FL_{True} is the true failure load.

Despite the fact that the exact failure load is unique, the optimum stress field does not have to be. It is conceivable that the same lower bounds could be provided by a variety of stress fields (Sloan, 2013).

3.3.1.1.2 Upper Bound Theorem

The upper bound solution calculates the predicted failure load by equating the dissipated internal work by plastic deformation to the rate of the work done by the external loads in a kinematically admissible velocity field (a failure mechanism) that satisfies the velocity boundary conditions and the associated flow rule. Hence, the upper bound theorem leads to:

$$FL_{UB} \geq FL_{True}$$

where FL_{UB} represents the predicted failure load from an upper bound solution.

It should be noted that the failure mechanism from the solution is not unique, and it is crucial to seek out the mechanism delivering the lowest upper bound value (Sloan, 2013).

In conclusion, when lower bound and upper bound theorems are performed for the same problem, the true failure load can be bracketed as follows:

$$FL_{LB} \leq FL_{True} \leq FL_{UB}$$

3.3.1.2 Finite Element Limit Analysis

Finite element limit analysis (FELA) employs finite element discretization to numerically apply the UB and LB theorems by implementing the stress and velocity fields. Although the LB and UB solutions are independent as stated before, it is sensible to use the same finite element discretization to formulate these approaches.

After discretizing the slope into finite elements, the LB and UB theorems are performed inside and between the adjacent elements. The variables and constraints imposed by the limit theorems are structured and solved in a way that produces the optimum LB (highest) and UB (lowest) load factors by a numerical optimization technique.

3.3.1.2.1 Lower Bound FELA

With the implementation of LB FELA, a piecewise continuous stress field is introduced into the adjacent FE mesh elements separated by statically admissible discontinuities. By this method, having additional degrees of freedom, better results are obtained compared to those generated by a fully continuous stress field (Makrodimopoulos and Martin, 2006). In early studies, quadratic stress elements for the LB limit analyses were employed by Belytschko and Hodge (1970); nevertheless, their approach required complex processes for verifying the yield criterion over each element.

Three-node triangle elements have been found to be useful for plane stress limit analyses and used widely in the following studies by Lysmer (1970), Pastor (1978), Sloan (1988), and

Makrodimopoulos and Martin (2006). This type of element possesses the advantage of securing to satisfy the yield criterion everywhere the element if it is enforced at the nodes placed at the vertices because the stress components vary linearly.

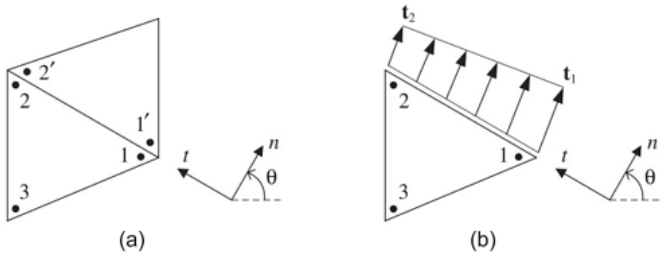

Figure 3.15 Three-node triangle mesh element illustrating interior edges (a) and exterior edges on a traction boundary (Makrodimopoulos and Martin, 2006)

Each element, internal edges between neighboring elements (Figure 3.15(a)), and outside edges (Figure 3.15(b)) must be in equilibrium in order to enforce a strict LB solution.

3.3.1.2.2 Upper Bound FELA

Numerous authors (e.g., Bottero et al., 1980; Abdi et al., 1994; Sloan and Kleeman, 1995; Pastor et al., 2000) have employed constant strain elements (three-node triangles) with discontinuities in the stress field to meet the associated flow rule when applying UB FELA, and it is considered to be a comprehensive solution for both drained and undrained clays.

However, according to Makrodimopoulos and Martin (2007), six-node triangles, first proposed by Yu et al. (1994) for purely cohesive materials, can be used for plane strain UB solutions instead of constant strain elements. This six-node triangle element is termed a "simplex strain element" and is demonstrated in Figure 3.16.

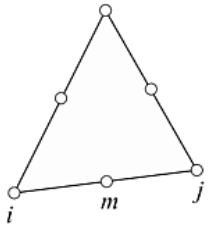

$$\mathbf{x}_m = \frac{1}{2}(\mathbf{x}_i + \mathbf{x}_j)$$

Figure 3.16 Six-node displacement element with straight sides for upper bound analysis

Makrodimopoulos and Martin (2007) revealed that this type of finite element outperforms constant strain elements with discontinuities while requiring a similar amount of computational time for a given problem. Their study performed on various numerical plane strain problems highlighted that the results from six-node triangular elements give smaller errors especially for unstructured meshes and/or materials with high friction angles.

3.3.1.3 Optimization Problem Solving by MOSEK

The present version of OxLim relies on MOSEK to solve optimization problems. MOSEK is a commercially available software package capable of efficient solution of large-scale optimization problems. Both optimization schemes arising from the LB and UB formulations are set up as second-order cone programming (SOCP) problems. Then a special algorithm introduced in Andersen et al (2003) and implemented in MOSEK (2014) can perform the SOCP analysis.

3.3.1.4 Mesh Generation by Triangle

OxLim uses another software called ‘Triangle’, developed by Shewckuk (2002), to perform unstructured triangular mesh generation using a Delaunay refinement algorithm for plane strain analysis. By utilizing unstructured meshes, elements can be concentrated in locations where they are needed most.

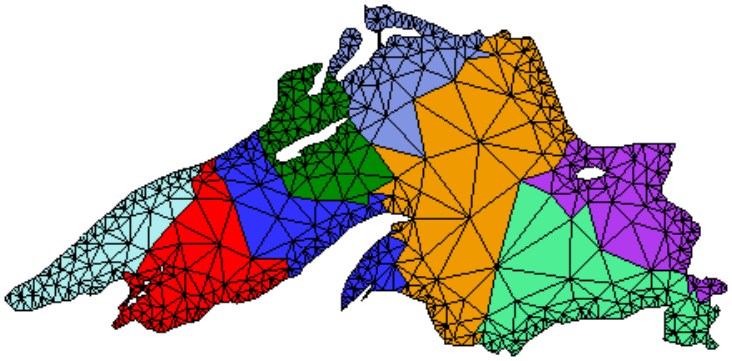

Figure 3.17 Triangular mesh generation of Lake Superior by Triangle software

Triangle software is launched at the beginning of the analysis to generate the initial coarse mesh and called again during each adaptive mesh refinement iteration to refine the FE mesh in the highly plastic regions in accordance with the target element number imposed by OxLim.

3.3.1.5 Adaptive Mesh Refinement and Determination of Factor of Safety

In order to provide an accurate collapse load estimate, the FELA algorithm seeks to minimize the gap between the upper and lower bound solutions. For the finite element limit analyses, this gap is highly dependent on how the mesh is discretized; therefore, a method of developing adaptively refined mesh becomes essential for accuracy.

Using an adaptive mesh refinement technique based on the spatial variation of the maximum shear strain rate in the FELA UB velocity field, OxLim refines the soil mesh around the plastically yielding regions. After a few cycles of adaptive mesh refinement, the finite element mesh itself begins to reflect the shape and the location of the failure mechanism.

The LB and UB theorems are solved on the same mesh after each mesh refinement, and the best estimate of the collapse load factor is output as the average of the LB and UB solutions,

$$LF_{estimated} = \frac{LB + UB}{2} \tag{3.6}$$

The precision of the solution is represented by the bracketing error of the estimated collapse load, calculating as

$$Error\ \% = \frac{UB - LB}{UB + LB} \times\ 100 \tag{3.7}$$

In OxLim's version used in this thesis, the user is required to specify the desired accuracy (maximum bracketing error) and/or the maximum number of mesh refinement. As soon as the estimated error value becomes equal to the user-defined maximum error or falls below that value, the mesh refinement cycle is terminated, and the results are displayed. Otherwise, the algorithm will continue to refine the mesh until the predefined number of mesh refinements is achieved.

This version of OxLim does not require the user to input the value of the target number of elements for a refined mesh; instead, the program automatically computes this number and refines the mesh accordingly.

3.3.2 Modeling of the Example Problem by OxLim

Finite element limit analysis of the representative slope stability problem (Figure 3.1) was performed by OxLim modeling.

OxLim is performed on a driver MATLAB script that consists of one main function and several other functions called by the main one. The MATLAB script's algorithm sequences the running of OxLim and Triangle program's executable files and the dynamic-link library (DLL)

file of MOSEK optimization software. In addition, the script checks whether the bracketing error is less than or equal to the target error and whether the program has reached the user-defined maximum number of mesh refinements. Furthermore, after each mesh refinement, it progressively prints the results, depicts the refined mesh, and plots the $LF_{estimated}$ values with associated LB and UB estimations.

Each OxLim round produces several output files that are interactively employed by OxLim, MOSEK, and Triangle.

3.3.2.1 Modeling Process in OxLim

A correctly laid out text file with extension *.dat for data entry is required to achieve a successful OxLim run. A correct data file for a slope stability analysis, shown in Figure 3.18, is comprised of 5 parts, namely, vertices, segments, regions, segment tags, and region tags.

```
*PLANE_STRAIN
*VERTEX
1      0.0          0.0
2   -35.0           0.0
3   -35.0         -20.0
4    52.475       -20.0
5    52.475       -10.0
6    27.475       -10.0
7   16.4849        -6.0
```

Figure 3.18 Data file for the analysis of the representative problem by OxLim

```
*SEGMENT
1 1 2 1
2 2 3 2
3 3 4 3
4 4 5 2
5 5 6 4
6 6 7 4
7 7 1 1
*REGION
1   -17.5   -10.0   1
*SEGMENT_TAG
1
 restraint = none   # free surface
2
 restraint = symmetry
3
 restraint = fixed
4
 p_live      =  -58.86
 dpdy_live =    -9.81
*REGION_TAG
1
 tresca_c   =     40.0
 by_live    =    -20.0
```

Figure 3.18 Continued

The model of the representative problem given in Figure 3.1 is illustrated in Figure 3.19 according to the data file. The model with the important parts of the data file will be discussed throughout this section.

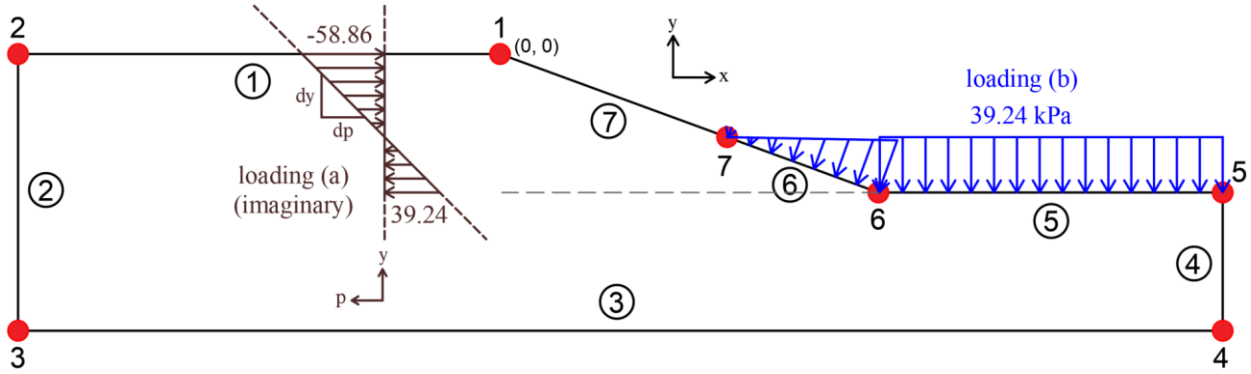

Figure 3.19 Illustration of the model according to the data file created for OxLim

Triangle software needs input data for vertices, segments, and regions to generate the initial mesh. Each vertex entry with its assigned label and (x, y) coordinates indicates the vertices to which the boundary segments will connect. In agreement with these vertex labels, each segment with a unique label is placed between two corresponding vertices. Then, segment tags are assigned to each segment so as to define the boundary conditions of the problem. To exemplify, a segment data entry should be as Figure 3.20 to generate a mesh properly, and it is directed to Triangle software by denoting regions in the data file. Regions should be designated in the way described in Figure 3.21, positioning an arbitrary interior point within an enclosed area. Since the focused slope problem in this chapter consists of a homogenous single soil formation, one region is defined for the whole enclosed area.

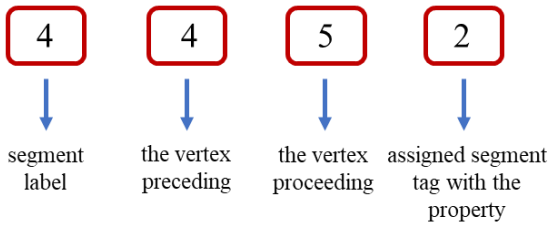

Figure 3.20 A sample segment data entry for Triangle

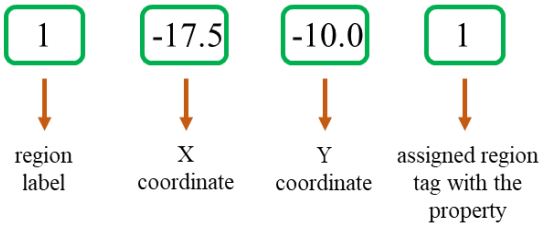

Figure 3.21 A sample region data entry for Triangle

Segment tags in the data file are associated with OxLim. In this section, restraint conditions, loading, and strength properties can be issued to be assigned to each segment. In this thesis, four types of segment tags are defined.

Segments representing open surfaces do not lead to any restraints, so "restraint = none" segment tag is used for the corresponding segments. "fixed" restraint is used to impose the behavior of rigid based stratum on the model and segment 3 is tagged with this behavior in all models in the thesis. The continuity of the stress field at the sides is provided by assigning "symmetry" restraint to the side segments (e.g., segments 2 and 4 in Figure 3.19). Finally, the fourth segment tag is associated with the modeling of reservoir loading.

In comparison to slope64, the reservoir loading should be modeled manually for OxLim in a way that the corresponding segments should be subjected to a distributed load due to the hydrostatic pressure. In order to introduce this hydrostatic pressure to the program, an imaginary linearly decreasing/increasing normal stress which infinitely lies along the y axis with its value at the crest and its stress gradient (dp/dy) should be defined as a segment tag. Then, this segment tag is assigned to the related segments to induce a loading.

For the given representative slope stability example in this chapter, this process can be illustrated by loading (a) and loading (b) in Figure 3.19. The reservoir level of 4 meters leads to

an external hydrostatic pressure illustrated by loading (b) in the figure, which is linearly increasing with depth on the slope surface and continues to be constant along the horizontal foundation level at the value of 39.24 kPa (9.81 kN/m^3 x 4 m). To subject the segments 5 and 6 to this loading, a linearly decreasing stress infinitely lying along the y axis, illustrated by loading (a), is defined with following attributes:

- Stress value at the crest (when $y = 0$) is -58.86 kPa
- Stress gradient (dp/dy) is -9.81 kPa, such that the stress value at the bottom of the reservoir will be 39.24 kPa

Then, when segments 5 and 6 are tagged by this distributed loading segment tag, loading (b) is introduced to OxLim properly. Note that this loading is applied as perpendicular to the segments. Besides, it may be noted that this defined loading (a) will only affect the tagged segments and will have no effect on the rest of the system.

The last part of the data file is about region tags and related to OxLim. The data lines beneath region tags determine the strength parameters and body forces of each region defined for Triangle. For the modeled slope problems in this thesis, one region tag is introduced with the Tresca cohesion (undrained shear strength s_u) and the total unit weight of the homogenous soil. The author of OxLim suggests, Martin (n.d.), that live body forces should be used instead of dead body forces for slope stability analyses.

3.3.2.2 OxLim Post Processing

OxLim, together with Triangle and MOSEK, produce numerous output files for the analysis of the initial mesh and each subsequent adaptively refined mesh. Accumulation of these

outputs can be challenging, particularly for batch runs where numerous files with large disk storage requirements may be needed. This issue will be further discussed in Section 3.3.3.

It should be noted that the precision and efficiency of the LB and UB FELA solutions are highly reliant on the finite element mesh. Coarse meshes result in a wider gap between the bounds. Very fine meshes, on the other hand, need a significant amount of processing time. Setting an extremely low target error and pushing the algorithm to repeat the mesh refinement many times will lead to the production of a very large number of mesh elements that may eventually exceed the computer's internal storage capacity. To avoid excessive file generation, care must be taken in the choice of the maximum number of mesh refinement cycles and the target error tolerance.

This requires the selection of optimum values for these two parameters. For the FELA analyses performed in this thesis, the target error is typically set to 0.3% and the maximum number of mesh refinement cycles is set to 7. On the basis of previous experience, it can be said that the target error will be reached mostly within five mesh refinements for the slope stability analyses under undrained loading.

mesh	elt	LB	UB	av	err%
1	679	1.439e+00 (k)	1.474e+00 (s)	1.456e+00	1.21
2	1409	1.447e+00 (k)	1.462e+00 (s)	1.455e+00	0.53
3	2933	1.450e+00 (k)	1.459e+00 (s)	1.454e+00	0.31
4	6034	1.451e+00 (k)	1.456e+00 (s)	1.453e+00	0.19

Figure 3.22 The generated result file summarizing each mesh refinement for the analysis of the example problem by OxLim

When FELA analysis for the chapter's example problem (Figure 3.1) is performed according to the modeling process in Section 3.3.2.1, the estimation's error dropped below the target error in the fourth analyzed mesh. The MATLAB driver script prints the summary of the analysis for each mesh generation on the display as shown in Figure 3.22, where:

- "elt" is the number of FE mesh elements
- "LB" is the LF obtained by an independent lower bound solution
- "UB" is the LF obtained by an independent upper bound solution
- "av" is the average LF value
- "err%" is the bracketing error according to Equation

The MATLAB script draws a graph that illustrates the progressive improvement on the estimated load factor after each mesh refinement. Convergence at the UB and LB FELA solutions can be observed in Figure 3.23. Frankly, it can be said that the first meshes' analyses for the investigated slope problem also perform very well.

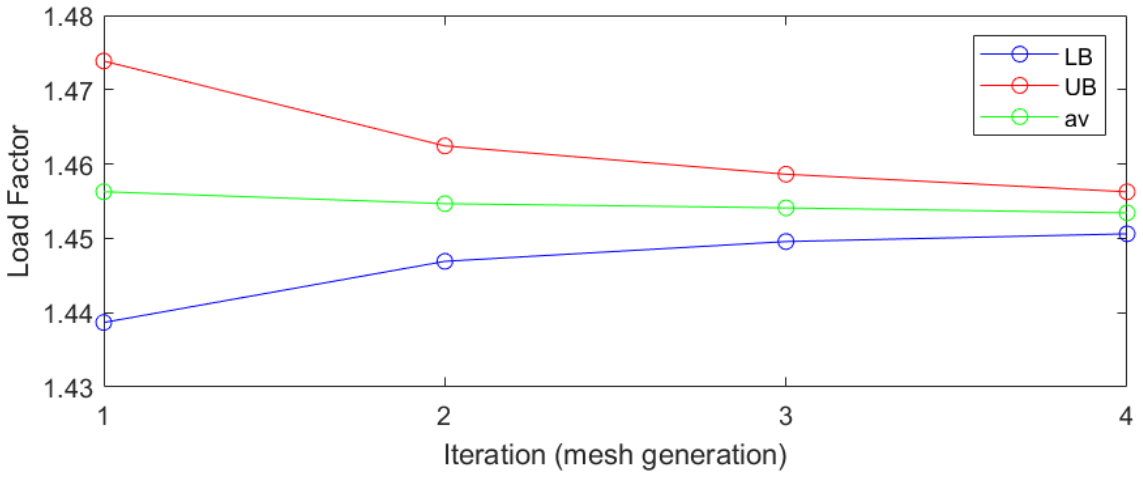

Figure 3.23 Bracketing the 'true' failure load with increasing accuracy by the adaptive mesh refinement

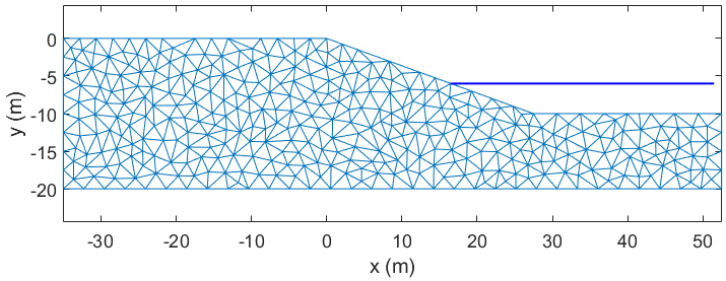

(a)

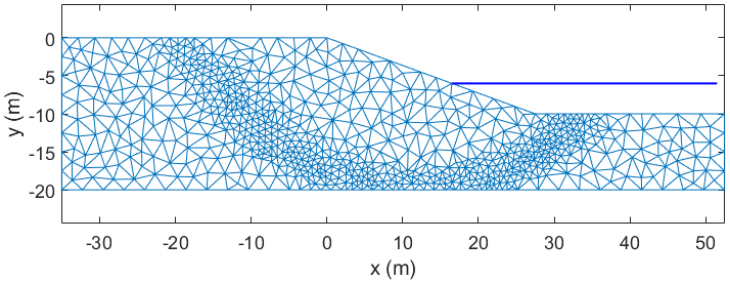

(b)

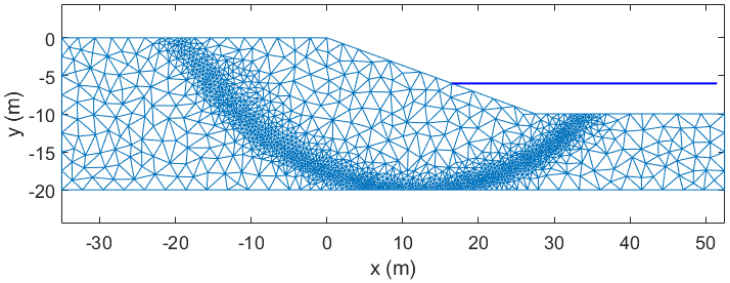

(c)

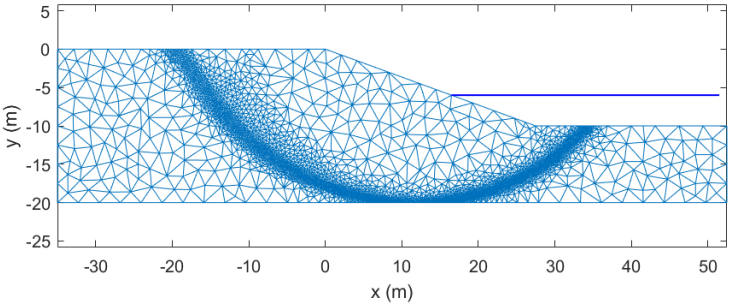

(d)

Figure 3.24 (a) initial mesh generation; (b), (c), and (d) the adaptive mesh refinement

According to Figure 3.22 and Figure 3.23, the true load factor lies between the LB estimation of 1.451 and the UB estimation of 1.456. Even though the true value may theoretically be equal to the bounding values, it will be rational to use the average of the bounds (1.453) as an estimate of the factor of safety. This estimation exactly matches the slope64's estimation in Section 3.2.2.2.

The driver script, moreover, prints and updates the generated mesh during the running process. As shown in Figure 3.24, the FE mesh is adaptively refined in the high plastic yielding zones and begins to display the failure mechanism itself.

OxLim outputs UB velocity field data in a *.vtu file that can be exported to the open-source program ParaView. ParaView visualizes this data and provides several graphics to assist in comprehending the failure. However, these *vtu files are large files, and they can consume a significant amount of disk space following a batch run of numerous data files, but they still provide the best visualization of the failure mechanism as shown in Figure 3.25.

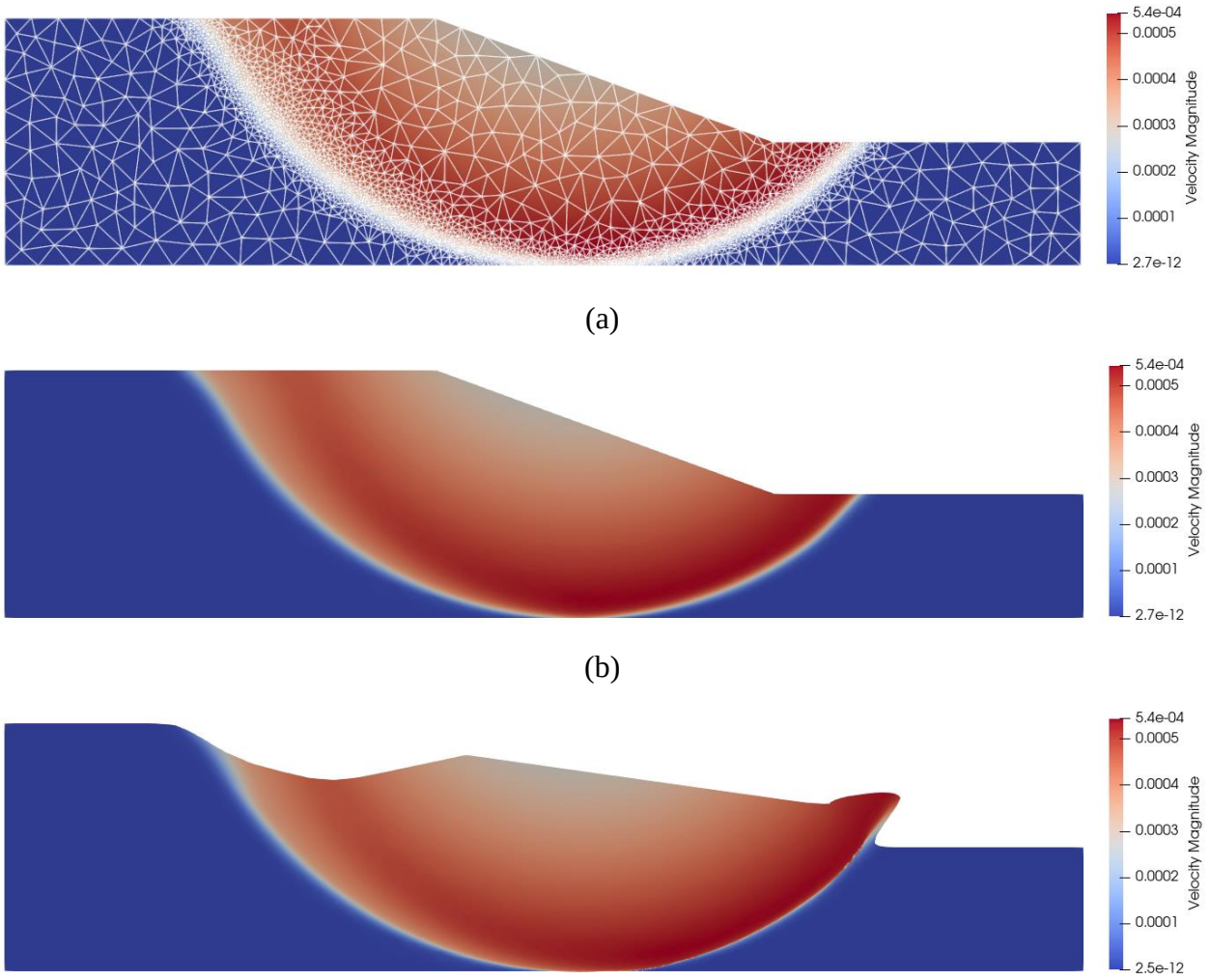

Figure 3.25 ParaView's outputs for velocity field data, with view options: (a) surface with edges; (b) surface view; (c) animated surface view

3.3.3 Python Scripts for Batch Run

As discussed in Section 3.2.3, doing a parametric analysis including thousands of simulations is challenging. Furthermore, a batch run with OxLim, in comparison to slope64, involves additional consideration due to its high output files in terms of both quantity and size. For example, a batch run of 1,000 cases would likely generate tens of thousands of output files,

consuming approximately 10 GB of disk space; and this would make sorting out the necessary files impossible. Therefore, two Python scripts similar to those described in Section 3.2.3 are employed to conduct the parametric studies in this thesis. Additionally, the driver MATLAB script of OxLim was slightly developed to make it batch-run-compatible.

The major tasks of the Python script regarding the modeling process are described in the following:

- prompt user to enter the soil and geometrical parameters
- prompt user to determine the target error and the maximum number of mesh refinement cycles
- create subfolders in the program's operating path for each H and H_w/H
- produce a data file for each slope stability problem in the parametric study and save it in a convenient path
- write parameters to a spreadsheet
- write a summary file
- create the modified version of OxLim's MATLAB driver script that run all data files sequentially, save the figure of final refined mesh, and save each analysis' result in a text file

whereas the other Python script is used for the post-processing work and is based on the following operations:

- read the summary file
- read FS estimates from each result file and detect the number of mesh refinement taken place

- write FS estimates to the spreadsheet
- delete all output files, or delete all but the result files, final refined mesh files, and *.vtu files belonging to the final mesh refinement

3.4 Summary

This chapter has explained the essential components of the two main programs with distinct algorithms used in this study, namely the elastic-perfectly plastic finite element method with strength reduction technique (slope64) and the finite element limit analysis method (OxLim). Included in this chapter was an example problem solved by both methods, a description of the input data files, and an explanation of the key output files generated.

Although both programs induce the soil mass to be discretized into finite elements, the models still have differences as follows:

- In the FELA model, the soil is rigid-plastic, while in the EPFE model, the soil is elastic-plastic.
- The computing time consumed by both models, it closely related to the mesh density, however, the FELA model generally runs faster than EPFE. This contrast is particularly noticed with EPFE when a dense mesh is implemented with numerous SRF trials. The computation time varies with the FS tolerance and iteration ceiling in slope64, whereas the target error in OxLim is the critical parameter affecting processing time.
- The FELA model is implemented by means of an unstructured mesh that is refined adaptively in the plastically yielding zones. No such adaptivity is currently available in slope64, but the mesh can be refined manually.

- While slope64 mesh discretization is in the form of eight-node quadrilateral elements, OxLim uses triangular elements (three-node for LB FELA and six-node for UB FELA).
- slope64 weakens the soil strength parameters (i.e., undrained shear strength in this study) with a strength reduction factor, OxLim increases the load multiplying by a load increase parameter to trigger the system to fail. It may be noted that in an undrained problem, these are essentially equivalent.

In conclusion, EPFE and FELA models both gave accurate estimates of the factor of safety value for the example slope stability problem considered in this chapter.

CHAPTER 4

PARAMETRIC STUDY

4.1 Overview

This chapter presents extensive parametric studies involving the variation of the soil and geometric parameters for the purpose of deriving the stability chart solutions using finite element methods for the estimation of factor of safety for homogenous undrained slope.

In advance of the derivation of the stability charts, a few preliminary studies are performed. First, the sufficient side widths of the slope model determined as a ratio of slope height with the goal of avoiding the excessively long execution time and incorrect estimations due to the geometrical constraints on the failure mechanism. Then, the effect of the reservoir water on the linear relationship of the stability number N with its terms is investigated. Following that, the EPFE and FELA results obtained by thousands of different cases are compared for undrained slopes. Some of the results are validated against the literature, and the results of both methods are used to discuss the stability of vertical cuts in undrained soils. Finally, stability charts for undrained slopes both with and without reservoir water are derived. The results are compared to the literature, and the new types of failure mechanisms are introduced after interpreting each visual output file.

The results of the parametric studies conducted throughout this chapter are interpreted in terms of the stability number N in the same manner as the literature, described in Section 2.3. The stability number N is defined as follows:

$$N = FS\frac{\gamma H}{s_u} \tag{4.1}$$

where the parameters are defined in Table 1.1 and illustrated in Figure 1.1.

The stability number N is a fundamental way to comprehend the results because it is a dimensionless expression that omits the considerations of soil parameters, slope height, and factor of safety. Thus, the subsequent analyses focus primarily on the geometric parameters, the slope gradient β and the depth factor D (see Figure 1.1 and Table 1.1 for the definitions).

The parametric studies in this chapter combine several parameters for various purposes, which results in the analysis of thousands of different cases using Slope64 and OxLim. Chapter 3 clearly demonstrates a single run of a slope stability problem; however, when a large number of parameters are involved, proper management of both programs' data and output files is required, as is the creation of batch files to run several simultaneous analyses and the presentation of the results. At this point, as introduced previously in Section 3.2.3 and Section 3.3.3, two python scripts written by the author assist in the efficient management of the parametric studies conducted throughout this chapter.

Additionally, Table 4.1 specify particular values for the input parameters of both programs that affect run-time and the precision in the assessment of factor of safety in the following parametric studies. These parameters were briefly discussed in Chapter 3. The Python scripts create the data files using these values. Despite the fact that increasing the accuracy of the analysis boosts the run-time significantly, these values were selected with the goal of performing very precise analyses, rather than prioritizing the execution time.

Table 4.1 Some of the specified inputs for slope64 and OxLim

	input parameters	specified as
Slope64	factor of safety tolerance	0.01
	iteration ceiling	1000
	number of elements (mesh density)	starting with two finite elements per unit length at the crest surface and deciding the rest consistently
OxLim	target error	0.30%
	number of max mesh refinement	7

4.2 Deciding Sufficient Side Widths for Slope Model

4.2.1 Analysis and Results

In slope stability finite element analyses, there is no doubt that having a dense mesh in the area of the model where the possible slip surface occurs improves the accuracy in the assessment of factor of safety. However, the number of mesh elements is one of the major factors that affect the run time in a FE analysis. Although a high run time might be tolerable for a single analysis, it becomes critical when considering a parametric study that involves batched runs of thousands of different data files. Therefore, it is important to optimize the factors that affect the run time in the model in advance of a parametric run. Several of these factors are discussed in Chapter 3, such as the FS tolerance and iteration ceiling for slope64, as well as the target error and number of mesh refinements for OxLim.

When a slope model is considered, the side widths of the slope are set by user input for both the crest and foundation sides. While wider side widths increase the number of mesh elements in the model, overly narrow side widths may result in inaccurate estimations due to the restrictions on the slip surface by the model's geometry.

Since OxLim utilizes an adaptive mesh refinement technique, it may tolerate an excessively large selection of the model's side widths during the analysis employing one or two more mesh refinements, but eventually accumulating the mesh elements around the slip surface. Although these extra mesh refinements do not increase the run time considerably, they may lead the program to reach the user-specified maximum number of mesh refinements before encountering the target error. In addition to the risk of not reaching the target error, it should be noted that these minor increases in run time can add up to a significant amount of time when applied to an extensive batched run.

As described in Section 3.2.2.1, slope64 prompts the user to specify the number of mesh elements in the crest and foundation sides in both the x and y dimensions, accordingly distributes the elements evenly across the corresponding region, and then performs the related algorithms for each mesh element throughout the model. Excessively enlarging the mesh on the sides introduces additional finite elements away from the slide mechanism into the analysis, and the mesh with greater number of elements will take longer to run. In this case, even a single analysis by slope64 may take a long time due to the unnecessary side elements while not improving the accuracy of the estimation.

One must also take into account that excessively narrowing the model's side widths will affect the FS estimation as illustrated in Figure 4.1.

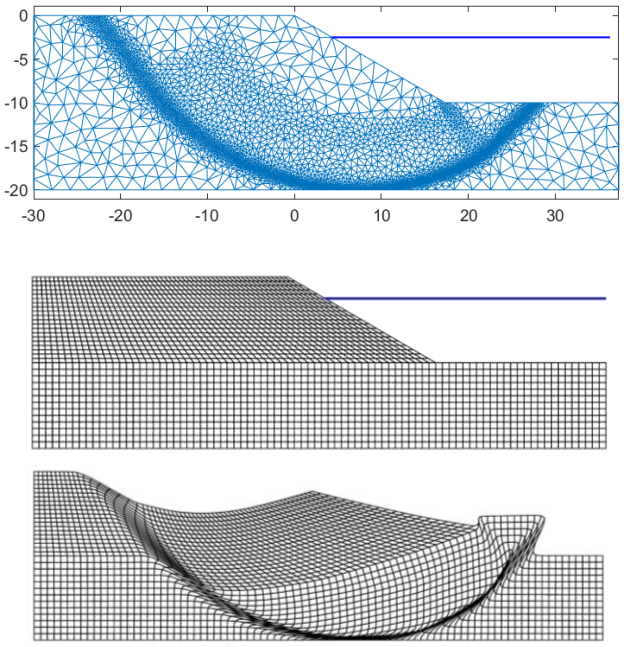

$FS_{OxLim} = 2.076$

$FS_{slope64} = 2.086$

(a)

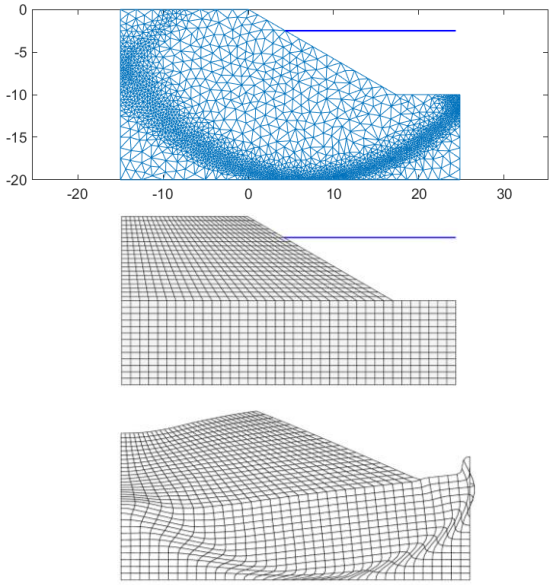

$FS_{OxLim} = 2.029$

$FS_{slope64} = 2.031$

(b)

Figure 4.1 FS estimation of the same slope by OxLim and slope64 with (a) a good selection of side widths and (b) a poor selection of side widths

In the light of the foregoing considerations, a parametric study that determines the slope model's appropriate side widths was conducted by using both slope64 and OxLim. The parameters listed in Table 4.2 were used as the input for the parametric run. The analysis was conducted at three different levels of submergence, taking into account the influence of resistant water in the reservoir on the failure mechanism. The slope angle β values were chosen to fall within the range that could result in a deep and wide failure mechanism. Lastly, the model's primary geometric restriction on the failure mechanism, the depth factor D, was selected as the values that Janbu's chart is based on and that will also be employed in this thesis's derivation of the major chart solution in the following sections.

Table 4.2 A data set to determine the proper side widths of the model

Parameter	***Values***	***Number of different values***
H_w/H	0, 0.5, 1.0	3
H (m)	10	1
D	1.0, 1.1, 1.2, 1.3, 1.5, 2.0, 2.5, 3.0, 4.0	9
β (°)	2.5, 5.0, 10.0, 15.0, 20.0, 25.0, 30.0, … 60.0	13
γ (kN/m^3)	20	1
s_u (kPa)	40	1
	Total Number of Cases	**351**

Following several trials with various side widths, the visual outputs of both programs were examined, and then the appropriate side widths for a homogenous slope model were concluded, as represented in Figure 4.2.

D	W_{crest} / H	$W_{foundation}$ /H
1.0	1.5 H	-
1.1	1.5 H	0.5 H
1.2	1.75 H	0.5 H
1.3	1.75 H	0.75 H
1.5	2 H	1 H
2.0	3 H	2 H
2.5	3.5 H	2.5 H
3.0	4.5 H	3.5 H
4.0	6 H	5 H

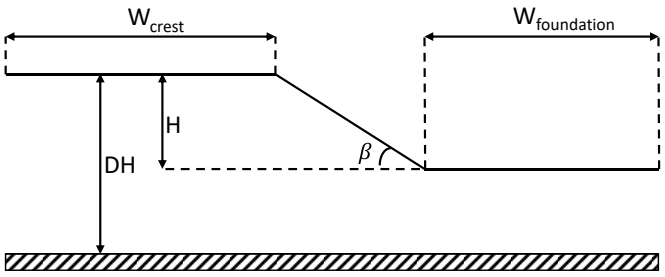

Figure 4.2 Appropriate selection of side widths for the FE analysis of a homogenous slope model

4.2.2 Discussion

It is wise to conduct a parametric study like above to determine the side widths prior to starting a lengthy parametric run. While an incorrect small selection of the side widths can result in inaccuracies in the estimations, as illustrated in Figure 4.1, the analysis can be significantly slowed down when the mesh is extremely large. Both of these scenarios could force the researchers to repeat the work, leading to a significant waste of time.

As a result, the following parametric runs in this chapter were conducted selecting the model's side widths according to suggested ratios in Figure 4.2.

4.3 Effect of s_u, γ, and H in Parametric Study

4.3.1 Analysis and Results

The soil parameters s_u and γ and the slope height H are parameters used for the stability number N as shown in Equation 4.1, and they are linearly proportional to N. In other words, as these values change, the factor of safety estimation changes proportionately, and the N value stays constant. That allows estimating the factor of safety of a slope from an N value obtained by

stability charts. However, before starting a lengthy parametric run, it is reasonable to perform a short parametric run to see whether this linear proportion is maintained in various cases, especially those involving reservoir water that contributes to the slope's stability. For that reason, a short parametric study is conducted based on the data set listed in Table 4.3.

Table 4.3 A data set to investigate the effect of s_u, γ, and H

Parameter	***Values***	***Number of different values***
H_w/H	0, 0.5, 1.0	3
H (m)	10, 20, 30	3
D	1.0, 2.0	2
β (°)	30.0, 60.0, 90.0	3
γ (kN/m^3)	18, 20, 22	3
s_u (kPa)	40, 80, 120	3
	Total Number of Cases	**486**

According to the results, it is revealed that s_u and H preserve their linear proportion to N regardless of the reservoir level. However, although unit weight of soil γ is linearly proportional when the reservoir is empty, this linear relation is disrupted as the reservoir fills. Table 4.4 lists the related results for γ values ranging from 18 to 22 kN/m^3 at three different reservoir level while keeping all other parameters constant.

Table 4.4 Effect of γ on N in the presence of reservoir water

H_w/H	H (m)	D	β (°)	γ (kN/m^3)	s_u (kPa)	FS	N	N_{ave}	Error	C
0	10	2	30	18	40	1.268	5.71	5.71	0.01%	1.000
				19		1.201	5.70		0.01%	1.000
				20		1.141	5.71		0.00%	1.000
				21		1.087	5.71		0.03%	1.000
				22		1.037	5.70		0.03%	1.000
0.5	10	2	30	18	40	1.661	7.47	7.27	2.74%	0.973
				19		1.549	7.36		1.20%	0.988
				20		1.452	7.26		0.13%	1.001
				21		1.365	7.17		1.44%	1.014
				22		1.289	7.09		2.54%	1.025
1	10	2	30	18	40	2.787	12.54	11.31	9.83%	0.902
				19		2.483	11.79		4.12%	0.959
				20		2.240	11.20		0.97%	1.010
				21		2.040	10.71		5.59%	1.056
				22		1.872	10.30		9.83%	1.098

This table calculates the stability number N for each γ value according to Equation 4.1, calculates the average of the N values along with a corresponding error (Equation 4.2), and finally introduces a new term, a correction factor C defined by Equation 4.3.

$$Error = \frac{|\, N_{ave} - N \,|}{N} \tag{4.2}$$

$$C = \frac{N_{ave}}{N} \tag{4.3}$$

Table 4.4 indicates that it is not possible to estimate the factor of safety of a slope from a single N value when the reservoir is not empty since different γ values lead to different values of N in the case of using Equation 4.1. Nevertheless, by employing a correction factor C (Equation 4.3), a single chart plotted by N_{ave} values could be used to estimate the factor of safety following Equation 4.4.

$$N_{ave} = FS\ \frac{\gamma H}{s_u}\ C \tag{4.4}$$

As a result, the stability charts for various reservoir levels are derived in Section 4.7 using the modified form of the stability number equation based on the average as seen in Equation 4.4.

4.3.2 Discussion

The parametric investigation from Section 4.3 shows that the predicted N value maintains unchanged regardless of the reservoir level as s_u and H vary since the value of FS changes proportionately. The parameter γ, on the other hand, is an exception. The presence of water in the reservoir breaks the linear relation between FS and γ, resulting in a range of N value estimates rather than a single value.

Given the foregoing, it is reasonable to set s_u and H values to a single value, which will reduce the total number of cases significantly for a large parametric run needed. However, data sets belonging to the following parametric studies should involve a variety of γ values in the presence of reservoir water. Therefore, the following data sets in this chapter set s_u and H to 40 kPa and 10 m, respectively, whereas the parametric cases are created for given five values of γ ranging from 18 to 22 kN/m^3.

The results of the small parametric study conducted in this section also introduces an idea of using an average value of N with a correction factor C for varying γ, and this idea is one of the fundamentals of the methodology used in the derivation of the submergence charts in Section 4.7.

4.4 Comparison of the Estimations of slope64 (EPFE) and OxLim (FELA)

4.4.1 Analysis and Results

As discussed in detail in Chapter 3, although both programs, slope64 and OxLim are based on finite element analysis, they use distinct algorithms to estimate the stability of slopes. For instance, whereas slope64 employs an elastic-perfectly plastic finite element model using a strength reduction technique (EPFE), OxLim's solutions are based on finite element limit analysis of a rigid plastic material (FELA).

slope64 and OxLim were used to execute a parametric run on the data set with the parameters specified in Table 4.5. In this way, the results of both programs (or both methods, EPFE and FELA) were thoroughly compared through the examination of about five thousand different cases.

Table 4.5 A data set used in the comparison of the results of EPFE and FELA

Parameter	***Values***	***Number of different values***
H_w/H	0, 0.1, 0.2, 0.3, 0.4, 0.5, 0.6, 0.7, 0.8, 0.9, 1.0	11
H (m)	10	1
D	1.0, 1.2, 1.5, 2.0, 4.0	5
β (°)	10.0, 15.0, 20.0 ……. 90.0	17
γ (kN/m^3)	18, 19, 20, 21, 22	5
s_u (kPa)	40	1
	Total Number of Cases	**4675**

When the results of this parametric run are analyzed, one could conclude that both methods exhibit strong agreement in assessing the factor of safety. However, it is also revealed

that EPFE estimations are always slightly higher than those obtained by FELA. At this point, a histogram chart, as shown in Figure 4.3, could assist in properly understanding this slight overestimation by slope64. This histogram chart is produced by examining the differences between the FS estimations of slope64 and OxLim over the total number of 4675 different cases. While the x-axis shows the bins for the FS overestimation ratio of slope64 to OxLim, the y-axis represents the percentage frequency distribution of the corresponding bin over the entire 4675 data. To illustrate, the difference in results of slope64 and OxLim varies between 0.5 and 1.0 percent in approximately 33% of the 4675 cases. Furthermore, the estimations of both programs are highly consistent, with slope64's overestimation ratio of the factor of safety being less than 2% in almost 85% of the cases.

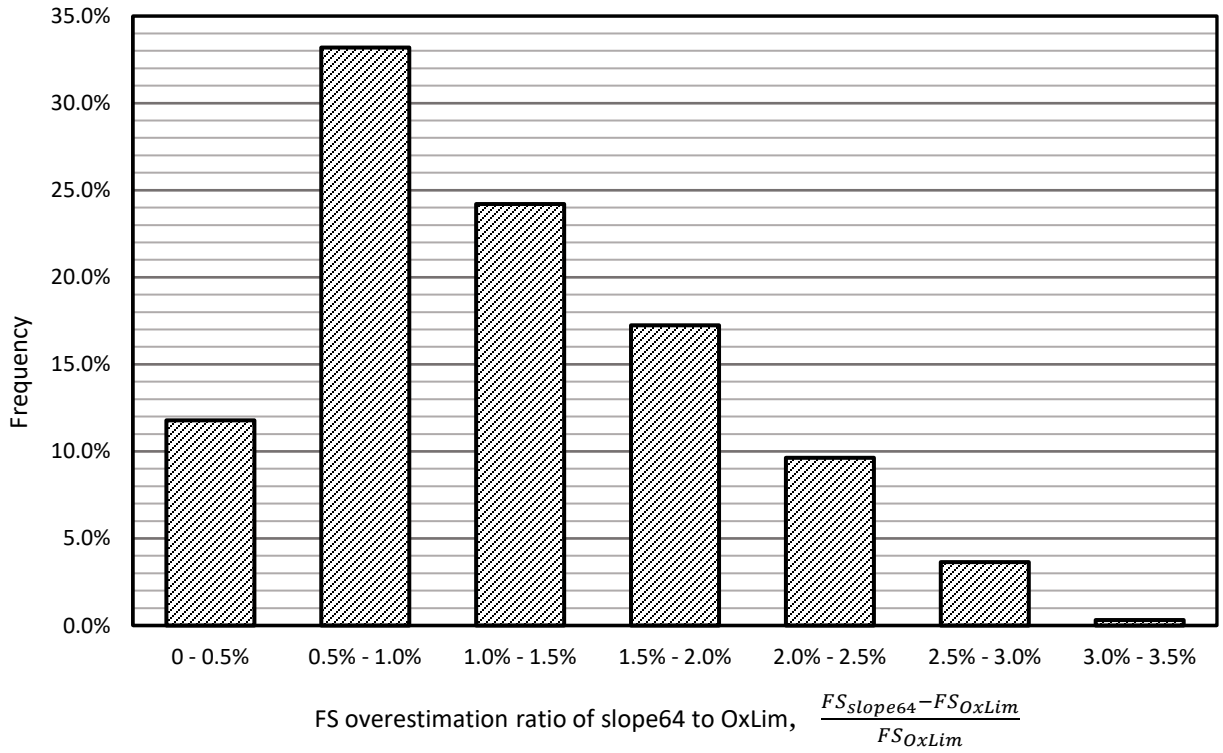

Figure 4.3 A histogram chart that depicts the overestimation ratio of slope64 to OxLim in the assessment of factor of safety over the total of 4675 different cases

Figure 4.4 depicts the distribution of slight overestimation of slope64 for different values of slope degree and depth factor when the reservoir is empty. Although there appears to be no pattern in terms of depth factor, the overestimation ratio tends to increase with increasing slope gradient in the range where a slip through the toe possibly occurs. However, these slight differences could be reduced further if the mesh used by slope64 was finer or the factor of safety tolerance was smaller, but this would dramatically boost the execution time. Improving the accuracy of slope64's estimates will be addressed along with the stability of vertical undrained cuts in the next section.

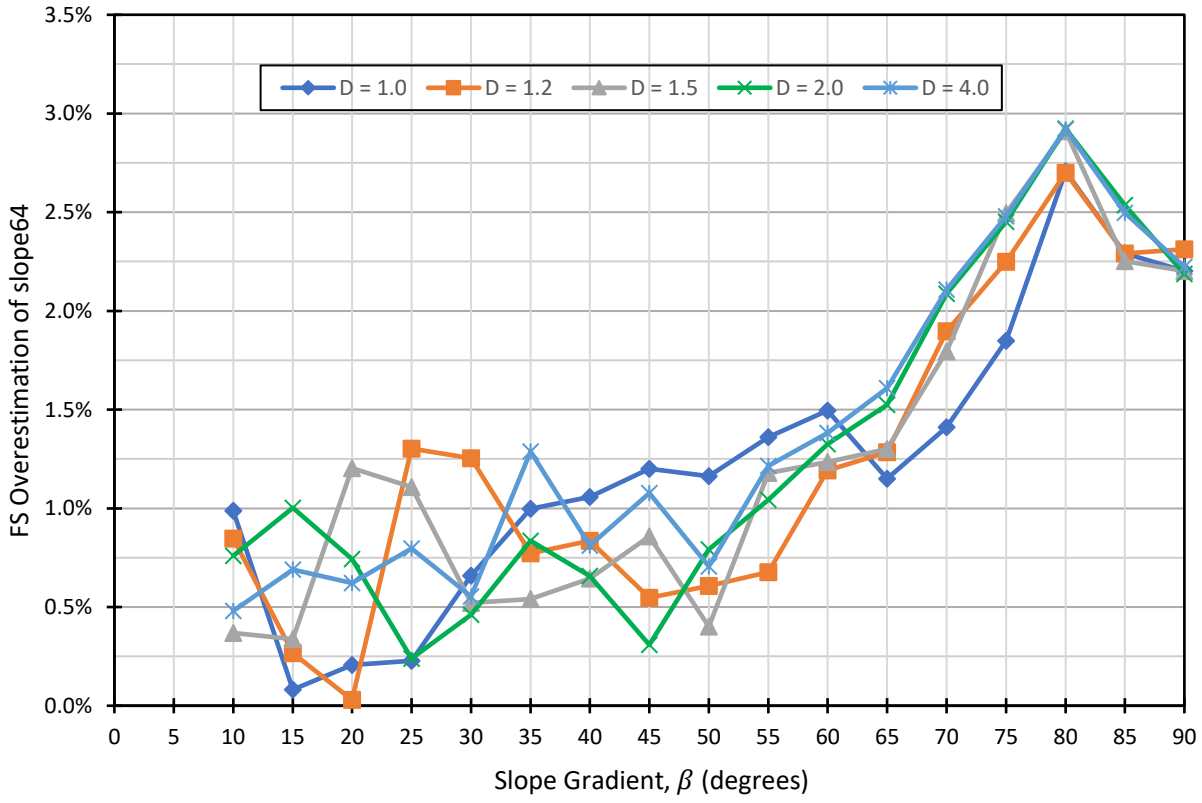

Figure 4.4 FS Overestimation of slope64 to OxLim for various depth factor D when $H_w/H = 0$

Table 4.6 compares the stability number values proposed by Griffiths and Martin (2020) for relatively flat slopes to the findings from the corresponding data of the parametric run conducted in this section adding those for $\beta = 5°$. In their study, the EPFE analysis is done by using another program called VG-SLOPE instead of slope64. VG-SLOPE is basically a similar program to slope64, and they share the same algorithms with the only exception of the way the mesh is discretized. While slope64 discretizes the soil into quadrilateral elements, VG-SLOPE generates the whole mesh trying to preserve all elements as being almost square. However, they estimate the exact same factor of safety when analyzing a sufficiently dense mesh as in the analyses conducted in this section. Figure 4.5 depicts the mesh discretization difference between the programs for the same slope model.

Table 4.6 Validating EPFE and FELA results against the data published by Griffiths and Martin (2020) for relatively flat slopes

	β = 5°					β = 10°				
	Griffiths and Martin (2020)		This study			Griffiths and Martin (2020)		This study		
	N_{FELA}	N_{EPFE}	N_{FELA}	N_{EPFE}	N_{EPFE} (Denser Mesh)	N_{FELA}	N_{EPFE}	N_{FELA}	N_{EPFE}	N_{EPFE} (Denser Mesh)
D = 1.0	22.5	23.1	22.47	22.80	22.62	14.2	14.4	14.19	14.34	14.26
D = 1.2	18.8	19.2	18.73	19.69	18.91	11.9	12.0	11.83	11.93	11.88
D = 1.5	15.1	15.3	14.99	15.63	15.16	9.7	9.7	9.59	9.65	9.61
D = 2.0	11.5	11.6	11.42	11.88	11.60	7.9	7.9	7.83	7.89	7.85
D = 3.0	8.7	8.7	8.63	8.67	8.67	6.5	6.5	6.46	6.52	6.52
D = 4.0	7.4	7.4	7.36	7.50	7.42	6.0	6.0	6.00	6.03	6.02

As seen in the table, this study's estimations closely agree with those by Griffiths and Martin, and the EPFE results tend to slightly overestimate the stability number; however, the results approach those obtained by FELA when the same analysis is repeated with a denser mesh in slope64. The stability numbers obtained by slope64 using the mesh density utilized in this study and a denser mesh are illustrated in Figure 4.5 (b) and (c).

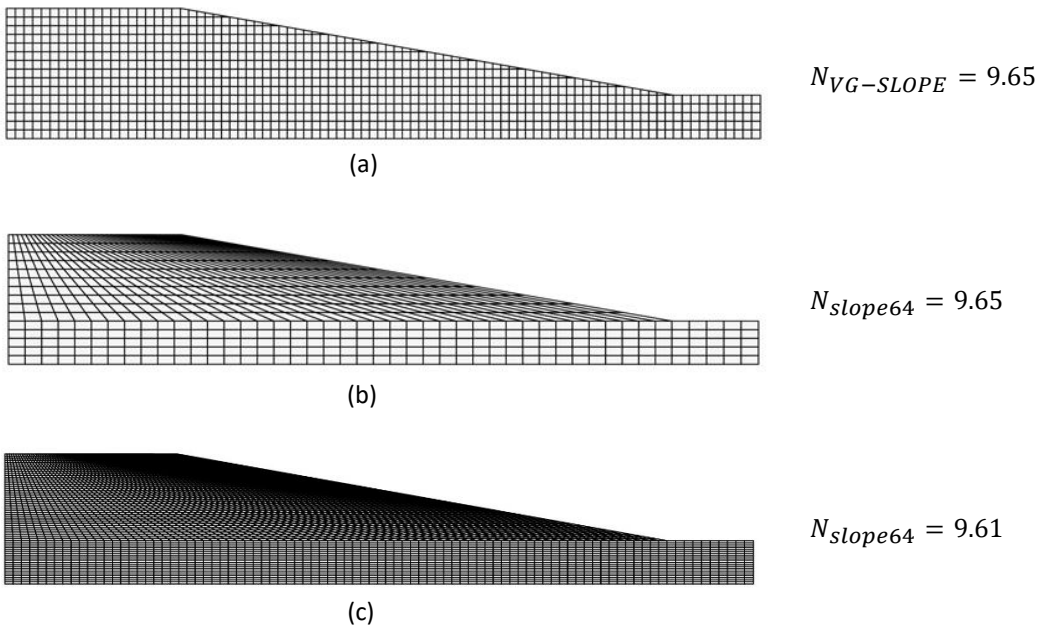

Figure 4.5 Comparison of (a) VG-SLOPE and slope64 with (b) the mesh density used in this study and (c) a denser mesh, when the parameters are $H = 10$ m, $H_w/H = 0$, $\beta = 10°$, $D = 1.5$, $\gamma = 20$ kN/m^3, and s_u = 40 kPa

4.4.2 Discussion

Despite the fact that slope64 and OxLim have different methodologies (EPFE and FELA, respectively) to estimate the factor of safety, the findings of the extensive parametric study conducted in this section reveal that the estimations from both methods are in close agreement. Additionally, it is shown that the EPFE results tend to be close to an upper bound solution and estimates factor of safety slightly higher as clearly indicated in Figure 4.3.

Apart from highlighting the minor differences between the estimations, this section also validates the models and associated estimations performed in this thesis using EPFE and FELA. Table 4.6 validates the results of this study against the data published by both programs' authors, Griffiths and Martin (2020). It could be also said that similarity of the estimates obtained through

two unique finite element programs validate the findings of the parametric studies done throughout this thesis.

Because of the strong agreement between the programs, only one software could be employed to perform the necessary analyses in the derivation of stability charts. Even though slope64 is also a strong tool to conduct such a study, OxLim is selected as the primary instrument for the analyses in the rest of this chapter. The following are the reasons for this choice:

- Despite the minor variation in estimations, a chart produced by FELA would be slightly more conservative.
- Although slope64 results, with increasing number of mesh elements, approach those obtained by OxLim, OxLim runs faster than slope64 especially in the case of the need of very precise estimations that requires a dense mesh since OxLim places the majority of the finite elements into the plastically yielding zones.
- The visual outputs of OxLim make it easier to define the failure mechanism.

However, while the data sets in the final chart derivations are not usually obtained by slope64, the program is frequently used to supplement and validate the findings.

Furthermore, the output of the parametric analysis in this section makes it possible to test multiple stability chart trials. It illuminates the necessary data and methods for deriving the final versions of stability charts proposed in this thesis.

4.5 Stability of Unbraced Vertical Cut in Undrained Clay

4.5.1 Analysis and Results

This chapter separately discusses the results for a vertical slope from the parametric study conducted in Section 4.4 since the stability of an unbraced vertical cut in undrained clay (also called a Tresca vertical slope) has always caught the researchers' attention. Besides, the estimation of Slope64 in Section 4.4 is improved by varying the relevant input parameters.

First stated as 4.00 by a planar failure surface assumption in very early studies (Coulomb, 1776; Rankine, 1857; Culmann, 1866), the stability number of a vertical slope was revised to 3.83 by Taylor (1937) and Janbu (1954) assuming a circular slip, and then it was improved to 3.78 by Pastor et al. (2009), Kammoun (2010) and Martin (2011) using FELA-based solutions.

The study in Section 4.4 shows that this value is obtained as 3.87 by slope64 with EPFE and as 3.78 by OxLim with FELA, implying a 2.4 percent overestimation of the value by Slope64, as seen in Figure 4.4.

As previously stated, slope64's outcomes can be enhanced by adjusting the factor of safety tolerance and the number of mesh elements. This is illustrated in Figure 4.6 in which the slope64's stability number estimate for a slope with $\beta = 90°$ is improved and gradually converges to the OxLim's estimation.

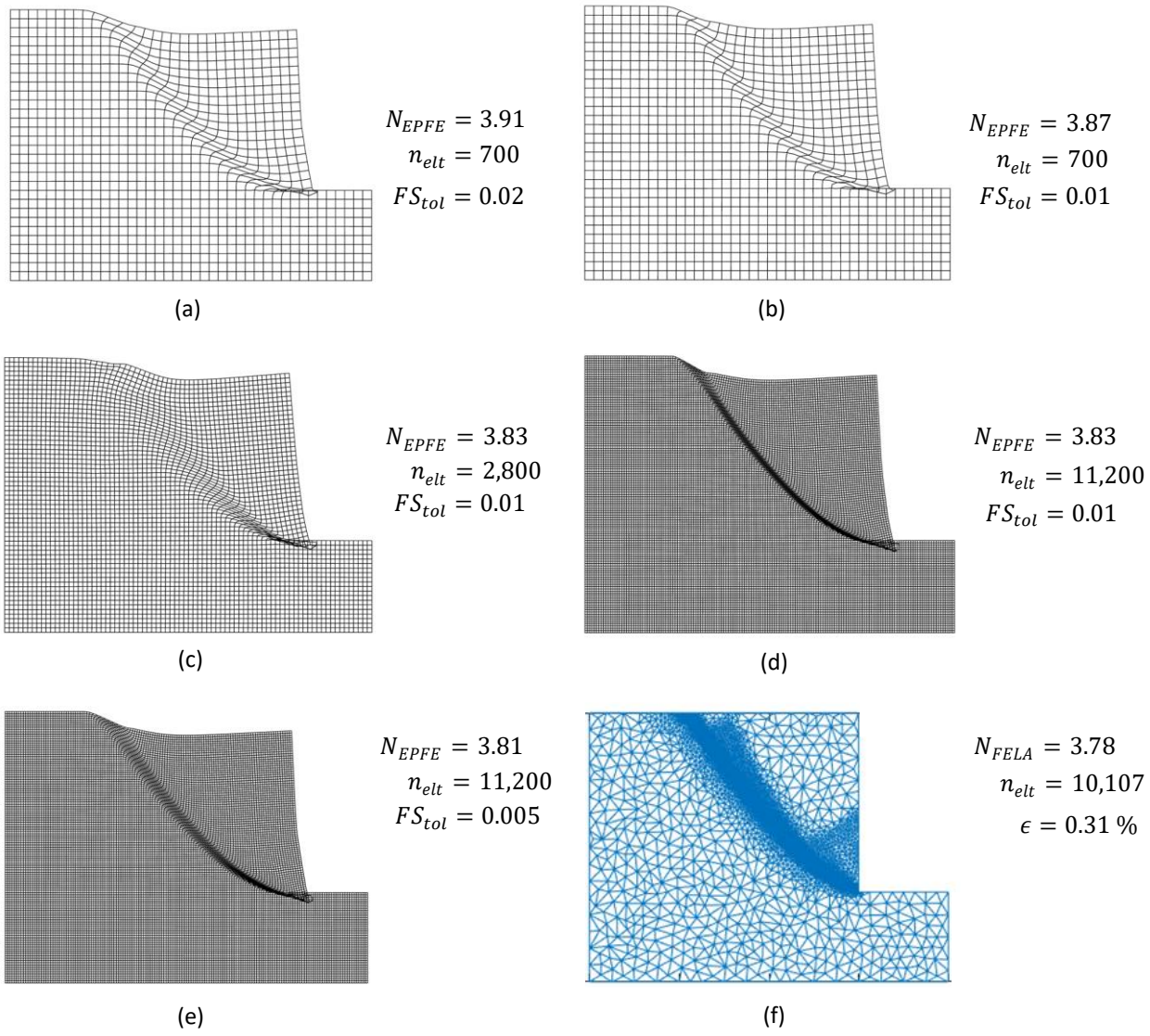

Figure 4.6 Stability number estimations for a vertical slope by slope64 from (a) to (e) and by OxLim (f)

Figure 4.6 (b) shares the same mesh density and factor of safety tolerance value with the analysis in Section 4.4. Noting that this model has even smaller side widths than Figure 4.2's suggestions (because of knowing the failure appears through the toe), the computing time consumed by slope64 to analyze this mesh density is around 2 minutes on a personal computer. This estimation can be improved to be 3.81 as seen in Figure 4.6 (e) by increasing the total

number of mesh elements to 11,200 and lowering the factor of safety tolerance value to 0.005. However, this alter boosts the computing time to be approximately 90 minutes. OxLim, on the other hand, discretizes the mesh into a nearly identical amount of mesh elements but places them around the plastically yield zone, resulting in the value of 3.78 with the bracketing error of 0.31% after four mesh refinements, as seen in Figure 4.6 (f). OxLim's computation time for such an analysis is around 30 seconds.

The term "factor of safety" can be defined as the ratio of a slope's critical height H_{cr} (a maximum height of a stable slope) to its height, as follows:

$$FS = \frac{H_{cr}}{H} \tag{4.5}$$

then substituting Equation (4.5) into Equation (4.1) and replacing the stability number N by 3.78, resulting in the following:

$$H_{cr} = 3.78\frac{s_u}{\gamma} \tag{4.6}$$

Equation (4.6) gives the theoretical maximum height of a stable vertical excavation in a clay in undrained condition.

4.5.2 Discussion

This section discussed the possible values of the stability number N than can be obtained by slope64 and OxLim for vertical Tresca slopes. As is usual, the slope64's estimate is slightly higher than the OxLim's; whereas the former is 3.87, the latter is 3.78 and matches with the value proposed by Pastour et al. (2009), Kammoun et al. (2010), and Martin (2011). Figure 4.6 demonstrates that the value of 3.87 obtained by slope64 can be improved further by altering the

mesh density and the factor of safety tolerance, then it reaches 3.81 converging to the OxLim's estimation. However, such a dense mesh and such a low FS tolerance value dramatically increase the computing time, making analysis of a large parametric research much more difficult. On the other hand, more accurate estimations within the same execution time would unquestionably be obtained if an adaptive mesh refinement technique were implemented to slope64's EPFE algorithm.

OxLim's precise estimation of N with 0.31% bracketing error shows that the theoretical maximum height of a stable unbraced vertical cut in undrained clay can be calculated by Equation 4.6. The value of 3.78 matches with Pastour et al. (2009), Kammoun et al. (2010), and Martin's (2011) proposed estimation that improved the value of 4 obtained by a planar slip assumption and the value of 3.83 obtained by a circular slip assumption in the literature.

4.6 Stability Charts for a Homogenous Undrained Slope and Failure Mechanisms

4.6.1 Analysis and Results

This section undertakes parametric research in order to derive a stability chart that enables estimating the factor of safety of a homogeneous simple undrained slope. The necessary data set to perform such a detailed study is listed in Table 4.7. OxLim was used to thoroughly analyze the total of 1620 unique cases generated by varying the parameters. The data set is constructed with a 2.5-degree slope increment, nine distinct depth factor values, and five distinct unit weight values in the range of 18 to 22 kN/m^3. While having β values every 2.5 degrees improves the precision in the derivation of the chart in comparison to Table 4.5, using nine depth factors, as Janbu (1954) did, reduces the interpolation error for the users. Although Table 4.4 indicates that the unit weight of the soil is in a linear relationship with the factor of safety in the

absence of reservoir water, five reasonable values are assigned to the parameter γ to determine if the linearity will be preserved for all possible geometries of the slope.

Table 4.7 A data set to derive the stability chart for a homogeneous simple undrained slope

Parameter	***Values***	***Number of different values***
H_w/H	0	1
H (m)	10	1
D	1.0, 1.1, 1.2, 1.3, 1.5, 2.0, 2.5, 3.0, 4.0	9
β (°)	2.5, 5.0, 7.5, 10.0, 12.5, ……. 90.0	36
γ (kN/m^3)	18, 19, 20, 21, 22	5
s_u (kPa)	40	1
	Total Number of Cases	**1620**

As mentioned in Chapter 3, OxLim produces a mass of output files even for a single analysis. When the data files created from the data set in Table 4.7 are run, it generates nearly a hundred thousand output files that consume approximately 15 GB of disk space. That is why managing the outputs with Python scripts is critical. The associated Python script reads each result file and writes the FS estimation to a spreadsheet. The results are then analyzed in the same manner described in Table 4.4. In all cases, the unit weight of the soil remains linearly proportional to the factor of safety, resulting in a single value of the stability number N for a range of γ values.

Since the different values of γ produce the same value of N for an empty reservoir, there are 324 distinct values of N in total (one-fifth of the total cases). These data points are placed onto a β versus N chart, as seen in Figure 4.7. Each *.vtu file belonging to the final mesh

refinement of each data point is imported into ParaView and each corresponding failure mechanism is colored according to a unique color code indicating the form of the slip. Along with those 324 points, nearly 200 additional data points are included and colored from the analyses of various intermediate D and β values at which the failure mechanism may change its form. According to the results, there appear to be a total of nine distinct failure mechanisms that could be obtained by a FELA analysis, with the majority falling into one of the six categories: compound slope, compound toe, tangent toe, compound deep, tangent deep, shallow toe. The remaining three types occur in exceptional circumstances. Tangent and compound failures occur only when $D = 1$ due to the model's geometrical constraint imposed by the rigid stratum. The last failure type is called transition zone and will be discussed later. As a result, Figure 4.7 clearly indicates the regions where the mechanisms form the same, which will be used later in the final chart.

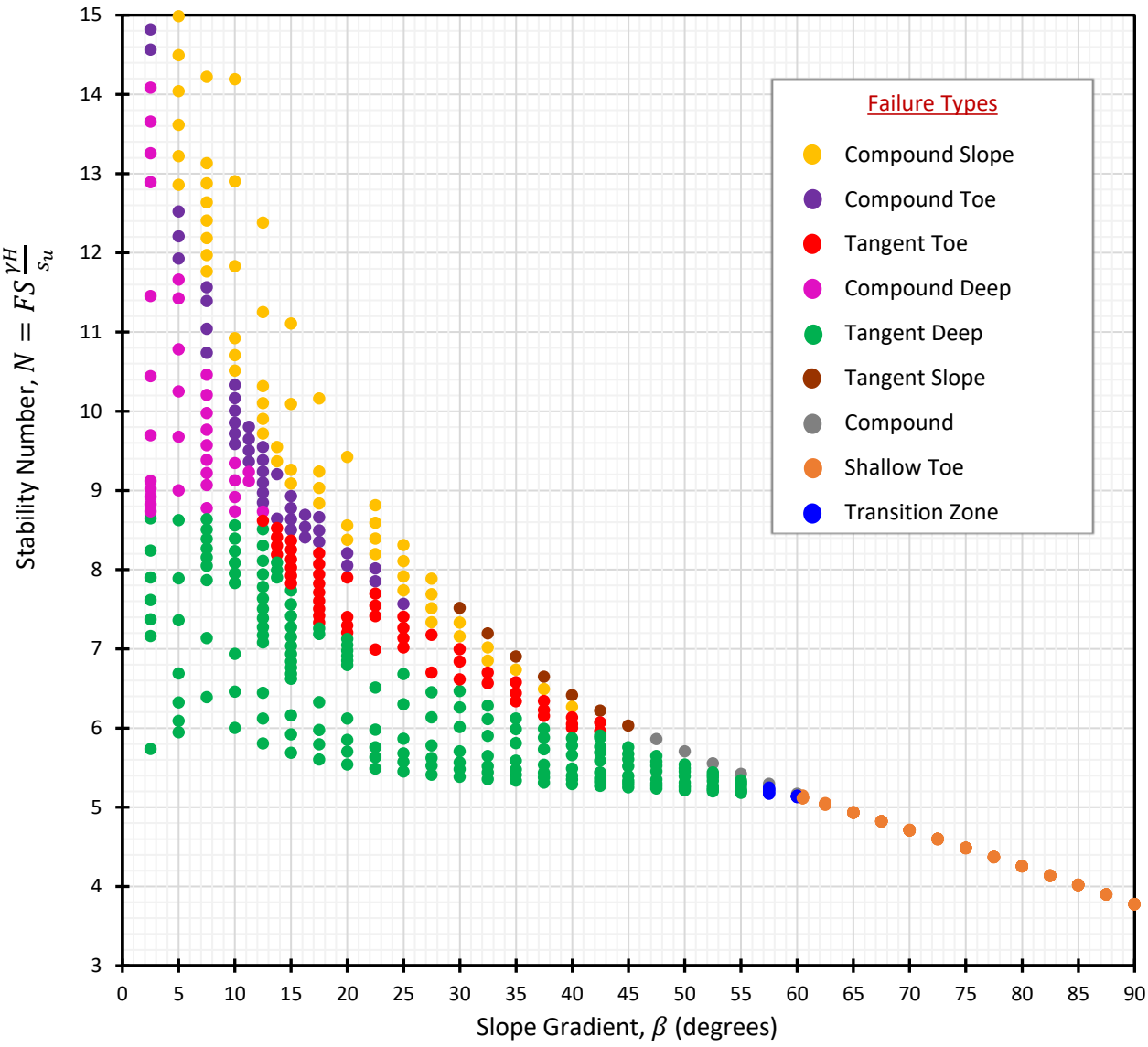

Figure 4.7 A chart coloring different failure forms obtained through the analysis of various β and D values

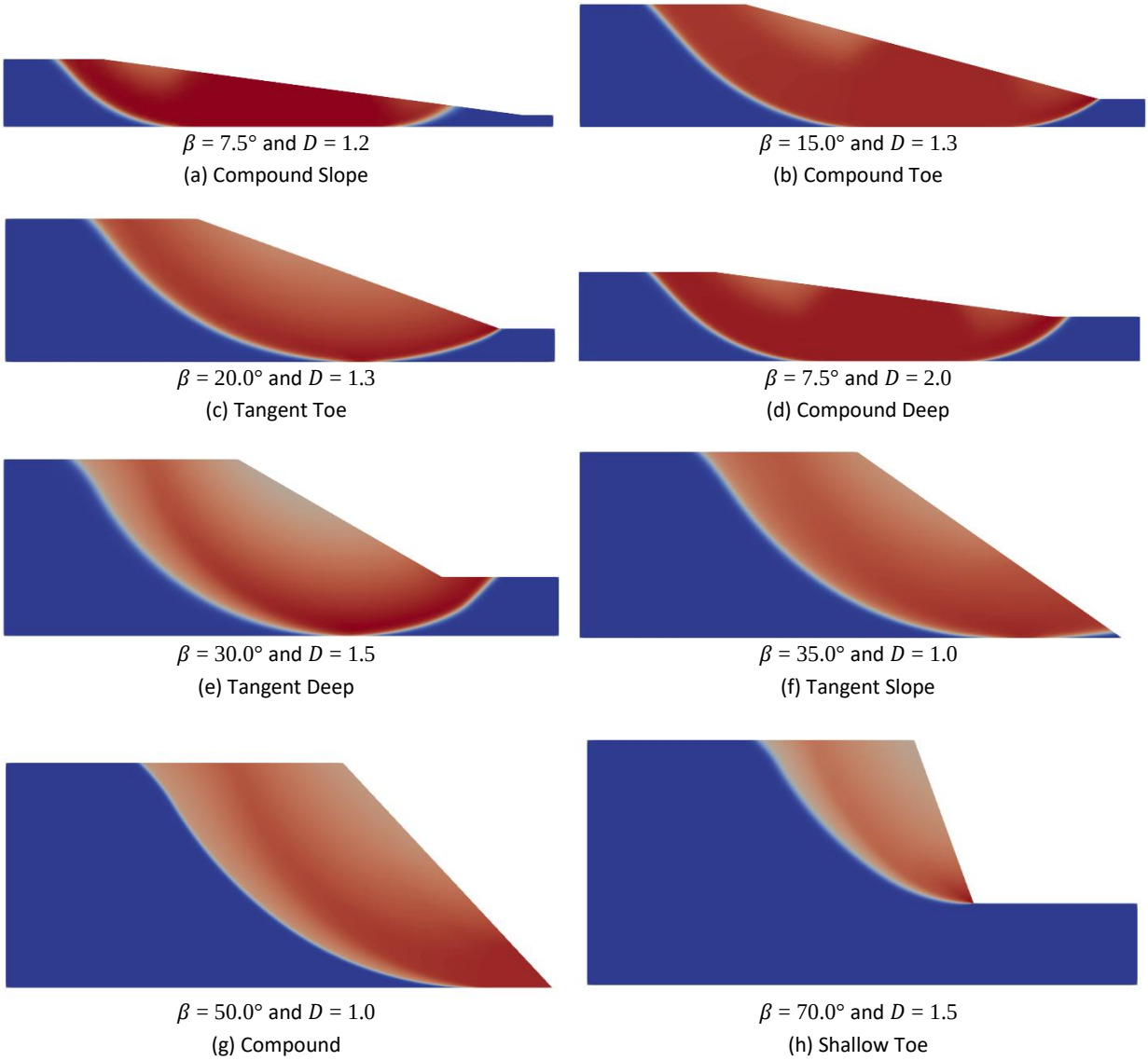

Figure 4.8 Failure mechanisms defined in the analysis of homogeneous slopes, with the corresponding geometrical parameters

The failure mechanisms Figure 4.7 indicates are illustrated in Figure 4.8 by OxLim's *.vtu outputs with coloring of the velocity field by ParaView (Ahrens et al., 2005). Each failure is presented with associated geometrical parameters of the slope in the figure.

It is worth noting that none of the mechanisms is called circular. While most failures resemble rotational slips, it is not possible to determine whether the slide is an arc or not since

the slip takes shape through the finite mesh. Moreover, as shown on the crest and foundation sides of the slip in Figure 4.9, there is some violation of the rotational trend throughout the slip. The findings reveal, as shown in Figure 4.9, a general trend that each exhibits a slight or more noticeable inflection point (a) on the crest side of the slip and the slips passing below the toe follow a straight path (b) before reaching the surface.

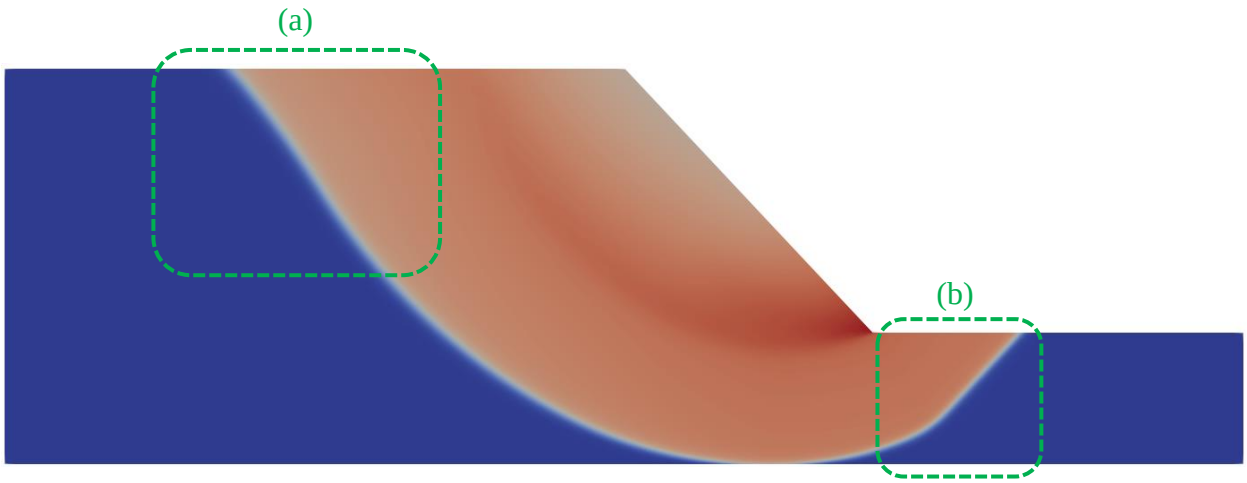

Figure 4.9 The failure mechanism for a homogenous undrained slope at $D = 1.5$ and $\beta = 45°$

Table 4.8 A data set focusing on the transition zone

Parameter	***Values***	***Number of different values***
H_w/H	0	1
H (m)	10	1
D	1.0, 1.1, 1.2, 1.3, 1.5, 2.0, 2.5, 3.0, 4.0	9
β (°)	50, 50.5, 51.0, 51.5, 52.0, ……. 70.0	41
γ (kN/m^3)	20	1
s_u (kPa)	40	1
	Total Number of Cases	**369**

The term "transition zone" refers to a region in which a tangent deep slip gradually rises and transforms into a shallow toe with increasing slope angle. After a parametric study based on the data set listed in Table 4.8, it is concluded that this transition trend appears in the range of β between $56.0°$ and $60.5°$ and becomes more noticeable with increasing D. Figure 4.10 illustrates how the failure mechanism transforms as the slope angle increases. When the slope angle reaches $60.5°$, all slopes become independent of the depth factor D and fail through the toe, resulting in a specific value of $N = 5.12$. Furthermore, the value of 5.12 represents the theoretical minimum stability number that can be obtained through a deep mechanism. All values less than 5.12 are only possible through a shallow toe mechanism.

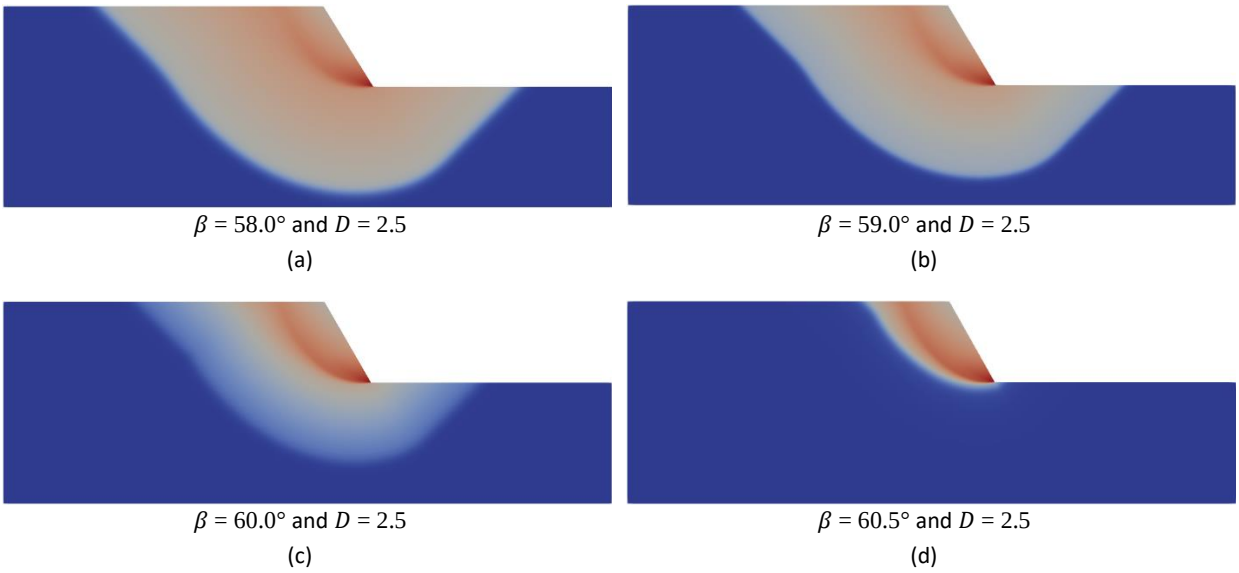

Figure 4.10 The gradual transformation of the failure mechanism within the transition zone

It is worth emphasizing that the failure mechanisms within the transition zones (Figure 4.10) have no sharp differences in the velocity magnitudes throughout the slip, implying the gray velocity zone, in contrast to other slip types as seen in Figure 4.8. This tendency is also visible in

the refined finite element mesh produced by OxLim. As demonstrated in Figure 4.11 (a) by a slope with $\beta = 60°$ and $D = 2.5$, the adaptive mesh refinement takes place within almost the entire sliding mass rather than around the specific sliding surface. This could imply that the mesh elements within the sliding exhibit similar plastic yielding. slope64's visual output for the same slope, shown in Figure 4.11(b), demonstrates that, the failure surface is not clearly visible unlike in most cases, and the majority of the elements in sliding mass exhibit similar displacements.

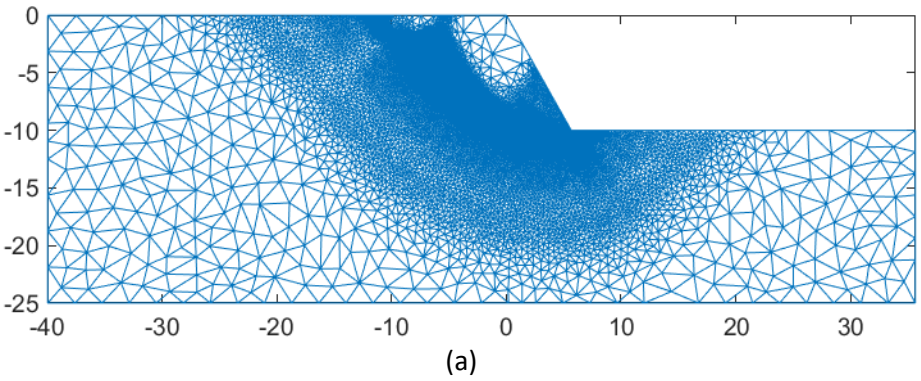

Figure 4.11 Visual outputs for the slope with $\beta = 60°$ and $D = 2.5$: (a) an adaptively refined mesh by OxLim; (b) a deformed mesh by slope64

Although slope64's failure mechanisms mostly match those of OxLim, slope64's deformed meshes in the transition zone do not reflect the progressive rise of the failure mechanism; instead, there appear to be several simultaneous slips. Figure 4.12 depicts three

simultaneous failure mechanisms that occur in a homogenous undrained slope with the geometrical parameters falling into the transition zone.

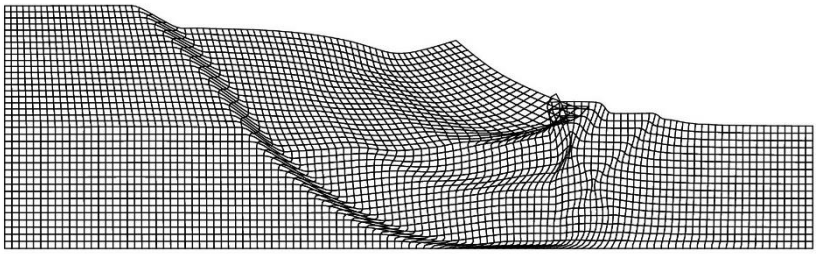

Figure 4.12 Three simultaneous slips in a homogeneous undrained slope with $\beta = 56°$ and $D = 2.5$

Taking all of the preceding results into account, the parametric studies in this section yield a stability chart that delivers the factor of safety along with an associated failure mechanism for a homogeneous undrained slope with $\phi = 0$, as given in Figure 4.13.

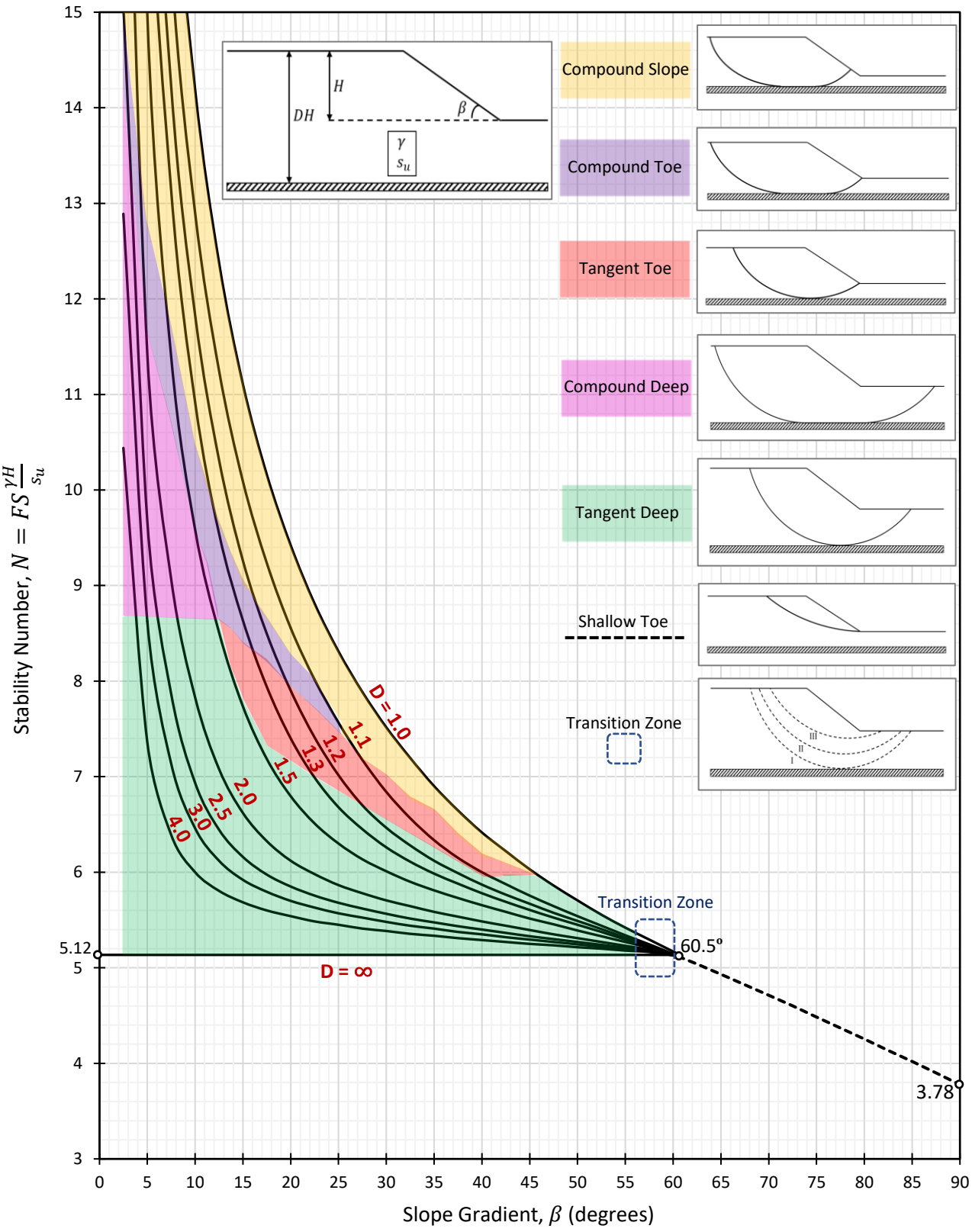

Figure 4.13 A stability chart for a homogeneous undrained slope with associated failure types

As discussed before, $D = 1.0$ is a special case where the rigid base stratum constrains the failure mechanism due to the lack of foundation. This geometrical constraint brings out two new types of failure mechanisms as illustrated in Figure 4.7. These two unique slip forms are omitted from Figure 4.13 because they only appear within a narrow range of slope angles and at $D = 1.0$ or very close values ($D < 1.025$). That is why the special case of $D = 1.0$ is separately provided along with its associated failure forms in Figure 4.14. The derivation of this chart is based on the analysis of the data set listed in Table 4.9.

Table 4.9 A data set to analyze the special case of $D = 1.0$

Parameter	***Values***	***Number of different values***
H_w/H	0	1
H (m)	10	1
D	1.0	1
β (°)	1.0, 2.0, 3.0, 4.0, 5.0, ……. 90.0	90
γ (kN/m^3)	20	1
s_u (kPa)	40	1
	Total Number of Cases	**90**

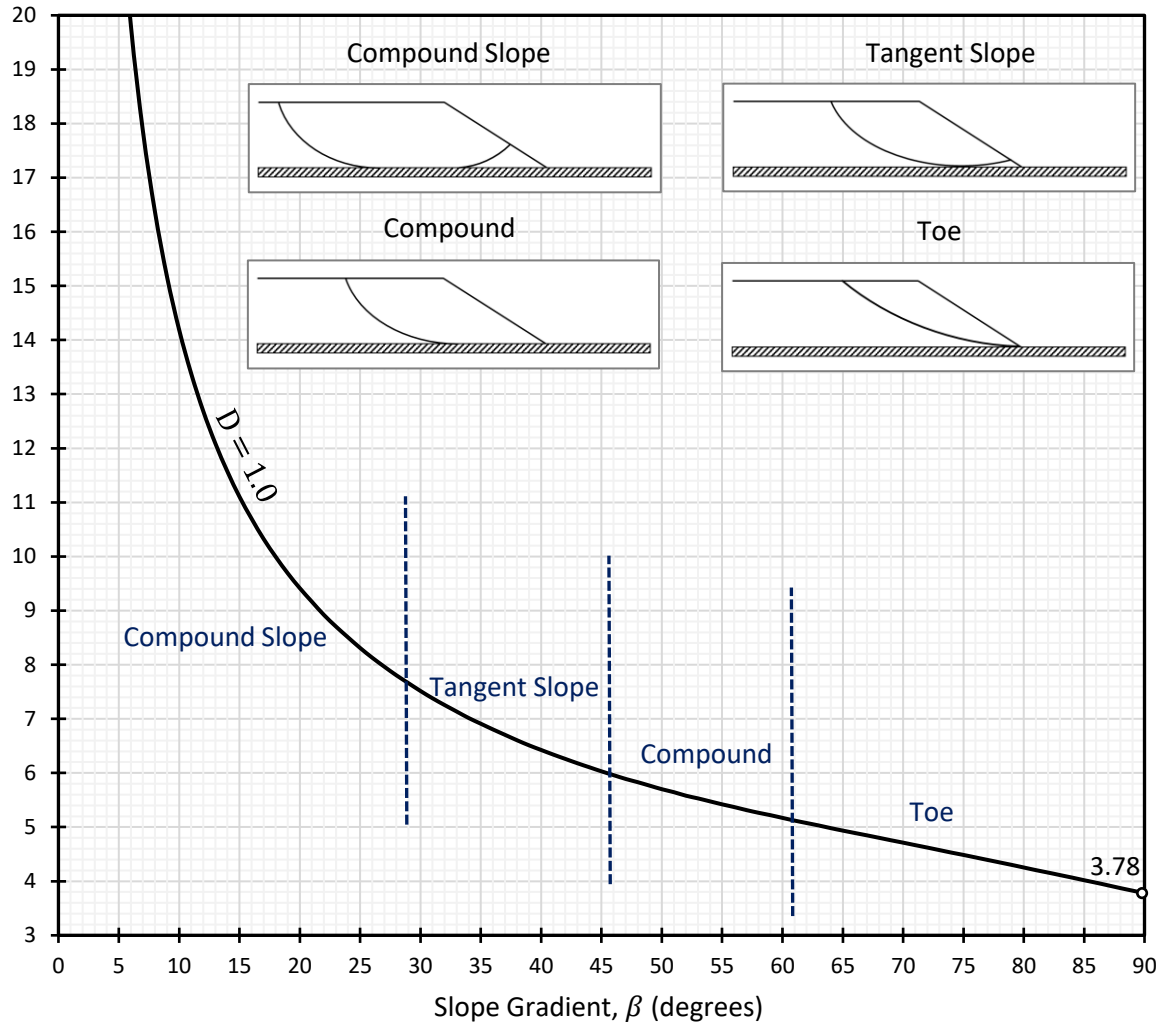

Figure 4.14 A stability chart for a homogeneous undrained slope with no foundation layer ($D = 1.0$)

4.6.2 Discussion

A stability chart for homogenous undrained slopes (Figure 4.13) was created using over a thousand FELA simulations with various parameter combinations. The chart is plotted in the same way as the literature, with the stability number N (Equation 4.1) and the slope angle β as the axes, and taking into account another geometrical parameter, a depth factor D, it delivers the factor of safety with an associated failure mechanism. It is built on nine reasonable values of D

stated by Janbu (1954), which inherently leads to less interpolation error than the charts proposed by Taylor (1937) and Steward et al. (2011).

The primary distinction in this thesis's proposed stability chart appears to be the shape of the failure mechanisms. Given that no prior assumptions regarding the shape or position of the critical failure mechanism are required for finite element methods, the failure mechanism will naturally choose the path of the least resistance, which means that the slope will collapse through zones with insufficient shear strength to resist the shear stresses. By utilizing an adaptive mesh refinement technique by OxLim, the mesh is discretized into thousands of finite elements gathered around the failure mechanism, which minimizes the effect of finite mesh on the final slip shape, so the failure mechanism forms into the most natural shape.

As a result, this thesis proposed nine unique failure types in total for homogeneous undrained slopes; with seven of those given in the main stability chart (Figure 4.13), and the other two, namely the tangent slope failure and compound failure, are only visible in the special case of $D = 1.0$ or at very close values. Figure 4.14 separately proposes a stability chart for an undrained slope with no foundation layer because the development of failure mechanism takes a different form than those in the main chart due to the geometrical restraints on the failure path imposed by the rigid base stratum.

None of the failure types proposed in this thesis is called an arc or a composite arc which consists of two arcs and a base straight line as assumed in the limit equilibrium methods. Even though the failure mechanism delivered by the finite element analyses appears to be similar in form to those in the literature, Figure 4.9 clearly demonstrates the complex geometry of the actual failure surfaces.

This thesis also proposes that there is a "transition zone" for case with a slope angle of between 56° and 65°. The findings by FELA show that the failure mechanisms gradually transform from a tangent deep mechanism to a shallow toe mechanism with increasing slope angles within the transition zone. This yields the most critical failure paths between the base and toe levels, which is more often observed in a slope with a layered soil formation. However, it is sensible to prioritize a tangent deep mechanism for slopes in the transition zone since a larger soil mass sliding might be more catastrophic. Furthermore, for a failure in this zone, the adaptive mesh refinement technique could not discretize the mesh around a sharp failure path, implying almost all the mesh elements in the sliding mass show similar yielding. This issue can be also noticeable from the deformed mesh produced by slope64 as seen in Figure 4.11; furthermore, slope64's EPFE analysis in the transition zone can yield multiple simultaneous failure mechanisms (Figure 4.12), which might be typical of a layered soil. Further research is needed on the differences between elastic-plastic and rigid-plastic analyses in this zone.

The following figures compare the stability number values determined by the proposed chart in this thesis to those obtained by Taylor (1937), Janbu (1954), and Steward et al. (2011), respectively. In general, while the proposed failure mechanisms in this thesis and the literature are notably different, they are not significantly different in the prediction of the factor of safety except for slopes in some specific geometries.

Taylor (1937), in agreement with Fellenius (1927), specifies that any slope steeper than 53° fails in the form of a toe circle. Taylor also indicates that the stability number value at this angle is 5.52, as the minimum stability number produced by an infinitely deep mechanism (N_{min}). In Janbu's chart, all the curves except for $D = 1.0$ intersects at around 53°, but Janbu highlights the 60° because the special case of $D = 1.0$ keeps failing as a slope circle until that

degree. However, Janbu very closely agrees with Taylor and Fellenius and proposes N_{min} as 5.53. On the other hand, Steward et al. (2011) replaces the angle of $53°$ by $58°$. Although they do not specify the value of N_{min}, the value appears to be around 5.40.

The value of 5.12 is given in this thesis as the theoretical minimum stability number that can be obtained through a tangent deep mechanism, and the corresponding angle is proposed as $60.5°$. Accordingly, all slopes steeper than $60.5°$ slide through the toe and the stability number or the factor of safety becomes independent of the depth factor D. Even though the intersection angle is close to those proposed by the other researchers, the value of $N_{min} = 5.12$ improves the literature by 7.8% on the safer side compared with methods that strictly enforce a circular failure mechanism.

Figure 4.15 shows that although Taylor assumed perfectly circular failure mechanisms in three distinct types and this study reveals, by a finite model, that the actual failure mechanism appears in possibly nine different forms, there is surprisingly no big difference in the estimation of the factor of safety in general.

However, Taylor's chart overestimates the factor of safety for some specific slopes. This study could agree with Griffiths and Martin (2020) that Taylor's chart overestimates the factor of safety for slopes at $\beta < 10°$. They point out an error of up to 12% in the estimation by Taylor's method for relatively flat slopes, particularly when the depth ratio D is small. This is not very clear in Figure 4.15 due to the lack of available data in Taylor's chart in which the range of the values for stability number N is given up to 11, but one could notice that Taylor's stability curves become very steep when $\beta < 10°$, implying great sensitivity to small changes in β. Additionally,

Taylor's chart delivers the factor of safety with an inaccuracy of up to 7.8 percent on the unsafe side for slopes with a foundation layer ($D \neq 1$) and slope gradients varying from 25° to 60.5°

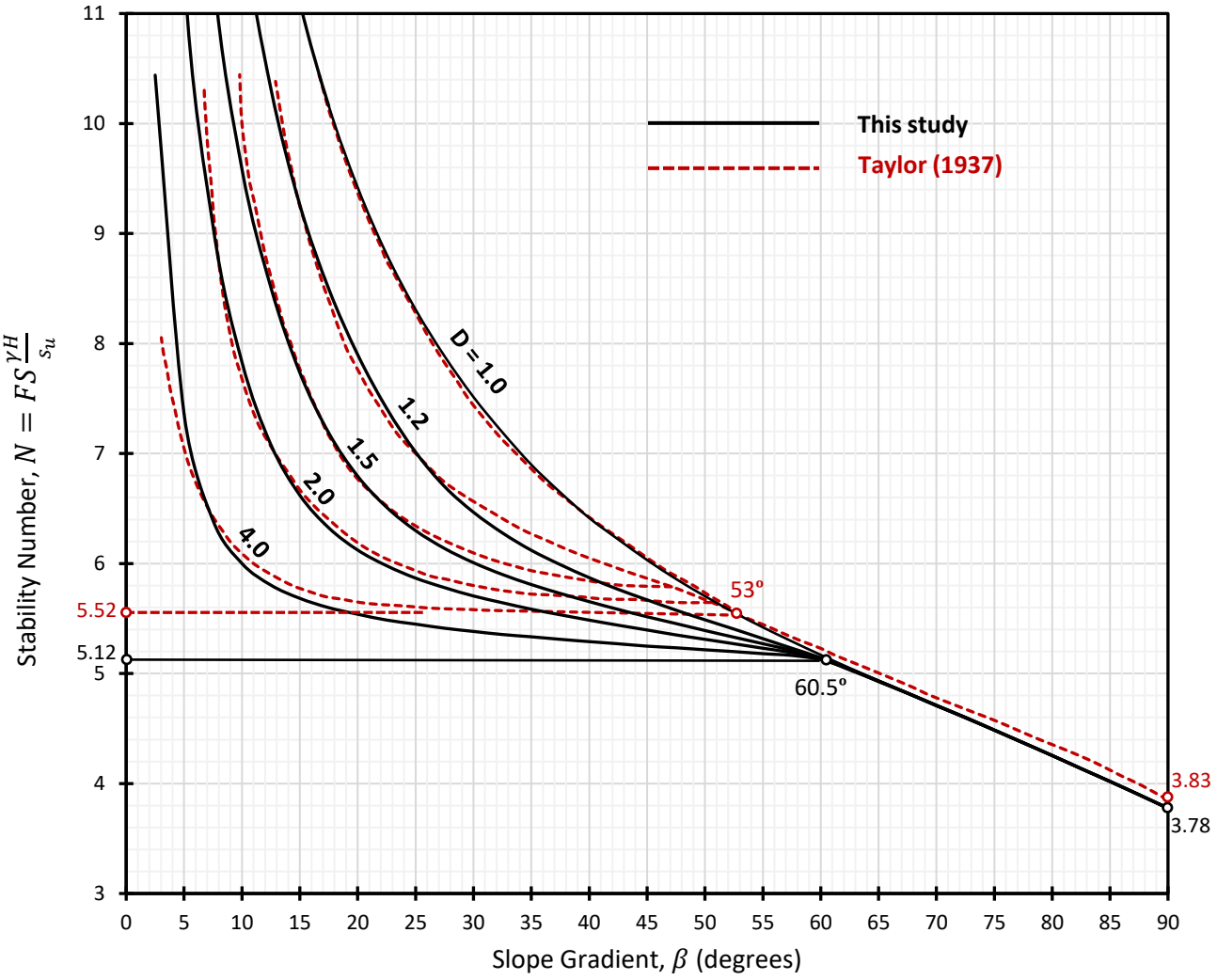

Figure 4.15 Comparison of the stability charts proposed by this study and Taylor (1937)

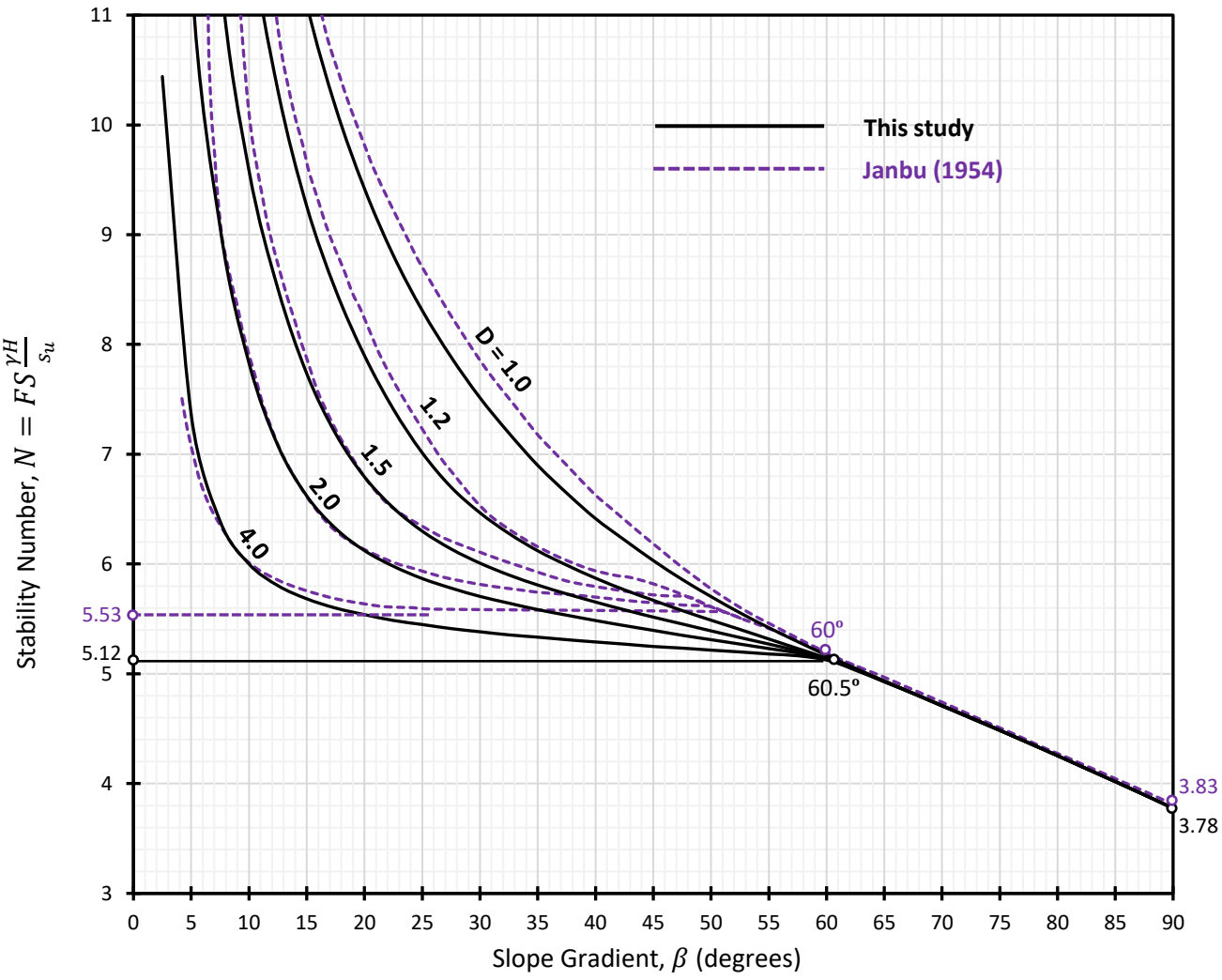

Figure 4.16 Comparison of the stability charts proposed by this study and Janbu (1954)

Figure 4.16 illustrates the comparison of the thesis's chart to Janbu's chart. One could say that Janbu's chart closely matches Taylor's chart, with slightly higher values. The trend appears very similar to Taylor's curves, and compared to the finite element chart, it overestimates the factor of safety for relatively flat slopes with very steep trend when $\beta < 10°$, slopes with no foundation layer ($D = 1$) or slopes having $D \geq 1.5$ and slope gradients varying from 25° to 60.5°.

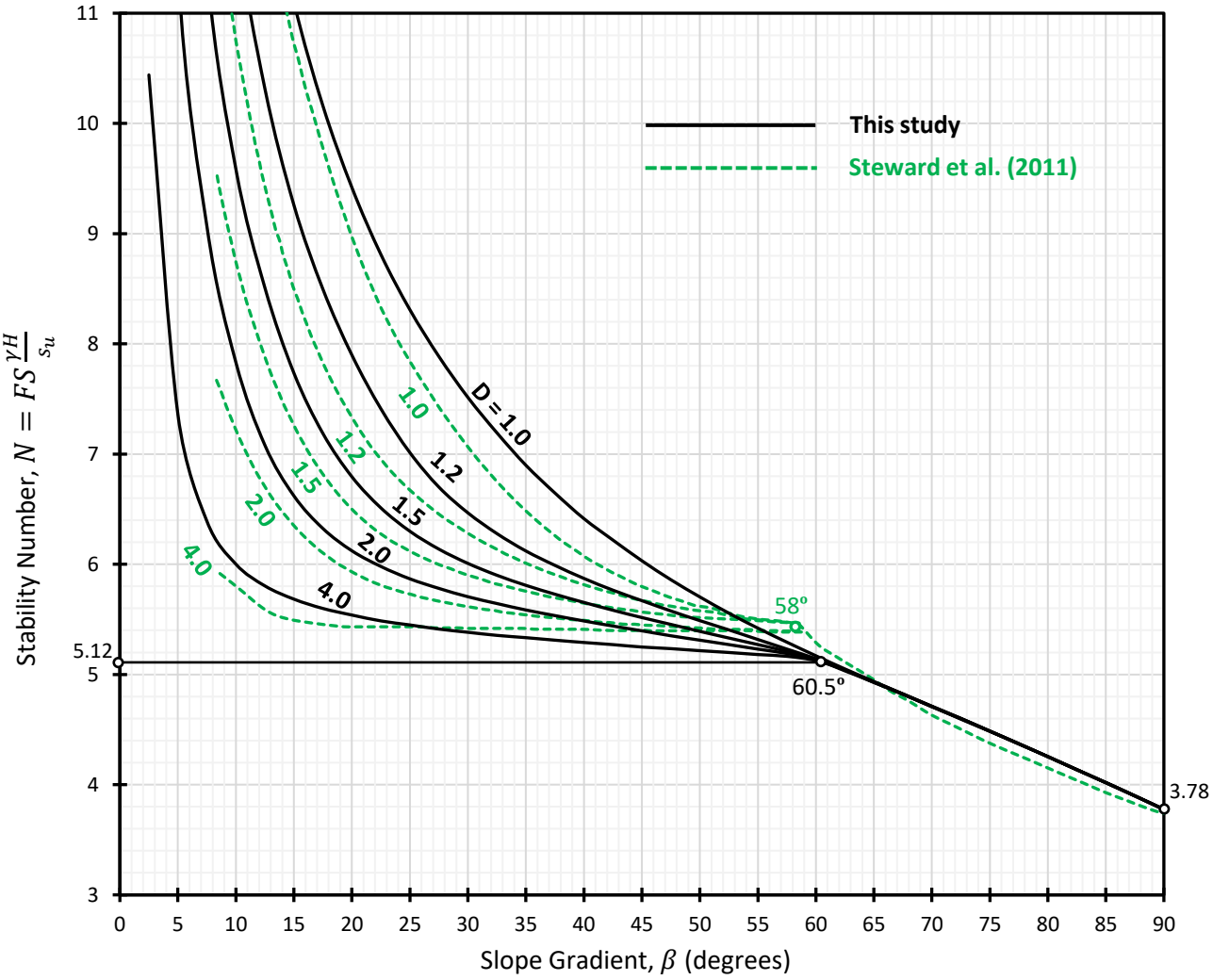

Figure 4.17 Comparison of the stability charts proposed by this study and Steward et al. (2011)

On the other hand, when the comparison chart in Figure 4.17 is examined, it could be seen that Steward et al.'s chart using Morgenstern and Price (1965) method mostly tends to underestimate the factor of safety, the difference being greatest for flatter slopes. For example, Steward's chart underestimates the factor of safety by about 10% for a slope having $\beta = 10°$ and having $D = 1.5$ or $D = 2.0$.

4.7 Stability Charts for Different Level of Reservoir Water

4.7.1 Analysis and Results

This section conducts a parametric study based on the data set described in Table 4.10, which is based on four reservoir levels and four times the size of the preceding section's data set. It takes a couple of days for OxLim to entirely analyze this amount of data and requires approximately 60 GB of available storage space.

H_w represents the height of the reservoir level above the toe, and it is defined in Figure 1.1 and Table 1.1 with other parameters.

Table 4.10 A data set for the derivation of stability charts at four different reservoir level

Parameter	***Values***	***Number of different values***
H_w/H	0.25, 0.50, 0.75, 1.00	4
H (m)	10	1
D	1.0, 1.1, 1.2, 1.3, 1.5, 2.0, 2.5, 3.0, 4.0	9
β (°)	2.5, 5.0, 7.5, 10.0, 12.5, ……. 90.0	36
γ (kN/m^3)	18, 19, 20, 21, 22	5
s_u (kPa)	40	1
	Total Number of Cases	**6480**

It is previously stated in Section 4.3, that the linear relationship between the unit weight of soil and the factor of safety is disrupted in the presence of reservoir water; as a result, the various γ values yield different N values, as illustrated in Table 4.4. Because of this, the stability charts in this section are constructed replacing N by N_{ave}.

N_{ave} is the average value of different N values obtained by varying γ values. However, after obtaining an N_{ave} value from the stability charts, a correction factor C proposed by this study is involved in the calculations in order to estimate the factor of safety correctly. In other words, the factor of safety is estimated by Equation 4.4.

The correction factor C is defined by Equation 4.3 for a single case in Section 4.3. However, a reasonable value of C should be found in order to accurately estimate the factor of safety for varying values of the parameters. The results of the extensive parametric study in this section show that the value of C mainly varies with changing the reservoir level H_w/H and unit weight γ. In the case of keeping these two parameters constant, altering the other parameters does not significantly affect the value of C. Thus, it is wise to utilize an average value of C belonging to varying γ values for each H_w/H value. In this case, the error due to using an average C value will not exceed 2% in the estimation of factor of safety, and the error will even stay below 0.5% in almost 65% of the total cases.

According to the aforementioned methods, the following stability charts are derived for homogeneous undrained slopes at four different reservoir levels.

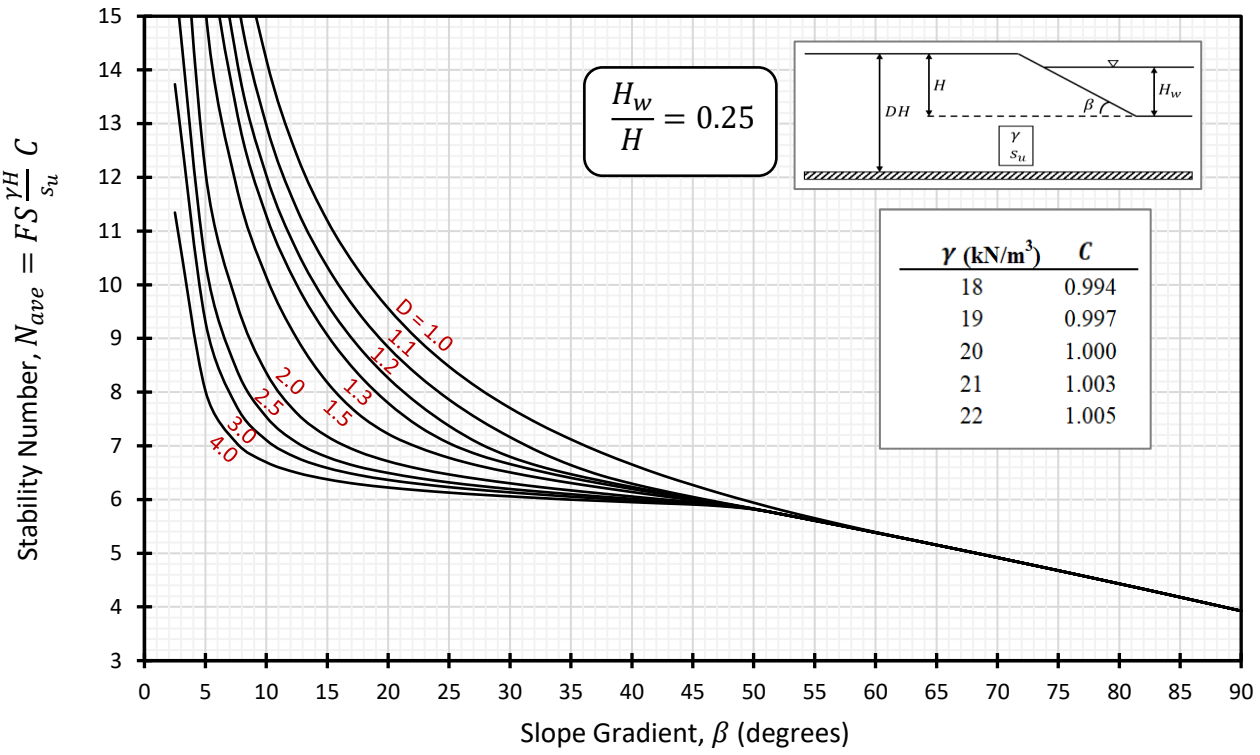

(a)

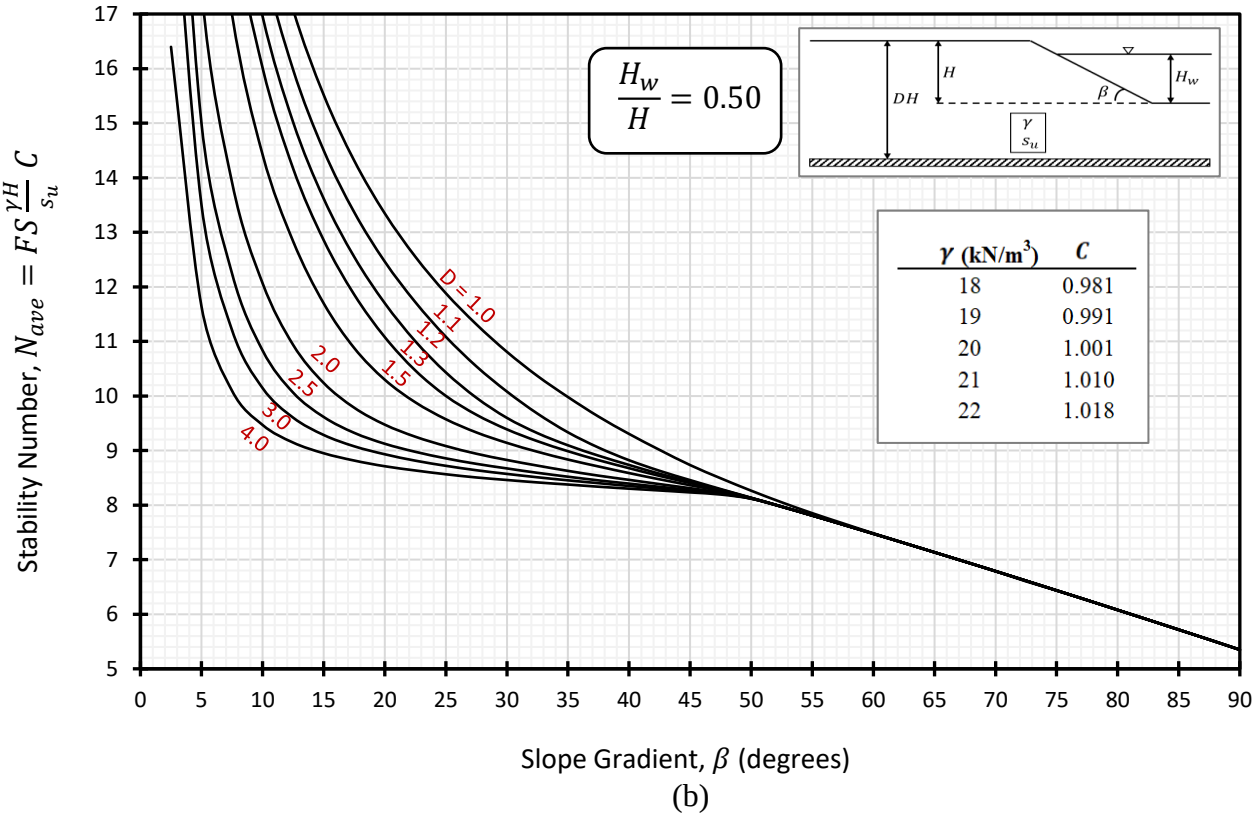

(b)

Figure 4.18 Stability charts for homogeneous undrained slopes in the presence of reservoir water

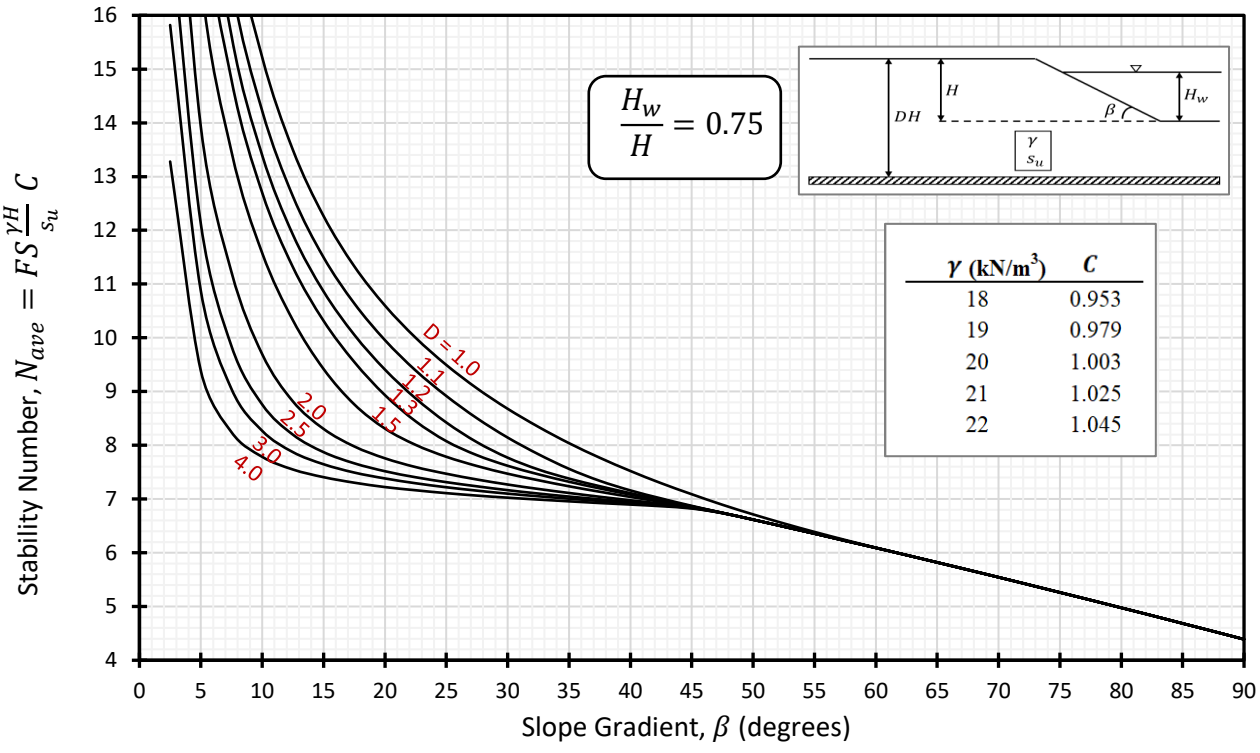

(c)

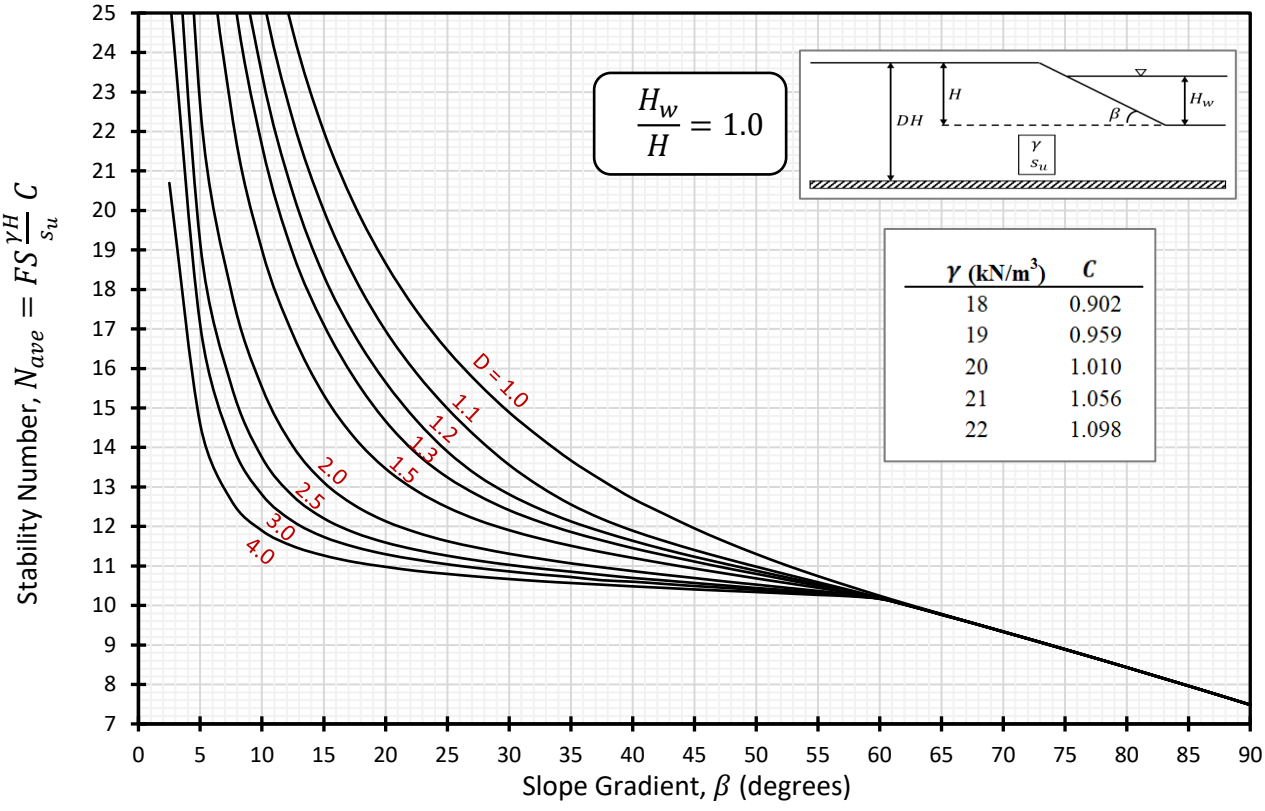

(d)

Figure 4.18 Continued

4.7.2 Discussion

In this section, stability charts for homogeneous undrained slopes in the presence of reservoir water are derived from an extensive parametric study conducted by utilizing FELA. In contrast to the previous charts, the charts are plotted by N_{ave} instead of N, where N_{ave} is the average of N values calculated by the factor of safety analyses of γ values with the range of 18 to 22 kN/m^3. Nevertheless, a correction factor C is needed for an accurate estimation of the factor of safety by using the stability charts. Figure 4.18 demonstrates each suggested C values associated with γ for each submergence level. It can be noticed that when the reservoir level increases, the range of C values increases, implying that the effect of γ increases.

A Python script is employed to re-interpret the Janbu's published study in order to provide a comprehensive comparison with the charts proposed in this thesis. A data set similar to those described in Chapter 4 can be inputted, and the program estimates the factor of safety of a given undrained slope problem by reading values from Janbu's main stability chart and charts for adjustment factor of reservoir loading. The program's algorithm is simply as follows:

- read the rigorously digitized data of Janbu's published charts
- write the variations of the parameters to a spreadsheet
- read N value from Figure 2.10; linear interpolation for intermediate β and D values
- read μ_w for a toe circle from Figure 2.13; linear interpolation for intermediate β values
- read μ_w for a toe circle from Figure 2.14; linear interpolation for intermediate D values
- estimate FS using Equation 2.9 for smaller μ_w
- write the FS estimate to the spreadsheet

With the help of the Python script, Janbu's chart solution in the presence of reservoir water was interpreted in the same manner as this thesis and compared to those proposed by this thesis. The comparison charts are given for $\gamma = 18$ kN/m^3 and illustrated in Figure 4.19. While Janbu's values in Figure 4.19 are derived by the Python script, this thesis's estimations are given after the correction factor C correlated to $\gamma = 18$ kN/m^3 is applied. In order to avoid interpolation of D values in the derivation of Janbu's modified charts, the comparison charts are presented with the four different depth factor values from Janbu's original chart (Figure 2.14).

According to Figure 4.19, one could observe that the charts proposed by this thesis for reservoir loading shows a reasonable agreement with Janbu's chart solution. However, as a general observation, Janbu's charts tend to overestimate the factor of safety. It can also be noticed that the error reaches its maximum in case of slopes with no foundation layer ($D = 1.0$). Moreover, it appears that the error reaches about 12.5% on the unsafe side when the parameters are $\gamma = 18$ kN/m^3; $H_w/H = 0.5$; $\beta = 20°$; and $D = 1$.

On the other hand, one should point out that the charts proposed in this thesis for the stability assessments in the presence of reservoir loading could be regarded more practical in comparison to Janbu's chart solution. That is because in order to obtain the adjustment factor μ_w (Figure 2.13 and Figure 2.14), interpolations for β and D values are mostly needed when it comes to Janbu's chart solution, not to mention that the intense use of interpolation may mislead the user, resulting in inaccurate estimations. On the contrary, the charts proposed by this thesis do not require as much interpolation as Janbu's charts require.

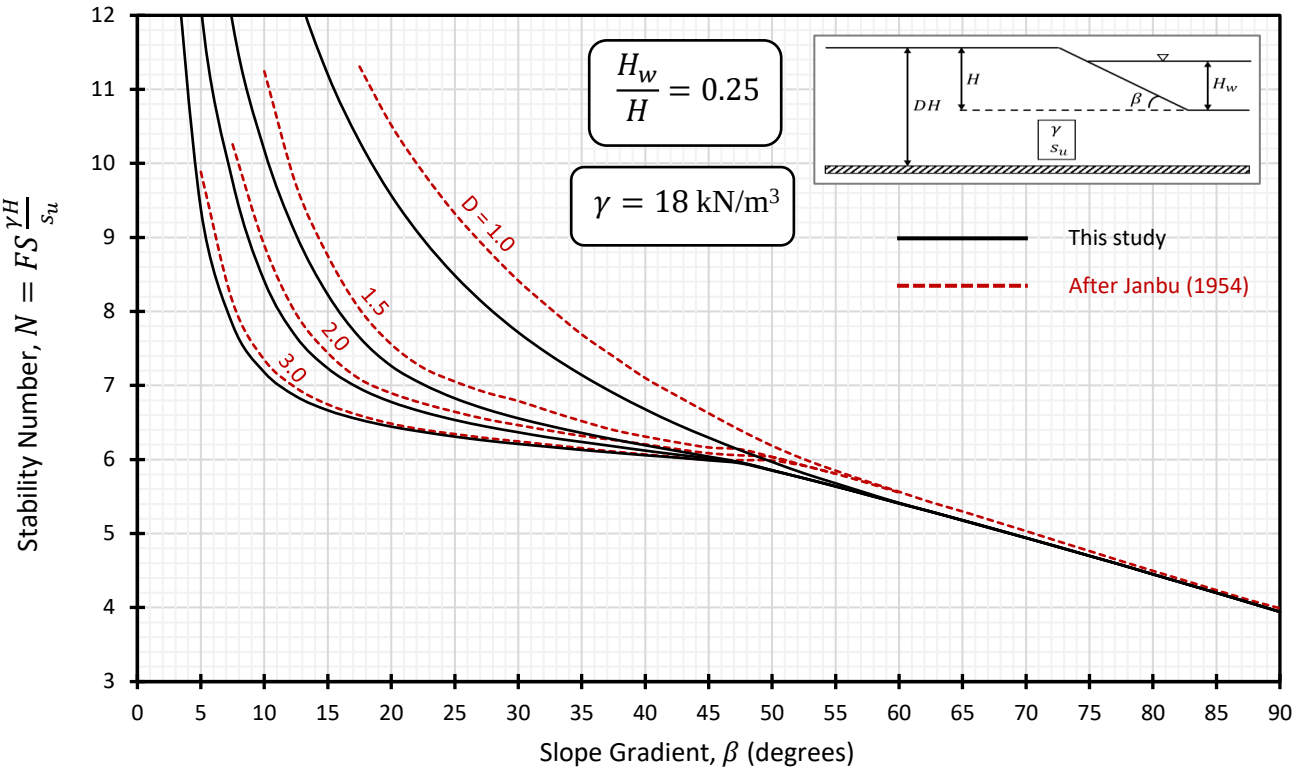

(a)

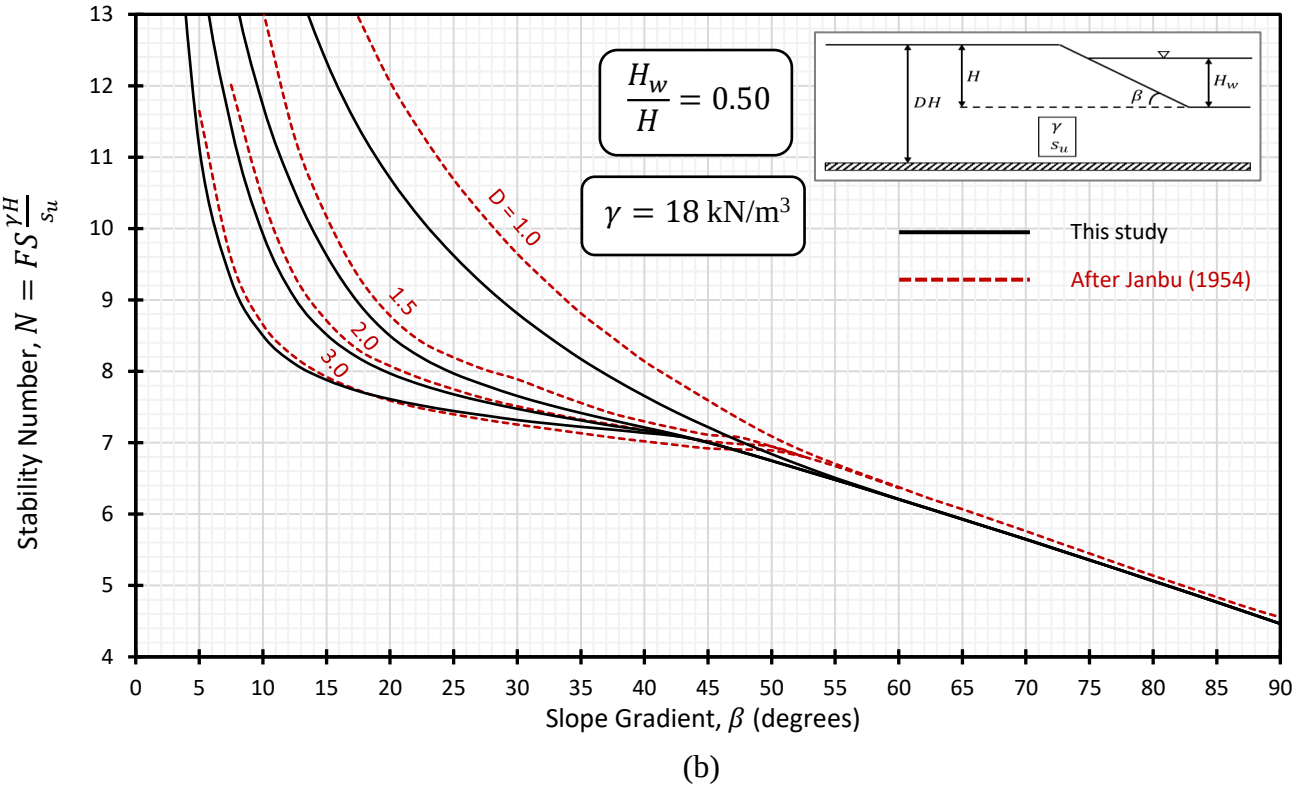

(b)

Figure 4.19 Comparison of the thesis's proposed charts to the charts derived after Janbu (1954) in the presence of reservoir water

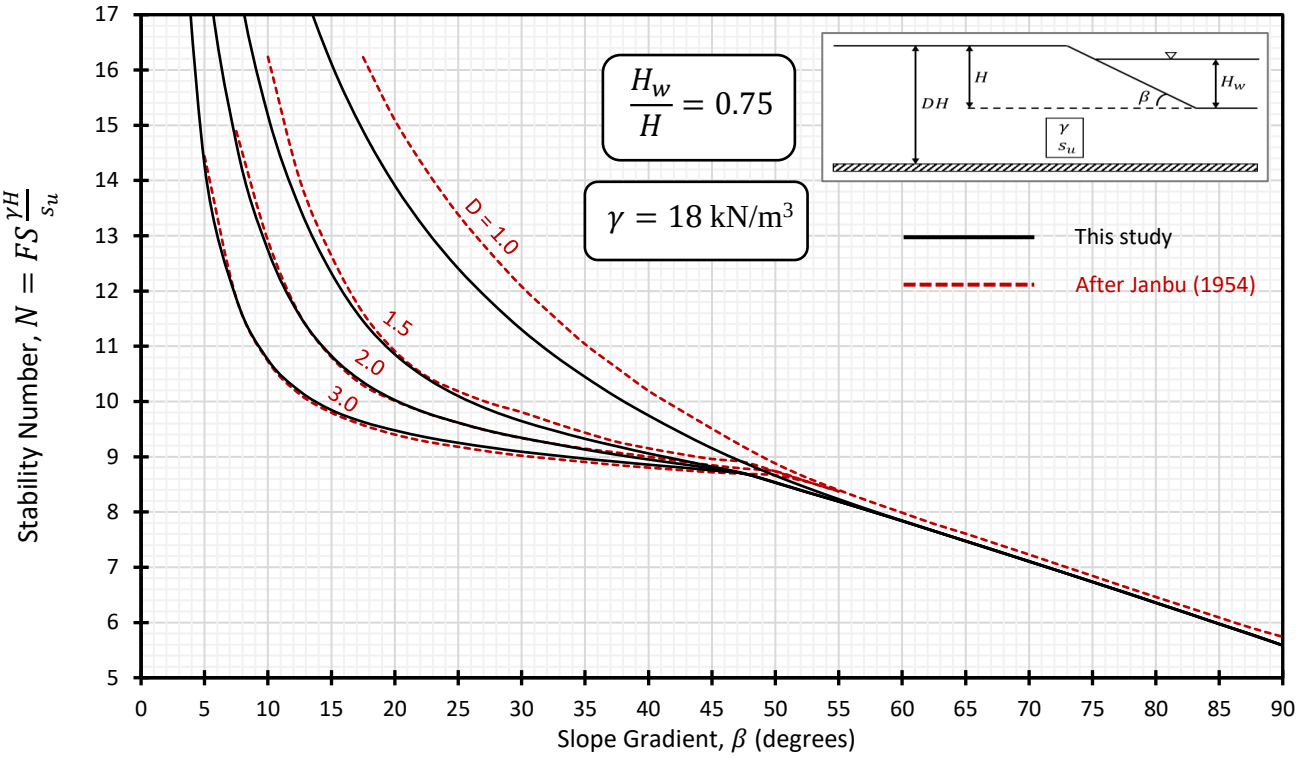

(c)

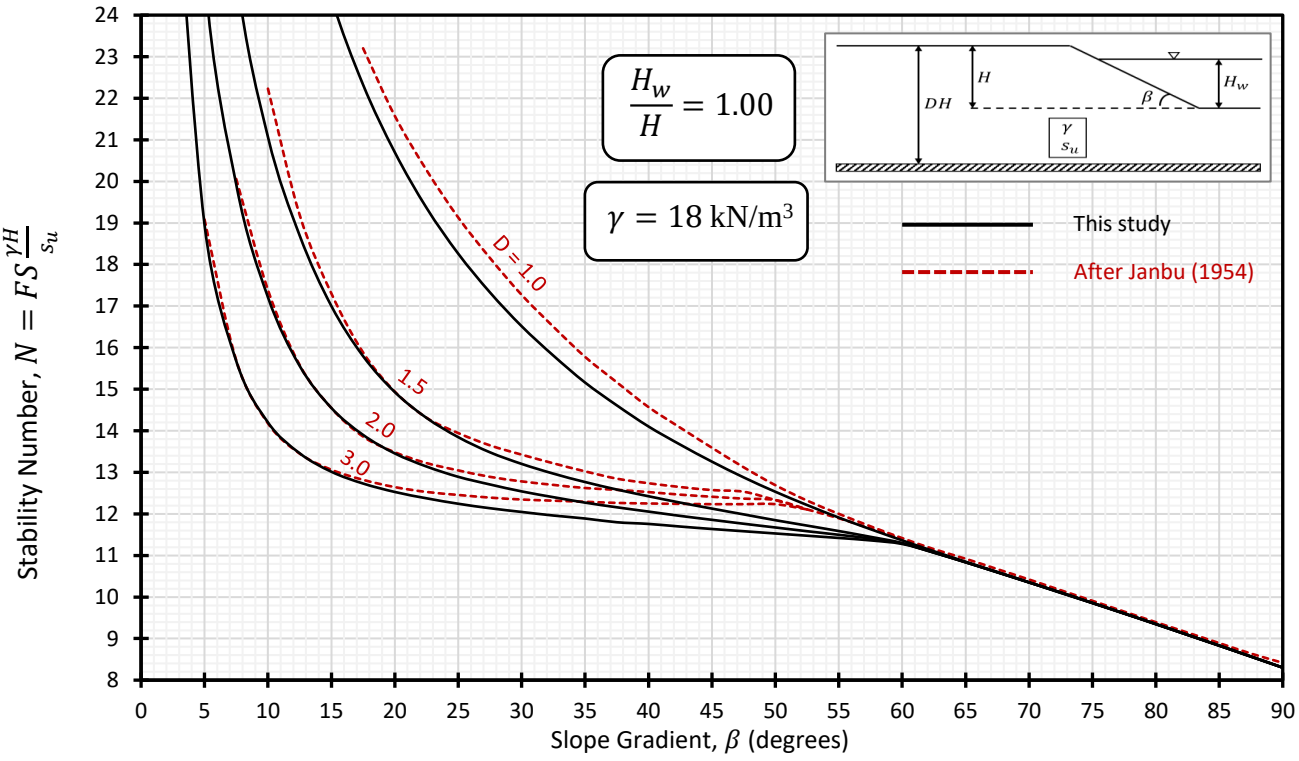

(d)

Figure 4.19 Continued

4.8 Summary

This chapter discussed numerous parametric studies changing the soil and geometric parameters with the main purpose of creating some stability charts for the estimation of the factor of safety for two dimensional homogenous undrained slopes.

Initially, sufficient side widths of a homogeneous FE slope model were determined as a ratio of slope height H, and these side ratios, proposed in Figure 4.2, were used throughout in order to reduce the run-time of the programs and remove possible inaccuracy due to an over-constrained mesh. Following that, the linear relationship of parameters H, s_u, and γ with the factor of safety was investigated prior to starting lengthy studies with thousands of cases. It is concluded that different values of γ will result in different N estimations in the presence of reservoir water, so it is proposed to use N_{ave} with a correction factor C.

Section 4.4 conducted a very detailed parametric study by employing two different methods, EPFE and FELA, and compared their factor of safety estimates. It is concluded that both methods closely agree with each other, and EPFE tends to slightly overestimates the factor of safety. While both methods' close estimations validate each other, some results are validated with the literature as well.

In Section 4.5, the stability of vertical slopes is separately investigated, the theoretical maximum height of a stable vertical excavation in undrained clays is formulated by Equation 4.6. This section also showed how EPFE results approach those obtained by FELA by altering some input parameters in slope64 but resulting in a dramatic boost in the program's execution time. It should be noted, however, that slope64 does not incorporate adaptive mesh refinement which could result in greatest run-time efficiency.

Stability charts were then derived for a homogenous undrained slope based on extensive parametric studies and compared to the charts proposed by Taylor (1937), Janbu (1954), and Steward et al. (2011). Even though there is mostly no significant difference in the estimation of the factor of safety, this study introduced nine distinct types of possible failure mechanisms.

This study lowers the previously accepted value of 5.52 to 5.12 as the minimum stability number that can be obtained by a deep mechanism. In addition, the angle associated with that minimum stability number, which has been first specified as $53°$ by Fellenius (1927) and Taylor (1937) and which has also further meaning as the angle at which the slope stability becomes independent of the depth factor D, was replaced to $60.5°$.

Finally, utilizing N_{ave}, similar stability charts are derived for 4 different reservoir levels. In order to accurately estimate the factor of safety, some values of the correction factor C are proposed according to the reservoir level and the unit weight of the soil. Then, with the help of a Python script, Janbu's submergence charts are presented in the same manner as the stability charts in this thesis, and the findings are compared. It is concluded that despite the existence of reasonable agreements for some cases, Janbu's chart solution mostly tends to overestimate the FS. This inaccuracy is particularly noticeable in the study of unique situation $D = 1,$ where it reaches approximately 12.5% on the unsafe side for a slope with $\gamma = 18$ kN/m^3; $H_w/H = 0.5$; $\beta = 20°$; and $D = 1$.

CHAPTER 5

CONCLUSIONS AND FUTURE RESEARCH RECOMMENDATIONS

5.1 Conclusion

The followings are the concluding remarks for the parametric studies conducted throughout this thesis:

- Taking into account the deep failure mechanisms from hundreds of analyses using a variety of geometrical parameters β and D, this thesis provides recommendations for the minimum side widths of the finite element mesh as a function of slope height H. These values guarantee reasonable computational efficiency while not interfering with the path of the failure mechanism.
- EPFE analyses always yield solutions between the upper and lower bounds of FELA analyses and generally closer to the upper bound. Nevertheless, the difference between the EPFE solution and the average FELA solution never exceeded 3.5% in any of the analyses undertaken for this thesis and was less than 1% in over half the analyses. Moreover, it is noted that EPFE results tend to converge to those obtained by FELA with an increasing number of mesh elements and a selection of a lower FS tolerance at the expense of much longer execution times.
- This thesis disagrees with existing charts regarding the shape of the failure mechanism. Based on finite element analyses, the stability charts for undrained slopes provided in this thesis deliver nine distinct types of failure mechanisms; seven of them are depicted in the main chart, while the remaining two correspond to a special case of a slope where $D = 1$.

- FELA analyses reveal a transition zone in which the failure mechanism gradually shifts from a tangent deep to a shallow toe mechanism, for slopes having a gradient of between $56°$ and $60.5°$.
- Based on more "realistic" failure surfaces developed by finite element methods, the charts proposed in this thesis estimate the factor of safety more accurately than the existing charts. This inaccuracy in the existing charts appears particularly noticeable for slopes having relatively flat gradients ($\beta \leq 10°$); while Taylor and Janbu's charts overestimate the FS of flat slopes by about 10%, Steward et al.'s chart, underestimates the FS of flat slopes by approximately 10%.
- The larger the depth factor is, the larger the error is, for slopes having a foundation layer ($D \neq 1$) and slope gradients varying from $25°$ to $60.5°$, reaching to a maximum of 7.8% error.
- This thesis replaces two previously accepted parameters by more accurate values. First, contrary to the previously published value of 5.52, the minimum stability number that can be obtained by analyzing a deep mechanism was found to be 5.12. Second, the slope angle at which the factor of safety becomes independent of the depth factor D is proposed as $60.5°$, while Taylor, Janbu, and Steward suggested as $53°$, $60°$, and $58°$, respectively.
- This thesis presents stability charts for reservoir loading at four different levels. These charts are more straightforward to utilize in the stability assessment since they require less interpolation associated with β and D values. Additionally, this study reveals that Janbu's published study overestimates the FS up to 12.5% for a variety of geometrical parameters β and D.

5.2 Future Research Recommendations

The followings are considered valuable research interests for future studies:

- The EPFE and FELA algorithms of slope64 and OxLim can be thoroughly investigated to determine why the EPFE-based estimations tend to be close to the FELA's upper bound solution.
- Another look at slope64's algorithm to find out why it generates multiple simultaneous failure mechanisms for analyses in the transition zone
- Performing LEM analyses on the failure surfaces in irregular shapes obtained by FEM analyses, and the comparison of the FS estimations to those obtained by FEM
- Implementation of an adaptive mesh refinement technique into slope64 to improve its accuracy and reduce its run-time
- Development of further stability charts based on FE analysis for other typical boundary conditions such as a surcharge on the slope crest and the formation of tension cracks
- Investigation of the effect of the typical boundary conditions mentioned above on the form of the failure mechanisms
- Review of stability charts for homogeneous slopes in drained condition

REFERENCES

Abdi, R., De Buhan, P., & Pastor, J. (1994). Calculation of the critical height of a homogenized reinforced soil wall: a numerical approach. International Journal for Numerical and Analytical Methods in Geomechanics, 18(7), 485-505.

Ahrens, J., Geveci, B., & Law, C. (2005). Paraview: An end-user tool for large data visualization. The visualization handbook, 717(8).

Andersen, E. D., Roos, C., & Terlaky, T. (2003). On implementing a primal-dual interior-point method for conic quadratic optimization. Mathematical Programming, 95(2), 249-277.

Baker, R. (2003). A second look at Taylor's stability chart. Journal of Geotechnical and Geoenvironmental Engineering, 129(12), 1102-1108.

Belytschko, T., & Hodge Jr, P. G. (1970). Plane stress limit analysis by finite elements. Journal of the Engineering Mechanics Division, 96(6), 931-944.

Bishop, A. W. (1955). The use of the slip circle in the stability analysis of slopes. Geotechnique, 5(1), 7-17.

Bishop, A. W., & Morgenstern, N. (1960). Stability coefficients for earth slopes. Geotechnique, 10(4), 129-153.

Bottero, A., Negre, R., Pastor, J., & Turgeman, S. (1980). Finite element method and limit analysis theory for soil mechanics problems. Computer Methods in Applied Mechanics and Engineering, 22(1), 131-149.

Clough, R. W., & Woodward III, R. J. (1967). Analysis of embankment stresses and deformations. Journal of the Soil Mechanics and Foundations Division, 93(4), 529-549.

Collin, A. (1956). Landslides in clays by Alexandre Collin, 1846. Toronto: University of Toronto Press.

Coulomb, C. A. (1776). Essai sur une application des règles de maximis & minimis à quelques problèmes de statique, relatifs à l'architecture. Paris: De l'Imprimerie Royale.

Culmann, K. (1866). Die graphische Statik. Zürich: Meyer & Zeller.

Drucker, D. C., Greenberg, H. J., & Prager, W. (1951). The safety factor of an elastic-plastic body in plane strain.

Drucker, D. C., Prager, W., & Greenberg, H. J. (1952). Extended limit design theorems for continuous media. Quarterly of applied mathematics, 9(4), 381-389.

Duncan, J. M. (1996a). State of the art: limit equilibrium and finite-element analysis of slopes. Journal of Geotechnical engineering, 122(7), 577-596.

Duncan, J. M. (1996b). Landslides: investigation and mitigation. Chapter 13-Soil slope stability analysis. Transportation Research Board Special Report, (247).

Dunne, H. P., Martin, C. M., Muir, L., Brown, N., & Wallerand, R. (2015). Undrained bearing capacity of skirted mudmats on inclined seabeds. In Frontiers in Offshore Geotechnics III: Proceedings of the 3rd International Symposium on Frontiers in Offshore Geotechnics (ISFOG 2015) (Vol. 1, pp. 783-788). Taylor & Francis Books Ltd.

Dunne, H. P., Martin, C. M., & Wallerand, R. (2017). Limit analysis of hybrid subsea foundations under horizontal and torsional loading. In Offshore Site Investigation Geotechnics 8th International Conference Proceeding (Vol. 818, No. 825, pp. 818-825). Society for Underwater Technology.

Dunne, H. P., & Martin, C. M. (2017). Capacity of rectangular mudmat foundations on clay under combined loading. Géotechnique, 67(2), 168-180.

Fellenius, W. (1927). Erdstatische Berechnungen mit Reibung und Kohasion (Adhasion) und unter Annahmekreiszylindrischer Gleitflachen. Ernst & Sohn, Berlin.

Fellenius, W. (1936). Calculation of stability of earth dam. In Transactions. 2nd Congress Large Dams, Washington, DC, 1936 (Vol. 4, pp. 445-462).

Francais, J. F. (1820). Recherches sur la pousee des terres, sur la forme et les dimensions des murs derevetement et sur les talus d'excavation Research on soil pressure on the form and dimensions of revetment walls and excavation slopes. Memoires de L'office d Genie, 4, 157-193.

Fredlund, D. G. (1981). The relationship between limit equilibrium slope stability methods. 10th. ICSMFE, 1981, 3, 409-416.

Griffiths, D. V. (1980). Finite element analysis of walls, footing and slopes. Symposium on Computer Applications to Geotechnical Problems in Highway Engineering, 122-146.

Griffiths, D. V. (1989). Computation of collapse loads in geomechanics by finite elements. Ingenieur-Archiv, 59(3), 237-244.

Griffiths, D. V., & Lane, P. A. (1999). Slope stability analysis by finite elements. Geotechnique, 49(3), 387-403.

Griffiths, D. V., & Martin, C. M. (2020). Critical failure mechanisms in relatively flat undrained slopes. Géotechnique Letters, 10(2), 95-99.

Hultin, S. (1916). Grusfyllnader for kajbyggnader. Teknisk Tidsskrift (Gravel fillings for quay construction), 31.

Hunter, J. H., & Schuster, R. L. (1968). Stability of simple cuttings in normally consolidated clays. Geotechnique, 18(3), 372-378.

Jaky, J. (1936). Stability of earth slopes. In Proceedings of the International Conference on Soil Mechanics (Vol. 2, pp. 125-129).

Janbu, N. (1954). Stability analysis of slopes with dimensionless parameters. Cambridge: Harvard University.

Janbu, N. (1968). Slope Stability Computations. Institutt for Geotknikk og Fundamenteringslære. Norges Tekniske Høgskole. Soils Mechanics and Foundation Engineering, the Technical University of Norway.

Kammoun, Z., Pastor, F., Smaoui, H., & Pastor, J. (2010). Large static problem in numerical limit analysis: A decomposition approach. International Journal for Numerical and Analytical Methods in Geomechanics, 34(18), 1960-1980.

Kohgo, Y., and Yamashita,T. (1988). Finite element analysis of fill type dams-Stability during construction by using the effective stress concept. In Proc. 6th Int. Conf. on Numer. Methods in Geomechanics, Balkema (pp. 1315-1322).

Kötter, F. (1903). Die Bestimmung des Drucks an gekru¨mmten Gleitfla¨ chen, eine Aufgabe aus der Lehre vom Erddruck, Sitzungsberichteder Akademie der Wissenschaften, Berlin, 229–233.

Lysmer, J. (1970). Limit analysis of plane problems in soil mechanics. Journal of the Soil Mechanics and Foundations Division, 96(4), 1311-1334.

Makrodimopoulos, A., & Martin, C. (2006). Lower bound limit analysis of cohesive-frictional materials using second-order cone programming. International Journal for Numerical Methods in Engineering, 66(4), 604-634.

Makrodimopoulos, A., & Martin, C. M. (2007). Upper bound limit analysis using simplex strain elements and second-order cone programming. International journal for numerical and analytical methods in geomechanics, 31(6), 835-865.

Makrodimopoulos, A., & Martin, C. M. (2008). Upper bound limit analysis using discontinuous quadratic displacement fields. Communications in Numerical Methods in Engineering, 24(11), 911-927.

Mana, D. S., Gourvenec, S., & Martin, C. M. (2013). Critical skirt spacing for shallow foundations under general loading. Journal of geotechnical and geoenvironmental engineering, 139(9), 1554-1566.

Martin, C. (n.d.). Introduction to finite element limit analysis using OxLim [PDF]. Retrieved from University Of Oxford Course Ultimate capacity of shallow foundations

Martin, C. M. (2011). The use of adaptive finite-element limit analysis to reveal slip-line fields. Géotechnique Letters, 1(2), 23-29.

Martin, C. M., & White, D. J. (2012). Limit analysis of the undrained bearing capacity of offshore pipelines. Géotechnique, 62(9), 847-863.

Massarsch, K. R., & Fellenius, B. H. (2012). Early swedish contributions to geotechnical engineering. In Full-Scale Testing and Foundation Design: Honoring Bengt H. Fellenius (pp. 239-256).

Matsui, T., & San, K. C. (1992). Finite element slope stability analysis by shear strength reduction technique. Soils and foundations, 32(1), 59-70.

Michalowski, R. L. (2002). Stability charts for uniform slopes. Journal of Geotechnical and Geoenvironmental Engineering, 128(4), 351-355.

Morgenstern, N. U., & Price, V. E. (1965). The analysis of the stability of general slip surfaces. Geotechnique, 15(1), 79-93.

MOSEK ApS (2014). The MOSEK C optimizer API manual, version 7.1.

Pastor, J. (1978). Analyse limit determination numerique de solutions statistique completes, Application au talus vertical. J. de Mechanique Appliquee, 2, 167-196.

Pastor, J., Thai, T. H., & Francescato, P. (2000). New bounds for the height limit of a vertical slope. International Journal for Numerical and Analytical Methods in Geomechanics, 24(2), 165-182.

Pastor, F., Loute, E., & Pastor, J. (2009). Limit analysis and convex programming: A decomposition approach of the kinematic mixed method. International journal for numerical methods in engineering, 78(3), 254-274.

Perzyna, P. (1966). Fundamental problems in viscoplasticity. In Advances in applied mechanics (Vol. 9, pp. 243-377). Elsevier.

Petterson, K. E. (1916). Kajraset i Goteborg des 5te mars 1916 (Collapse of a quay wall at Gothenburg, Xarch 5th, 1916). Teknisk Tidskrift, 46 : 289.

Potts, D.M., Dounias, G., & Vaughan, P.R. (1990). Finite element analysis of progressive failure of Carsington embankment. Geotechnique, 40, 79-101.

Prandtl, L. (1921). Eindringungsfestigkeit und Festigkeit von Schneiden. Z. Angew. Math Mech. 1, 15.

Rankine, W. J. M. (1857). II. On the stability of loose earth. Philosophical transactions of the Royal Society of London, (147), 9-27.

Rendulic, L. (1935). Ein beitrag zur bestimmung der gleitsicherheit. Der Bauingenieur, 16(19/20), 230-233.

Sarma, S. K. (1973). Stability analysis of embankments and slopes. Geotechnique, 23(3), 423-433.

Shewchuk, J. R. (2002). Delaunay refinement algorithms for triangular mesh generation. Computational geometry, 22(1-3), 21-74.

Sloan, S. W. (1988). Lower bound limit analysis using finite elements and linear programming. International Journal for Numerical and Analytical Methods in Geomechanics, 12(1), 61-77.

Sloan, S. W., & Kleeman, P. W. (1995). Upper bound limit analysis using discontinuous velocity fields. Computer methods in applied mechanics and engineering, 127(1-4), 293-314.

Sloan, S. W. (2013). Geotechnical stability analysis. Géotechnique, 63(7), 531-571.

SLOPE/W 2007–GeoStudio Student Edition [Computer software]. GEOSLOPE International Ltd, Calgary, AB, Canada.

Smith, I. M., & Hobbs, R. (1974). Finite element analysis of centrifuged and built-up slopes. Geotechnique, 24(4), 531-559.

Smith, I. M., & Griffiths, D. V. (1988). Programming the finite element method. New York: John Wiley & Sons.

Smith, I. M., Griffiths, D. V., & Margetts, L. (2014). Programming the finite element method. John Wiley & Sons.

Spencer, E. (1967). A method of analysis of the stability of embankments assuming parallel inter-slice forces. Geotechnique, 17(1), 11-26.

Steward, T., Sivakugan, N., Shukla, S. K., & Das, B. M. (2011). Taylor's slope stability charts revisited. International Journal of Geomechanics, 11(4), 348-352.

Terzaghi, K. (1943). Theoretical soil mechanics. johnwiley & sons. New York, 11-15.

Terzaghi, K., & Peck, R. B. (1948). Soil mechanics in engineering practice. New York: J. Wiley & Sons.

Taylor, D. W. (1937). Stability of earth slopes. J. Boston Soc. Civil Engineers, 24(3), 197-247.

Yu, H. S., Sloan, S. W., & Kleeman, P. W. (1994). A quadratic element for upper bound limit analysis. Engineering Computations.

Zienkiewicz, O. C., & Cormeau, I. C. (1974). Visco-plasticity—plasticity and creep in elastic solids—a unified numerical solution approach. International Journal for Numerical Methods in Engineering, 8(4), 821-845.

Zienkiewicz, O. C., Humpheson, C., & Lewis, R. W. (1975). Associated and non-associated visco-plasticity and plasticity in soil mechanics. Geotechnique, 25(4), 671-689.